NASA CR137621
R73AEG360

AVAILABLE TO THE PUBLIC

ACOUSTIC RESULTS FROM TESTING OF A 36 INCH (0.914m) DIAMETER STATORLESS LIFT FAN

by

D.L. Stimpert

GENERAL ELECTRIC COMPANY

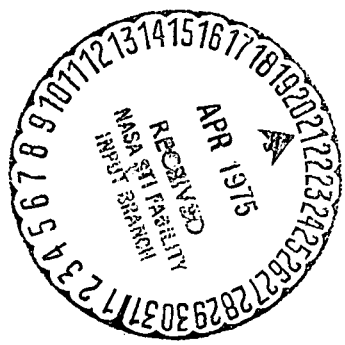

prepared for

NATIONAL AERONAUTICS AND SPACE ADMINISTRATION

NASA-Ames Research Center

1. Report No.	2. Government Accession No.	3. Recipient's Catalog No.
NASA CR137621		

4. Title and Subtitle	5. Report Date
Acoustic Results from Testing of A 36 Inch (0.914m) Diameter Statorless Lift Fan	January 1975
	6. Performing Organization Code

7. Author(s)	8. Performing Organization Report No.
D.L. Stimpert	R73AEG360
	10. Work Unit No.

9. Performing Organization Name and Address	11. Contract or Grant No.
General Electric Company Aircraft Engine Group Cincinnati, Ohio 45215	

12. Sponsoring Agency Name and Address	13. Type of Report and Period Covered
National Aeronautics and Space Administration Washington, D.C. 20546	Contractor Report
	14. Sponsoring Agency Code

15. Supplementary Notes

16. Abstract

A statorless, turbotip lift fan was tested statically outdoors at General Electric Edwards Flight Test Center and at NASA Ames Research Center to determine its acoustic characteristics.

Spectral and directivity results are presented with comparison to data from the same family of lift fan designs having stator vanes. Modifications to the fan were tested to evaluate circular inlet guide vanes and exhaust treatment. A comparison was made of results obtained at General Electric Edwards Flight Test Center and NASA Ames Research Center with regards to test data and differences in site characteristics.

17. Key Words (Suggested by Author(s))	18. Distribution Statement
LF336/E Statorless Lift Fan Rotor-alone Noise Lift Fan Acoustics	Unclassified - Unlimited

19. Security Classif. (of this report)	20. Security Classif. (of this page)	21. No. of Pages	22. Price*
Unclassified	Unclassified	94	

* For sale by the National Technical Information Service, Springfield, Virginia 22151

TABLE OF CONTENTS

TABLE OF CONTENTS (Cont'd)

LIST OF TABLES

LIST OF FIGURES

LIST OF FIGURES (Cont'd)

LIST OF FIGURES (Cont'd)

LIST OF FIGURES (Cont'd)

LIST OF FIGURES (Cont'd)

SECTION I

SUMMARY

A statorless, turbotip, lift fan (LF336/E) was tested statically outdoors to determine its acoustic characteristics. The tests were conducted at the General Electric Edwards Flight Test Center (EFTC) at Edwards AFB, California and at the NASA Ames Research Center outdoor test site at Moffett Field, California.

The LF336/E is a 36 inch (91.4 cm) tip diameter fan with an aerodynamic design pressure ratio of 1.25 at a design tip speed of 1060 feet per second (324 meters per second). The statorless fan is designed for operation without a stage inlet guide vane or exit stator row; thus, it is a rotor only configuration and is driven by a tip turbine using the exhaust gases of the General Electric J85-GE-5 (dry) turbojet engine.

Directivity comparisons, on an equal tip speed basis indicate that the statorless lift fan is 1 to 3 PNdB quieter in the forward quadrant and equal to 2PNdB quieter in the aft quadrant than a conventional two chord spacing rotor-stator lift fan. A massive fan inlet suppressor was installed which indicated that fan exhaust radiated noise levels are 5 to 8 PNdB below the inlet radiated levels in the forward quadrant. Installation of a circular IGV increased forward PNL's by 3 to 5 PNdB and aft PNL's by 1 to 2 PNdB due primarily to an increase at the BPF. Treated exit louvers achieved 2 to 4 PNdB suppression from 80 to 100 degrees at 6000 RPM. Near field fan levels were unchanged from EFTC to NASA Ames and that the asphalt surface at NASA Ames and the desert sand at EFTC have similar reflectivity characteristics.

SECTION II

INTRODUCTION

The General Electric Company has been conducting extensive research programs in conjunction with NASA to develop acoustic technology for advanced, lightweight lift fans for applications to V/STOL aircraft systems. These research programs have studied the generation of lift fan noise and its alleviation by judicious selections of fan geometry using the LF336 lift fan as a test vehicle.

Reference 1 has shown that increased axial spacing between the fan rotor and outlet guide vanes (OGV) is a significant parameter in reducing lift fan noise. Increased spacing reduces noise generated by viscous wake interaction and a logical extension of technology would be to eliminate the OGV's creating a statorless lift fan and thus eliminating any viscous wake interaction noise.

In addition to noise reduction potential due to elimination of viscous wake interaction noise, previous conceptual design studies, Reference 2, have shown that the remote tip turbine statorless fan is an attractive V/STOL propulsion system in terms of thrust-to-weight, installed thickness, and overall rotor disk loading.

A program sponsored by NASA Ames Research Center under NASA Contract NAS2-5462 was initiated to design, fabricate, and test the LF336/E statorless fan system. The fan was tested for mechanical and aerodynamic performance at the General Electric Edwards Flight Test Center (EFTC). In addition, acoustic testing was conducted at EFTC and a NASA Ames Research Center outdoor test site. Unsuppressed, baseline noise levels were determined at both sites and are presented in this report. Further acoustic configurations were tested to measure exhaust radiated noise levels, to determine the effect of circular inlet guide vanes, and to measure the suppression achieved with acoustically treated fan exit louvers. These results are also presented here. A summary of the configurations tested at both locations is presented in Table I.

SECTION III

TEST HARDWARE

The basic test propulsion system consisted of the LF336/E statorless fan, the J85-5 engine, and interconnecting ducting as shown in Figure 1. The system was installed in a test stand which provided for mounting the fan and engine system with the fan inlet oriented in a vertical plane. The fan inlet bellmouth was installed flush with a flat plane surface which simulated a wing upper surface of a fan-in-wing installation.

A. LF336/E Fan System

The LF336/E fan is a single stage statorless turbotip lift fan which is designed to operate without either inlet guide vanes or exit stator rows. The fan has a 36 inch (91.44 cm) diameter and incorporates 42 blades in a tip turbine driven, single stage rotor. The single stage rotor develops a fan pressure ratio of 1.25 at a fan design tip speed of 1060 feet per second (323 m per second). The design pressure ratio of 1.25 assumes no recovery of the exit swirl component. Accordingly, the overall total-to-total pressure ratio is 1.32 at design operating conditions.

A sketch of the fan is shown in Figure 2 with selected design parameters presented in Table II. When the fan was tested it was modified by the installation of tip turbine exit stators.

B. J85-5 Engine

The fan tip turbine was driven by a J85-5 engine modified to a conventional turbojet engine configuration. The gas generator is shown in Figure 1 coupled to the lift fan. Also evident in this photograph is the acoustic suppressor which was installed on the J85-5 inlet to suppress gas generator inlet radiated noise. The engine exhaust is direct-coupled to the fan scroll inlet through a transition duct. Engine serial number 231-233 was used during these tests.

C. LF336/E Fan Inlet Suppressor

During the testing at EFTC a massive fan inlet suppressor was installed to suppress fan inlet radiated noise and to allow determination of exhaust radiated statorless lift fan noise. Details of the design of the massive fan inlet suppressor are given in Reference 3. The fan inlet suppressor is shown in Figure 3. In addition to suppressing the inlet radiated fan noise, the massive inlet suppressor provided a 90 degree directivity shift to further reduce the levels at the microphone locations. Note that the inlet duct was wrapped with lead-vinyl blanket to reduce any structure-born transmission of noise.

SECTION IV

TEST SITES

A. Edwards Flight Test Center

The test program was conducted at an outdoor test facility designed and constructed for testing full scale lift fans and engines. The site shown in Figure 4 is located at the General Electric Edwards Flight Test Center at Edwards Air Force Base, California and is in an area free of buildings and obstructions. The area surrounding the acoustic test site consists of desert sand and brush. Figure 4 is a photograph taken across the top of the control room which extends only thirty inches (76.2 cm) above the ground. The photograph shows the large bellmouth positioned in front of the LF336/E fan and the J85 with its inlet suppressor removed.

The test stand is attached to four concrete columns which protruded above the asphalt apron and the fan was mounted in the stand ten feet (3.05 m) above the ground with the fan flow parallel to the ground. No portion of the test stand was forward of the lift fan upper wing simulation surface which prevented any turbulence being generated by test stand structures.

A sketch of the microphone locations at EFTC is shown in Figure 5. There were seventeen microphones located at 10 degree increments from 0 to 160 degrees relative to the fan inlet on a 150 foot (45.7 m) arc. Seven near field microphones were located on a 20 foot (6.1m) arc at angles of 90, 110, 130, 150, 210, 230, and 250 degrees relative to the fan inlet. The near field mikes can be seen in Figure 1. All microphones were in a horizontal plane through the fan centerline.

B. NASA Ames Outdoor Test Site

Additional LF336/E fan testing was conducted at an outdoor test site located at NASA Ames Research Center. An aerial view of the test site is presented in Figure 6. As the photograph shows, the acoustic path to a given microphone was in some places asphalt and concrete, and in others short grass and asphalt. The microphone layout is sketched in Figure 7. Far field microphones were on a 150 foot (45.7 m) arc in ten degree increments from 0 to 160 degrees. Two arrangements of near field microphones were used - both on a 20 foot (6.1 m) arc. The first, used for Runs 1 and 2, had the microphones located at 20 degree increments from 30 to 150 degrees. The second arrangement, for Run 3 and all successive runs, had the seven microphones located at 90, 110, 130, 150, 210, 230, and 250 degrees. This latter arrangement duplicated the near field microphone locations used at Edwards Flight Test Center, and in the NASA Ames 40' by 80' (12.2 m x 24.4 m) wind tunnel.

Engine and fan centerline height at NASA Ames was 9 feet 8 inches (2.95 m) and all microphones were located in a horizontal plane through the fan centerline.

SECTION V

SOUND DATA ACQUISITION AND PROCESSING

A. Data Acquisition

1. Edwards Flight Test Center

All data acquisition for the near and far sound fields was made using Bruel-Kjaer model 4133 microphone systems in conjunction with an AR200 tape recorder operating at 60 inches per second (152 cm per second). Figure 8 includes a schematic of the data acquisition system at EFTC, and a photograph of some of the equipment.

All far field microphones were oriented to point at the test vehicle and had Bruel-Kjaer UA0237 windscreens installed on the microphone heads. The near field microphones were oriented to point in the same direction as the J85 inlet and used Bruel-Kjaer model UA0052 nose cones.

The free field frequency response of each microphone head is derived from a pressure response curve recorded automatically by the electro-static actuator method traceable to the Bureau of Standards. The free field characteristics for various angles of incidence for microphones with protecting grid, nose cones, and windscreens are given by the microphone manufacturer. Individual microphone head sensitivities are determined by the insertion of a Bruel-Kjaer pistonphone on the cartridge mounted to a standard microphone system. Both the pistonphone and standard microphone system are traceable to the Bureau of Standards.

Prior to initiation of testing, a frequency response of each data channel (minus microphone head) was made by the insertion of a Hewlett-Packard Pseudo-Random Pink Noise Generator into each cathode follower and recorded on magnetic tape.

Prior to and subsequent to each day's testing, an absolute calibration was made by the insertion of a pistonphone on each microphone and recorded on tape. Since the test site is 2300 feet (701 m) above sea level, a barometric correction was made to the pistonphone output as provided by manufacturer's specifications. Any microphone whose voltage output with the pistonphone applied was found to deviate more than $\pm$ 1.5 dB from the laboratory calibration was replaced.

2. NASA Ames Research Center

Data acquisition at NASA Ames was similar to that at EFTC as the sketch in Figure 9 shows, except that the tape recorder was a Honeywell Model 7600 operated at 30 inches per second (76 cm per second). The step amplifier, tape recorder, monitor scope, and monitor voltmeter were all located in the General Electric Mobile Sound Evaluation Unit (Figure 6).

During test operations at both test sites, sound was recorded continuously for a minimum of two minutes to allow enough sample length for data processing.

B. Data Processing

1. 1/3 Octave Bands

All 1/3 octave band data processing was performed at the General Electric Edwards Flight Test Center facilities using a General Ratio real time analyzer in conjunction with a Honeywell 316 and SDS930 computer. Thirty-two second averaging time was used for data processing with data for each angle sampled from the same period of time for each data point.

Before data processing could be initiated, the total data acquisition and reduction system frequency response characteristics had to be determined and made available in the computer for final data processing. The first step in this process was to analyze the Pink Noise calibration tapes for each data channel, and determine the response characteristics for the total system as referenced to 250 Hz (frequency of the pistonphone) at each 1/3 octave band. Final one-third octave data processing was made by determining absolute sound pressure levels, for the 150 foot (45.7 m) arc and 200, 500 foot (61 m, 151 m) sidelines, corrected to standard day (59° F (15° C), 70% relative humidity) conditions as per Reference 4 and for ground attenuation effects as per Reference 5.

2. 20 Hz Narrowbands

All narrowband analysis was made at the General Electric Evendale facilities using a Federal Scientific Ubiquitous Spectrum Analyzer and a 139B Digital Averager. All data was processed using a 20 Hz bandwidth filter and an averaging time of 12.8 seconds. No corrections for humidity or acquisition/processing responses were included in the narrowband plots.

SECTION VI

RESULTS AND COMPARISONS

Extensive testing of the LF336/E statorless lift fan was conducted at the General Electric Edwards Flight Test Center and at a NASA Ames Research Center outdoor test site. All succeeding 1/3 octave band SPL and PNL comparisons are made on a 200 foot (61 m) sideline while all 20 Hz narrowband SPL's are compared at a 150 foot (45.7 m) arc.

A. Statorless Fan Comparisons to Other LF336 Fans

In this section, acoustic levels of the LF336/E statorless fan from NASA Ames Research Center testing are compared to LF336/A, LF336/B, LF336/C-1 and LF336/C-11 fans (Reference 1). Table I-VII lists the design parameters of these fans of the LF336 family.

Comparison of statorless and conventional rotor-stator fan configurations has shown that equal fan thrust can be achieved through proper selection of fan pressure ratio. For equal thrust, the statorless fan will require a larger fan diameter at a lower pressure ratio with minor increases in overall installation diameter in exchange for the reduced thickness of the fan relative to the more conventional design. This trade-off of fan diameter for thickness is one of the merits of the statorless fan concept.

Comparisons will be made at equal tip speeds and equal absolute pressure ratios. Comparisons of noise generation at equal tip speed is equivalent to comparing fans having equal thrust but different pressure ratios. Comparison at equal absolute pressure ratio implies similar fan loading characteristics and equal thrust for the same diameter. Pressure ratio has been used as a correlating parameter of aft radiated fan noise or rotor-stator noise while equal tip speed comparisons have been associated with inlet radiated or rotor alone noise. Comparisons will be made both ways but in applications, the statorless fan would be designed to operate at a lower pressure ratio than conventional fans.

1. Equal Tip Speed Comparison

Figure 10 compares statorless fan 1/3 octave band BPF directivity patterns to the LF336/B and LF336/C-11 fans at three fan speeds (no C-11 data available at 6000 RPM). Since all three fans are the same diameter, equal fan speed is equal tip speed. At the forward angles the statorless fan is lower than the other two fans. In the aft quadrant the statorless fan BPF levels are consistently lower than the LF336/B and at least as quiet as the LF336/C-11 at the critical angles of 110° to 130°. These angles are the most critical for sideline noise measurements with lift fans. Narrowband BPF directivity patterns for the statorless and LF336/B fans are compared in Figure 11 at 6000 RPM (950 fps, 290 m/sec tip speed) and show similar trends as Figure 10. PNL directivity patterns are presented in Figure 12 and show

that the statorless fan forward quadrant PNL's are quieter than the LF336/B and equal to or slightly lower than the LF336/C-11. In the aft quadrant (110° to 130°), statorless fan levels are the same or quieter than LF336/B but 1 to 3 PNdB higher than LF336/C-11. Since the statorless fan is not significantly lower than the conventional rotor-OGV lift fan this implies that the maximum effect of spacing has been reached at two chord spacing. This is shown more clearly in Figure 13 where the effect of spacing is shown on aft quadrant 110° PNL at several fan speeds (tip speeds) using several LF336 series fans. This figure indicates little change with increased spacing beyond two rotor chords which means that two chord spacing can be considered the spacing at which rotor alone noise dominates over that caused by rotor-OGV interaction effects.

Figure 14 compares the LF336/E, LF336/B, and LF336/C-11 PNL's as a function of fan speed (and tip speed) at several acoustic angles. At 40 and 60 degrees the statorless fan is lower than the LF336/B at all speeds and generally the same as LF336/C-11. At 110 and 120 degrees, the statorless fan is the same as LF336/B at high speeds, but 3 PNdB lower at low fan speeds. At the same angles it is 2 to 3 PNdB higher than LF336/C-11 at high speeds, but the same at lower speeds.

2. Equal Absolute Pressure Ratio Comparisons

Figure 15 compares the fan pressure ratio of the LF336/A (which was assumed for the LF336/B and C) with the absolute pressure ratios developed by the LF336/E statorless fan. The absolute pressure of the LF336/E fan is based on the average total pressure at the fan exit measured in the direction of the swirling flow.

Directivity patterns of the 1/3 octave band which contains the BPF are compared in Figure 16 at equal absolute pressure ratios. In the forward quadrant, the trends are the same as in the previous section with statorless fan levels generally lower than LF336/B but equal to LF336/C-11. In the critical aft angles between 110 and 130 degrees, the statorless fan is generally the same as LF336/C-11 and lower than LF336/B at the lower two pressure ratios. At the higher pressure ratio, the statorless fan is 1 to 3 dB above LF336/C-11. On a PNL directivity comparison, as shown in Figure 17, the statorless fan is the same as LF336/B at forward angles and 1 to 2 PNdB higher in the aft quadrant. Figure 18 compares the three LF336 lift fans as a function of absolute pressure ratio at four acoustic angles. At 40 and 60 degrees, the LF336/E is consistently lower than LF336/B at all pressure ratios but about 2 PNdB higher than the treated LF336/C-11 configuration. At 110 and 120 degrees, the LF336/B and LF336/E are almost identical at all pressure ratios and both are 2 to 3 PNdB above the LF336/C-11 levels.

On either basis - equal tip speed or equal pressure ratio - the statorless fan has noise levels comparable to the quietest conventional fan modified for minimum noise. Therefore, the statorless fan would seem to be a viable candidate, from the acoustic point of view, for quiet lift fan applications.

B. Fan Exhaust Directivity Patterns

In analyzing lift fan systems, it is sometimes useful to know the split between inlet radiated noise and exhaust radiated noise levels. To determine this split a massive fan inlet suppressor was designed (Reference 3) as part of the LF336 Discharge Noise Suppression Test. In addition to suppressing fan inlet radiated noise, the suppressor - shown in Figure 3 - provided a 90 degree directivity shift to any fan inlet radiated noise. When tested, the massive fan inlet suppressor effectively suppressed fan inlet radiated noise and permitted measurement of exhaust radiated noise. The same fan inlet suppressor was installed on the statorless fan during testing at Edwards Flight Test Center.

Fan PNL directivities are presented in Figure 19 with and without the fan inlet suppressor at 6000, 5400, and 4800 rpm. The exhaust radiated levels in the forward quadrant are 5 to 8 PNdB below the unsuppressed levels. In Figure 20, the 40 and 60 degree microphone PNL's are compared as a function of fan speed. At 40 degrees the exhaust radiated noise levels are 6 to 10 PNdB lower than the unsuppressed levels at 6000 to 3000 rpm. At 60 degrees, there is 5 to 6 PNdB difference over the speed range.

Looking at Figure 19, installing the inlet suppressor appeared to slightly increase the PNL levels in the aft quadrant. Figure 21 shows the 110 and 120 degree PNL's as a function of physical fan speed. At 110 degrees the inlet suppressor has no effect; however, at 120 degrees there is an increase of 2 PNdB near 4700 rpm and very little effect at other speeds. These slight changes are probably due to increased turbulence from the massive fan inlet suppressor or, as will be discussed later, due to velocity changes in the fan tip region when the inlet duct was installed.

Figure 22 compares the directivity patterns of the 1/3 octave band which contains the BPF at three fan speeds with and without the inlet suppressor. At the 40 degree microphone the fan exhaust radiated levels are 6 to 10 dB below the unsuppressed levels. In the aft quadrant at 5400 and 4800 rpm, the exhaust radiated SPL's are higher than the total or unsuppressed levels. However, Figure 23 compares the 20 Hz narrowband BPF directivity patterns with and without the inlet suppressor and indicates that inlet radiated BPF noise has been eliminated to 120 degrees at 6000 RPM. At lower speeds, Figure 24 indicates that the 90 degree exhaust radiated BPF SPL's are 1 to 2 dB higher at 5400 and 4800 rpm and these are lower than the unsuppressed levels. At 110 degrees the exhaust radiated levels are lower at all speeds; however, at 120 degrees the exhaust radiated BPF levels have increased 4 to 7 dB over the unsuppressed levels at speeds from 4000 to 5400 rpm.

1/3 octave band spectra are compared in Figure 25 at the 40 degree microphone. At this microphone, fan inlet radiated noise is evident down to 500 Hz at all speeds. The 20 Hz narrowband spectra in Figure 26 show that fan broadband suppression is about the same at all frequencies. At the 60 degree microphone in Figure 27, the 1/3 octave band spectra again indicate fan inlet radiated noise is present down to 500 Hz. 20 Hz narrowbands in Figure 28 indicate that the fan broadband suppression is not as much as at

the 40 degree microphone. Looking at the 20 Hz BPF directivity as a function of fan speed, Figure 29 indicates that the fan exhaust radiated BPF SPL is 16 to 9 dB below the unsuppressed fan levels at the 40 degree microphone. At the 60 degree microphone the exhaust radiated BPF SPL is 12 to 8 dB down except for 3800 rpm. Why this particular speed does not agree trendwise with the other speeds is unknown.

The split between exhaust radiated and inlet radiated noise levels can be easily determined. To calculate inlet radiated levels, one only has to logarithmically subtract the exhaust radiated levels from the unsuppressed levels. This provides the capability of evaluating different exhaust and inlet suppression requirements and determining the effect on the overall noise levels.

C. Circular IGV Effects

During testing of the statorless fan in the 40' by 80' (12.2 m by 24.4 m) wind tunnel, a circular inlet guide vane (IGV) was installed and tested to determine its effect on crosswind performance. The same IGV was installed and tested outdoors. While in the wind tunnel the fan major strut was horizontal and the IGV covered from 12 o'clock to 6 o'clock looking into the fan. Outdoors, the fan major strut was vertical and covered from 3 o'clock to 9 o'clock. IGV to rotor spacing was approximately 0.25 inches (0.63 cm) or about 0.06 IGV true chords.

PNL directivity patterns of the fan without (unsuppressed) and with the circular IGV installed are compared in Figure 30 at 6000 and 5400 rpm. Forward angles of 60 and 70 degrees show an increase of 3 to 5 PNdB. Aft angles show a slight increase of 1 to 2 PNdB at both speeds. Figure 31 shows that the effect of the IGV at 60 degrees decreases from 5 PNdB at 6000 rpm to zero at 3000 rpm. At the 110 degree microphone, the effect remains essentially constant with speed. A comparison of 1/3 octave band spectra in Figure 32 at 60, 70, and 110 degrees shows a big change in the 1/3 octave band which contains the BPF. Fan broadband levels are unchanged. Narrowbands of the same spectra used in Figure 32 confirm that the IGV has caused a large increase in the BPF level with no change in fan broadband noise. These narrowbands are shown in Figure 33. A comparison in Figure 34 of the narrowband BPF directivity patterns at 6000 rpm clearly shows the BPF increase at forward and aft angles.

That the aft quadrant PNL's show only a small (1 to 2 PNdB) change due to the IGV's may be explained by closer examination of the 110 degree spectra in Figure 33. When the 20 Hz bandwidth SPL's are converted to 1/3 octave band levels, the BPF does not control the band. 10 log (0.23 x 4000 Hz/20 Hz) = 16.5 dB is added to the fan broadband levels and since they are unchanged except for some modulation near the BPF, the 1/3 octave band SPL shows only a little change. In the forward angles, the signal-to-noise ratio of the BPF is such that the BPF controls the 1/3 octave band.

If circular inlet guide vanes are installed to improve crossflow characteristics of the fan, one can expect sharp increases in the BPF sound pressure levels. At forward angles, there will be a 3 to 5 PNdB increase. while aft angles will be increased 1 to 2 PNdB.

D. Treated Exit Louver Suppression

Acoustically treated exit louvers were installed and tested on the statorless fan at NASA Ames. The louver cascade is shown in Figure 35 and was previously used in the LF336/C test program (Reference 1). It consisted of eight airfoils, each 0.58 inch (1.48 cm) thick with a 7.9 inch (20.1 cm) chord. The airfoils were treated on both sides with two degree-of-freedom resonators and had acoustic design parameters $L/H \sim 1.3$ and $H/\lambda \sim 1.4$. They were located about 8 inches (20.3 cm) downstream of the rotor trailing edge. Reference 1 determined that little appreciable acoustic energy was radiated from the open ends of the louver cascade.

A comparison of the PNL directivity patterns with and without the treated exit louvers is shown in Figure 36 at 6000, 5400, and 4800 rpm. Suppression of 2 to 4 PNdB was achieved at angles of 80 to 110 degrees. Figure 37 presents the directivity patterns of the 1/3 octave band which contains the BPF. Again suppression is evident from 80 to 110 degrees at all speeds. 1/3 octave band spectra at the 110 degree microphone are compared in Figure 38. Fan BPF and fan broadband suppression is evident for frequencies at and above the BPF; however, there is an increase in noise in the 630 Hz to 2500 Hz bands and a decrease at frequencies below 250 Hz. Narrowbands of 110 degree microphone spectra at 6000 and 5400 rpm are shown in Figure 38 and show broadband humps of noise near 1200 and 2100 Hz at 6000 rpm. This increase in the midfrequency range is due to wake scrubbing and interaction noise over the louvers. The flow out of the statorless fan has swirl in it which would tend to increase the scrubbing noise.

In Reference 1, it was shown that for the LF336/C fan at 95 percent fan speed (5750 rpm), there was no suppression from the louvers; however, at 80 percent fan speed (4800 rpm) 1 to 2 PNdB suppression was realized. At that time it was observed at high power settings, the Mach number of the flow over the louvers was of the order of 0.7. High Mach numbers are known to reduce the effectiveness of resonator treatment. At lower fan speeds, the Mach number was lower; therefore, the treatment was more effective. At the highest fan speed of the statorless fan (6000 rpm), the Mach number based on the above calculations is about 0.5 at which the treatment should be more effective and indeed is as shown in Figure 36.

E. Inlet Radiated Power Level Predictions

A theoretical analysis of the noise generated by inlet turbulence-rotor interaction was conducted and a mathematical model developed to predict the inlet radiated sound power levels.

At the time of testing, no inlet turbulence measurements had been made for the LF336/E statorless fan. Thus it was necessary to estimate levels by scaling turbulence measurements taken during testing of a fan with radius ratio and axial Mach number that were similar to the LF336/E; however, the statorless fan is a radial inflow fan while the fan was an axial inflow design.

SPL levels were calculated at several radial locations from hub to tip and integrated over the annulus area to obtain sound power level. A comparison of the measured and predicted inlet radiated sound power levels is shown in Figure 40. The measured inlet sound power levels were obtained by integrating the measured far field SPL's from 0 to 90 degrees. In Figure 40, the measured and predicted level of the 1/3 octave band which contains the blade passing frequency are in good agreement; but the location of the BPF is not consistently predicted by the theoretical analysis. In an attempt to better place the BPF in the 1/3 octave band, the eddy size was systematically varied at various radial locations. The initial scaled longitudinal eddy sizes were 2.0 inches (5.12 cm) in length. In Figure 41 the assumed eddy sizes were increased by a factor of ten at all radial locations, at the outer two radial locations, at the outer radial location. It appears that increasing the eddy size at the outer one or two radial locations causes the BPF to fall in the correct 1/3 octave band. The effect of increasing the eddy size by factors of 5, 10, and 15 at the two outer radial locations is shown in Figure 42. The best fit is provided with a factor of 15 increase; however, the signal to broadband ratio obviously does not match the measured levels. In Figure 43, the outer radial location eddy size was increased by a factor of 5, 10, 15. Again the best fit of the BPF occurs with the factor of 15 increase and the broadband levels do not agree.

The theoretical model used in these few comparisons gives encouraging results and the model does seem sensitive to inlet turbulence eddy sizes when placing the BPF in the correct 1/3 octave band.

F. Effects of Fan Tip Region Changes on Noise Levels

In the course of testing the statorless fan, several configurations were tested which indicated that the fan is sensitive to both mechanical and aerodynamic changes in the fan tip region.

Earlier LF336 tests with conventional rotor-stator life fans were conducted with tip tang cooling dams on the fan flowpath side of the carrier to alleviate a temperature problem associated with the titanium blades. When the statorless fan was assembled, the carriers from previous fans were used and the tip tang cooling dams were left in place even though the statorless fan blades were made of INCO 718 which would not experience the same temperature problems. Figure 44 shows the statorless fan and location of the tip tang cooling dams. During testing at NASA Ames Research Center these tip tang cooling dams were removed to investigate sensitivitiy of fan tip region changes on fan noise.

Removal of the tip tang cooling dams resulted in a 1 to 3 PNdB reduction from 80 degrees rearward as shown in Figure 45 at 6000, 5400, and 4800 rpm. No changes are evident at forward angles except that the 70 degree microphone PNL was up 3 PNdB at 6000 rpm when the dams were removed. At 6000 rpm, the 20 Hz narrowband directivity pattern of the BPF in Figure 46 shows a BPF increase at 70 degrees similar to the PNL directivity and a slight decrease at the aft angles.

A comparison of 1/3 octave band spectra with and without tip tang cooling dams in Figure 47 shows that fan broadband levels have been reduced. 20 Hz narrowband spectra are shown in Figure 48 at 6000 and 5400 rpm. The observed reduction is primarily a fan broadband noise reduction, not a BPF reduction.

Another indication of the sensitivity of the statorless fan to changes in the tip region occurred during mechanical checkout testing of the fan while at EFTC. The large bellmouth and inlet duct which connected the massive fan inlet suppressor to the fan was installed as sketched in Figure 49 to permit measurement of fan airflow. The SPL's showed a sharp increase in the forward radiated SPL of the 1/3 octave band which contained the BPF as shown in Figure 50. A 20 Hz narrowband spectral comparison at 40 and 60 degree microphones with and without the bellmouth installed indicates that the change is primarily in the BPF. Figure 51 makes the comparison at 40 degrees while Figure 52 is at the 60 degree microphone location. The narrowband BPF directivity pattern is shown in Figure 53.

Aerodynamically, stator pressure taps on the fan bellmouth surface indicate a 6 to 10 percent decrease in the velocity in the fan tip region. This would increase the incidence angle slightly and tend to load the blade more which may account for the observed BPF increase.

The final configuration tested at NASA Ames had the large bellmouth and inlet duct installed, tip tang cooling dams removed, and treated exit louvers installed. As at EFTC, the large bellmouth permitted measurement of fan airflow. Tip tang coooling dams and treated exit louvers were discussed earlier; however, some results are applicable to the discussion at hand. As at EFTC, the forward angles of the BPF directivity pattern show a sharp increase in level as indicated by Figure 54. There also appears to be some shielding taking place at 70-90 degrees which was also indicated in the EFTC directivity pattern in Figure 53. As Figure 55 shows, the BPF was increased at 40 degrees when the large bellmouth was installed, but fan broadband levels were essentially unchanged.

These results emphasize that mechanical and aerodynamic changes in the tip region of the radial statorless fan can cause marked increases in the forward radiated BPF levels.

SECTION VII

SITE COMPARISONS

A. Near Field Comparisons

The near field microphone sound fields as described in a previous section were utilized for two reasons. First, they provided a means of comparing fan source noise at two different test sites without having to account for possible differences in site reflectivity characteristics. Secondly, the sites duplicated the sound field used to record noise levels when the fan was tested in the NASA Ames Research Center 40' by 80' (12.2 m by 24.4 m) wind tunnel.

In Figure 56, PNL's measured by the 20 foot (6.1 m) near field microphones at Edwards Flight Test Center and NASA Ames are compared at 90, 110, 130, and 150 degrees as a function of fan speed. The PNL's from the two sites are in excellent agreement. 1/3 octave band spectral comparisons are shown at five fan speeds in Figures 57 and 58. On a spectral basis, source noise agreement between the two sites is very good.

Looking more closely at the spectral comparisons in Figure 57 the fan BPF is clearly visible. At 3400 rpm, the 10K band is influenced by a tip turbine tone at 10600 Hz (3400 rpm x 180 blades/60 = 10600). All three speeds show a J85 one-per-rev signal in the 250 Hz band. This one-per-rev signal is also visible in the EFTC data at 5400 rpm in Figure 58. Similar good agreement is shown in Figures 59 and 60 at 130 degrees and 150 degrees respectively at the top three speeds.

In the near field microphone arrangement, there were microphones located at 210, 230, and 250 degrees or on the J85 side of the near field microphone arc as shown in Figures 5 and 7. Although the J85 was fitted with an inlet suppressor, it should be determined if any J85 inlet radiated noise was influencing the near field levels. Accordingly, in Figure 61, PNL's at the microphones which are symmetrical about the fan exhaust are compared as a function of fan speed. It appears that at 3400 rpm, J85 inlet radiated noise is raising the noise levels of the 250 and 230 degree microphones by 2 PNdB. At the 250 degree microphone, which is nearest to the J85 inlet, one can see the J85 influence up to 4800 rpm. Comparisons of the 110 and 250 degree 1/3 octave band spectra are made for 3400, 4100, and 4800 rpm in Figure 62. 20 Hz narrowbands for the same spectra are compared in Figure 63. At all speeds the broadband levels of the 250 degree microphone are higher than the 110 degree levels.

The point here is that at low fan speeds, microphones in the near field on the J85 side may be influenced by J85 inlet radiated noise. At higher speeds, there is good agreement between microphones located symmetrically about the fan exhaust, and no indication of J85 inlet noise.

B. Far Field Comparisons

From Figure 7, the acoustic path to the thirty degree microphone at the NASA Ames test site is mostly over asphalt; however, at EFTC the path was over desert sand. Figure 64 compares 1/3 octave band far field spectra at the thirty degree microphone from both test sites at 6000, 5400, and 4800 rpm. The ground reflection null for EFTC is in the 315 Hz band and appears to be near the 400 to 500 Hz band at NASA Ames. Calculating the ground null based upon the source and receiver geometries and assuming a phase factor of 1, one would predict the ground null to occur at 350 Hz and 450 Hz respectively at EFTC and NASA Ames. On a 1/3 octave band basis 350 Hz falls in the 315 Hz band and 450 Hz falls in the 500 Hz band but close to the lower limit. Figure 64 confirms these results. The magnitude of the null relative to the jet noise peak at 160 Hz is about the same at both sites at each speed. Similar results are observed at lower speeds at the thirty degree microphone and at the other microphones which are located on the asphalt. This implies that there is very little difference in reflection characteristics between the desert sand of Edwards Flight Test Center and the asphalt of NASA Ames.

The acoustic path to the 110 degree mike is mostly short grass at NASA Ames in contrast to the desert sand at EFTC. In Figure 65 EFTC and NASA Ames 1/3 octave band spectra are compared at the 110 degree microphone location at three speeds - 6000, 5400, and 4800 rpm. There is good agreement between SPL's from the two test sites at this microphone location. The predicted ground null at NASA Ames would occur at 450 Hz and at 315 Hz at EFTC. Figure 65 shows that the NASA Ames 110 degree ground null falls in the 315 Hz 1/3 octave band. This means that the short grass of NASA Ames has a phase factor of 0.8 or less - 0.8 being the phase factor necessary to shift the ground null from 450 Hz to the 315 Hz 1/3 octave band.

Perceived noise level directivity patterns from EFTC and NASA Ames testing of the unsuppressed fan are compared in Figure 66 at 6000 and 5400 rpm. There is excellent agreement at all angles except at 80 and 100 degrees. 1/3 octave band spectra from these two angles are shown in Figures 67 and 68 At both angles and both speeds the fan broadband SPL's from NASA Ames testing are 2 to 4 dB higher than the EFTC SPL's. The reason for this is not known at this time. 20 Hz narrowband BPF directivity patterns in Figure 69 also shows good agreement between the two test sites except at 80 degrees and 100 degrees.

C. Near to Far Field Comparisons

Noise levels from both the near and the far field microphones were extrapolated to a 200 foot (61 m) sideline to have a common basis for comparison. NASA Ames data will be used in these comparisons.

On a PNL directivity basis, Figure 70 indicates that PNL's from the near and far field microphones are in good agreement at 4800, 5400, and 6000 rpm in both the front and the rear quadrants. Next 1/3 octave band spectral comparisons are made for the forward and rear quadrant angles of 50 and 110

degrees, respectively. Figure 71, at 50 degrees shows good agreement between the far and near field extraploated SPL's at frequencies above 315 Hz for the three speeds considered. Similar results are evident at the 110 degree microphone in Figure 72. Here there is also good agreement above 315 Hz.

In the above spectral comparisons, the good agreement occurs above 315 Hz or at frequencies where the number of wavelengths between the source and receiver is five or greater. At lower frequencies the extrapolated near field levels fair through the ground null and reflection SPL's. Generally, distances greater than five wavelengths are considered to be far field and may be extrapolated according to usual and accepted extrapolation procedures.

SECTION VIII

CONCLUSIONS

1. When compared on an equal tip speed (or equal size) basis the LF336/E statorless lift fan is 1 to 3 PNdB lower than the LF336/B lift fan in the forward quadrant and the same to 2 PNdB quieter in the aft quadrant. The lack of substantial reduction when comparing the statorless fan to the two chord LF336 conventional rotor-OGV lift fan indicates that at two chord spacing the noise is primarily rotor alone noise and not interaction noise.

2. On an equal absolute pressure ratio basis, the statorless lift fan is 1 to 2 PNdB lower than the LF336/B at forward angle and the same or slightly higher in the aft quadrant.

3. Statorless fan exhaust radiated noise levels are 5-8 PNdB below the inlet radiated levels in the forward quadrant.

4. Installation of a circular IGV on the LF336/E caused an increase of 3 to 5 PNdB at forward angles and 1 to 2 PNdB increase at aft angles. The change is primarily in the SPL at the fan BPF.

5. Treated exit louvers achieved 2 to 4 PNdB suppression from 80 to 110 degrees. At 6000 rpm, an increase in SPL was observed at mid frequencies which appears to be due to wake scrubbing noise over the louvers.

6. Fan baseline near field levels measured at EFTC are the same as those measured at NASA Ames.

7. Reflection characteristics between EFTC desert sand and NASA Ames asphalt are similar.

8. Extrapolation of near field levels to far field levels gives good agreement at or above 315 Hz where the number of wavelengths between the source and near field receiver is 5 or greater.

9. Predicted inlet levels based on a theoretical rotor-turbulence interaction theory give encouraging results.

10. Sensitivity of the fan to changes in the tip region is indicated by the increase in level observed when the large bellmouth was installed and the decrease when the tip tang cooling dams were removed.

SECTION IX

NOMENCLATURE

Symbol or Abbreviation	Definition	Units
BPF	Blade Passing Frequency	Hz
d	Characteristic dimension	inches (cm)
EFTC	Edwards Flight Test Center	---
f	Frequency	Hz
H	Duct height	feet (m)
IGV	Inlet guide vane	---
L	Treatment Length	feet (m)
OGV	Outlet guide vane	---
PNL	Perceived Noise Level	PNdB
S_N	Strouhal number	---
SPL	Sound pressure level re: 0.0002 dynes/cm^2	dB
V	Velocity	feet per second (meters per second)
λ	Wavelength	feet (m)

SECTION X

REFERENCES

1. Kazin, S.B.; Volk, L.J.; "LF336 Lift Fan Modification and Acoustic Test Program," General Electric Company, NASA CR-1934, December, 1971.

2. Przedpelski, Z.J.; "Lift Fan Technology Studies," General Electric Company, NASA CR-761, April, 1967.

3. Stimpert, D.L., and Uhl, W.R., "Aero-Acoustic Design and Test of a Multiple Splitter Exhaust Noise Suppressor for a 0.914 m Diameter Lift Fan," NASA CR 121108, January, 1973.

4. Standard Values of Atmospheric Absorption as a Function of Temperature and Humidity for Use in Evaluating Aircraft Flyover Noise. S.A.E. ARP 866, August 31, 1964.

5. Method of Calculating the Attenuation of Aircraft Ground to Ground Noise Propagation during Takeoff and Landing. Aerospace Information Report 923, Society of Automative Engineers, Inc., August 15, 1966.

Table I. LF336/E Acoustic Test Summary.

Location	Run	Configuration	Nominal Fan Speed (RPM) 3000	3375	4050	4200	4800	5400	6000
EFTC	15	GE4 Bellmouth						1	1
	16,17	Unsuppressed Fan		2*	2		2	2	2
	18	Massive Fan Inlet Suppression		2	2		2	3	3
NASA Ames	1	Unsuppressed	1	1	1	1	1	1	1
Research Center	2	Circular IGV	1			1	1	2	2
	3	Unsuppressed	1	1	1	1			
	4	Exhaust Louvers	2	1	2	1	2	2	2
	7	Unsuppressed Without Tip Tang Cooling Dams	2			2	2	2	2
	8	Exhaust Louvers Without Tip Cooling Dams With GE4 Bellmouth	2			2	2	2	2

* denotes number of data points at each speed

Table II. LF336/E Lift Fan Design Parameters.

	Design Point	Mechanical Limit Speed
Fan pressure ratio	1.25	1.196
Fan flow, lbm/sec (kg/sec)	172 (78)	152 (69.4)
Fan tip speed, ft/sec (m/sec)	1060 (323)	950 (290)
Fan speed, rpm	6748	6048
Blade number	42	
Fan tip diameter, inches (cm)	36 (91.44)	
Radius ratio (rotor inlet)	0.554	

Table III. LF336 Lift Fan Configurations.

Fan	Test Number	Date	Vanes	Spacing Chords	Acoustic Splitter	Acoustic Treatment	Test Location
LF336/A	1	1-69	45	.15	No	No	EFTC
LF336/B	1	2-69	45	2	No	No	EFTC
LF336/C	1	12-69	45	1	No	No	EFTC
LF336/C	11	6-70	90/Leaned	2	Yes	Yes	EFTC
LF336/E	16,17	1-73	0	∞	No	No	EFTC
LF336/E	1	3-73	0	∞	No	No	NASA Ames

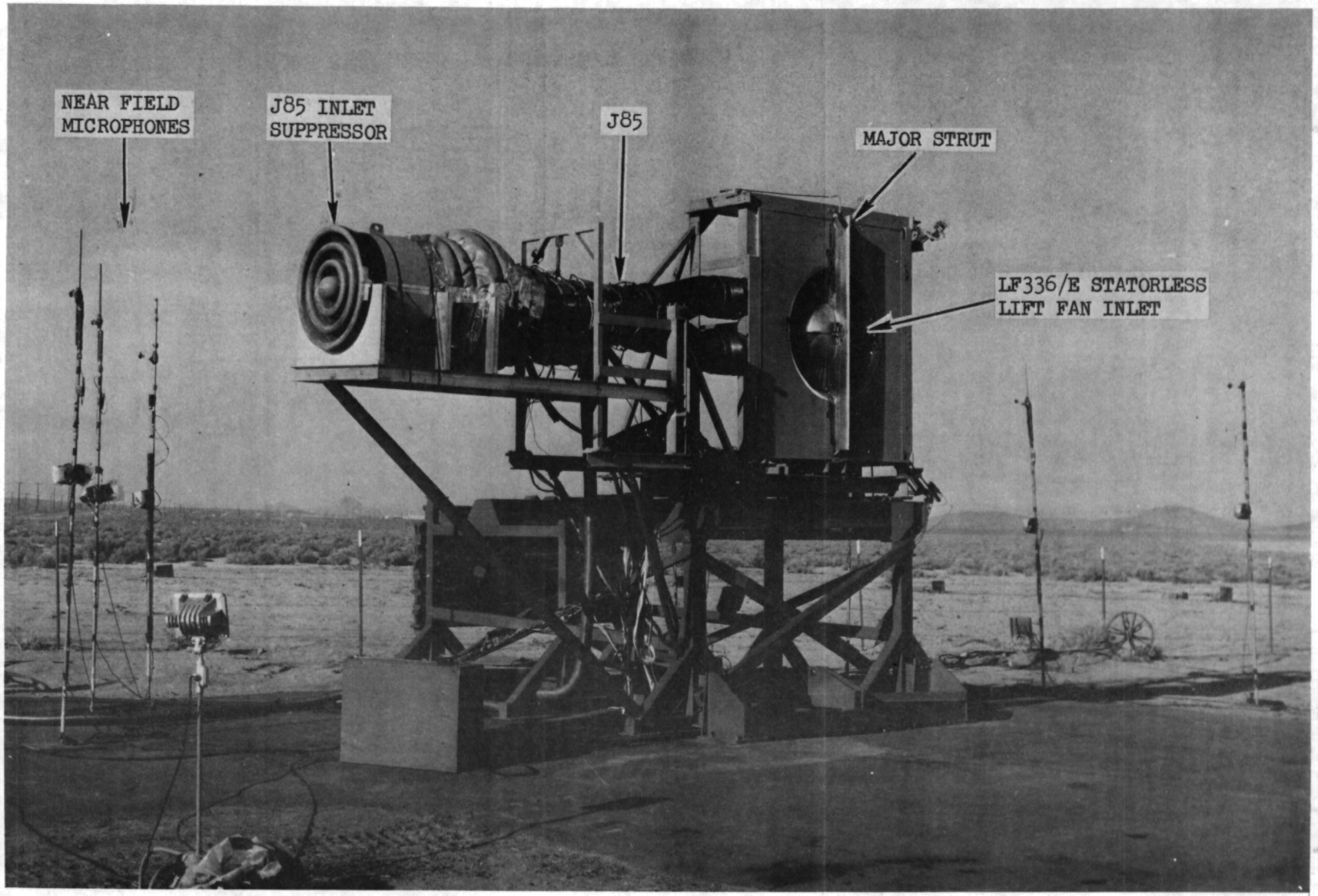

FIGURE 1 PHOTOGRAPH OF THE LF336/E STATORLESS FAN AT EDWARDS FLIGHT TEST CENTER

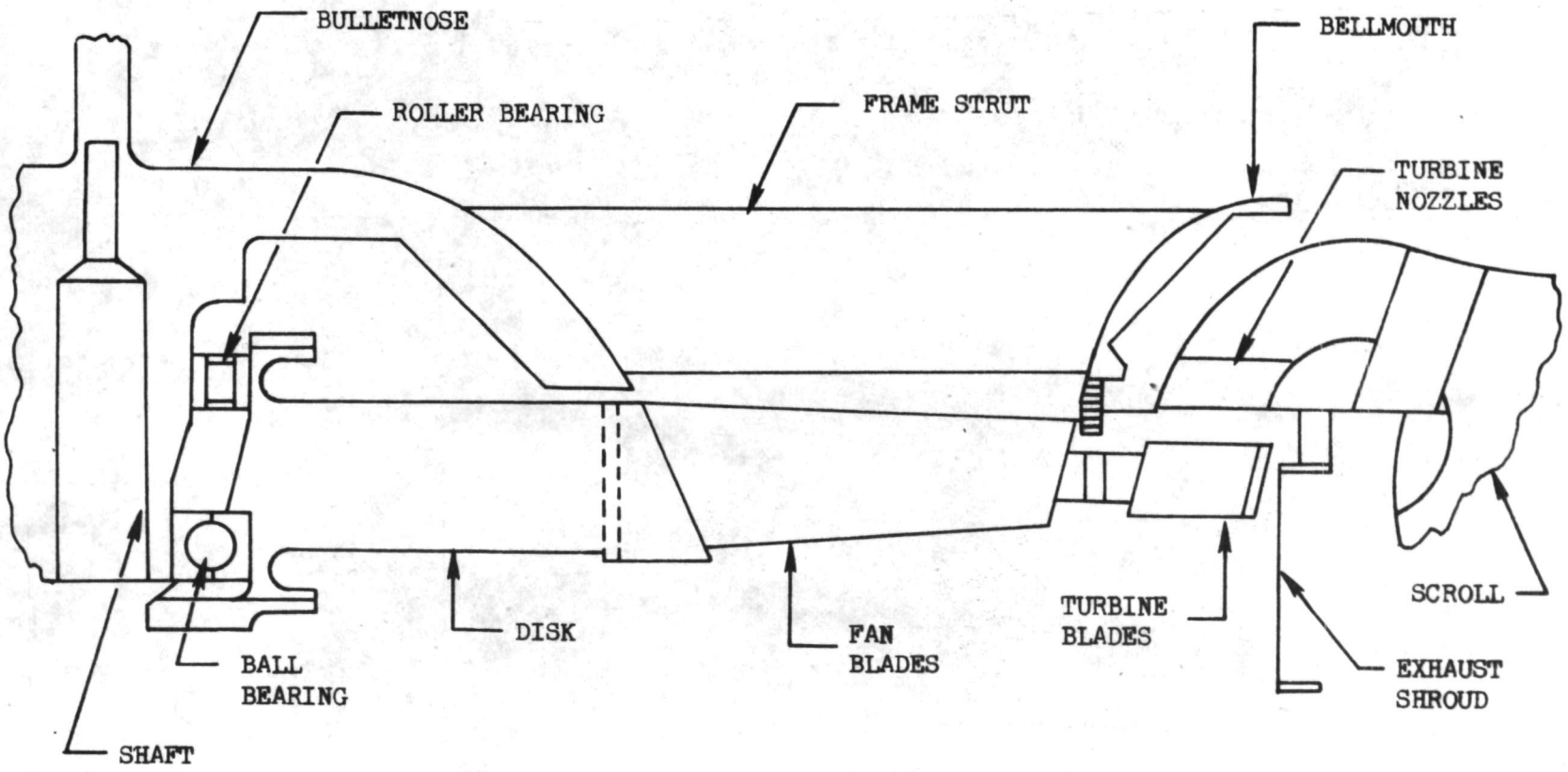

FIGURE 2 CROSS SECTION OF THE LF336/E STATORLESS FAN

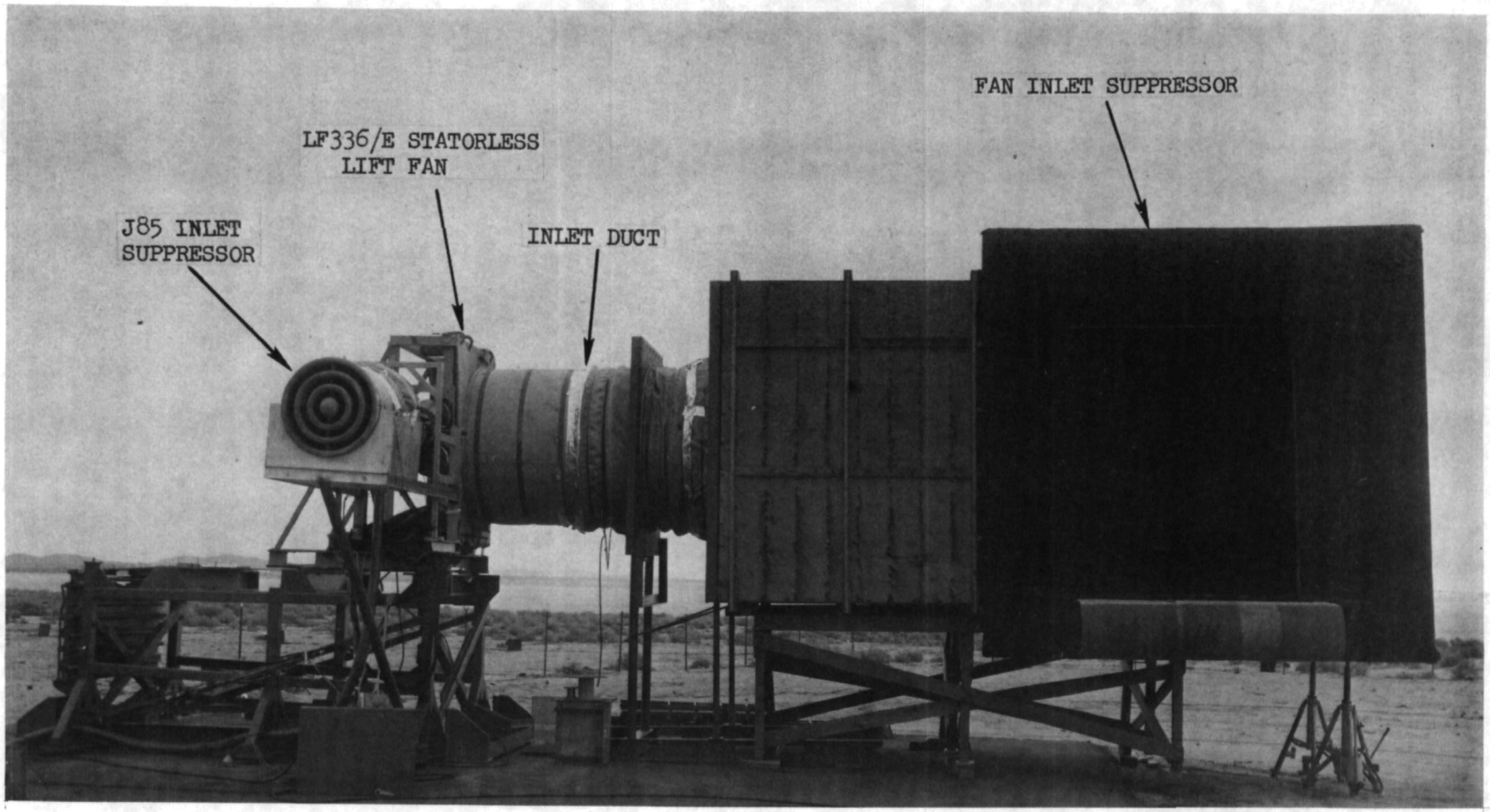

FIGURE 3 PHOTOGRAPH OF THE LF336/E STATORLESS FAN WITH MASSIVE INLET SUPPRESSION

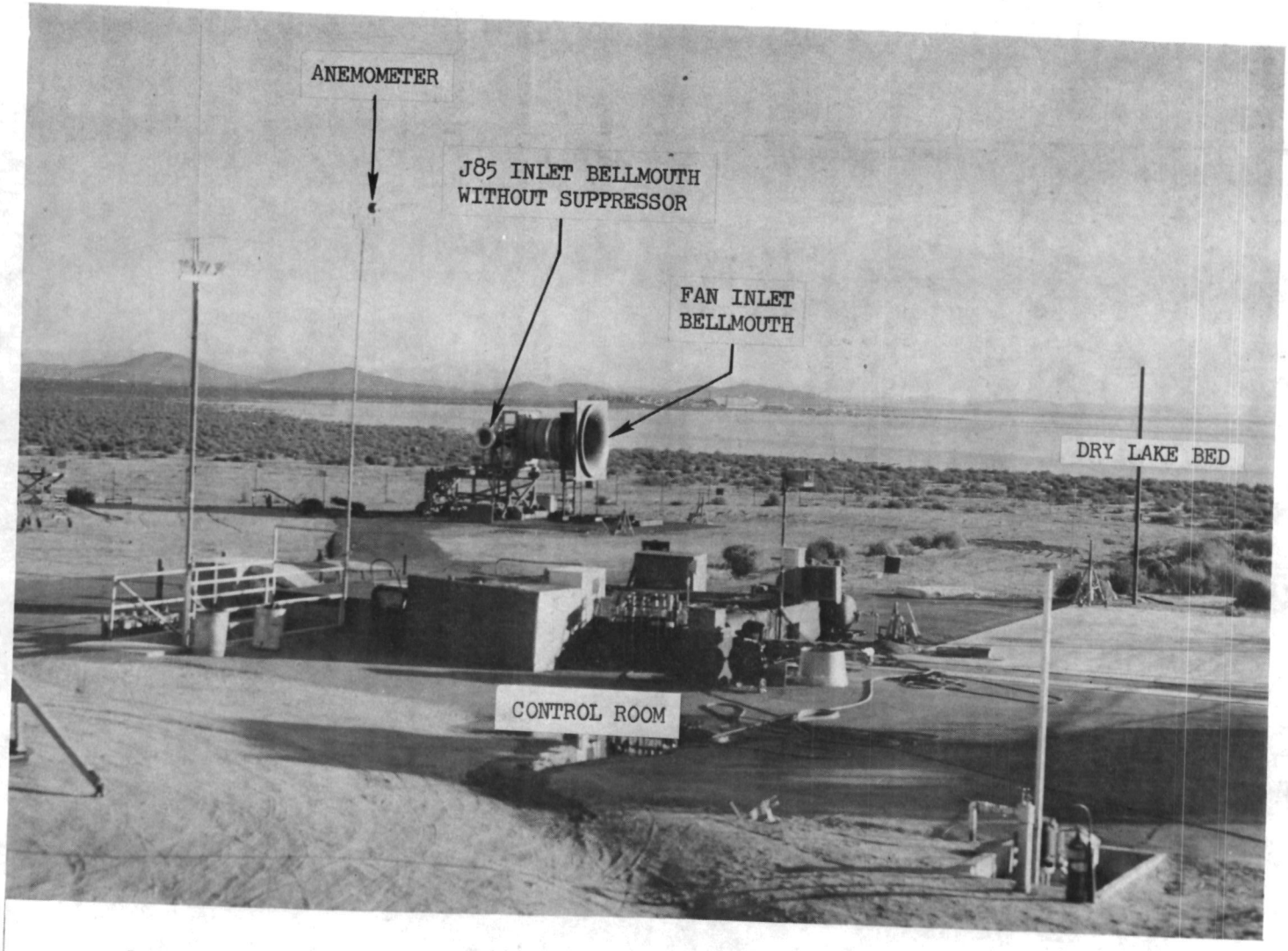

FIGURE 4 PHOTOGRAPH OF ACOUSTIC TEST SITE AT EDWARDS FLIGHT TEST CENTER

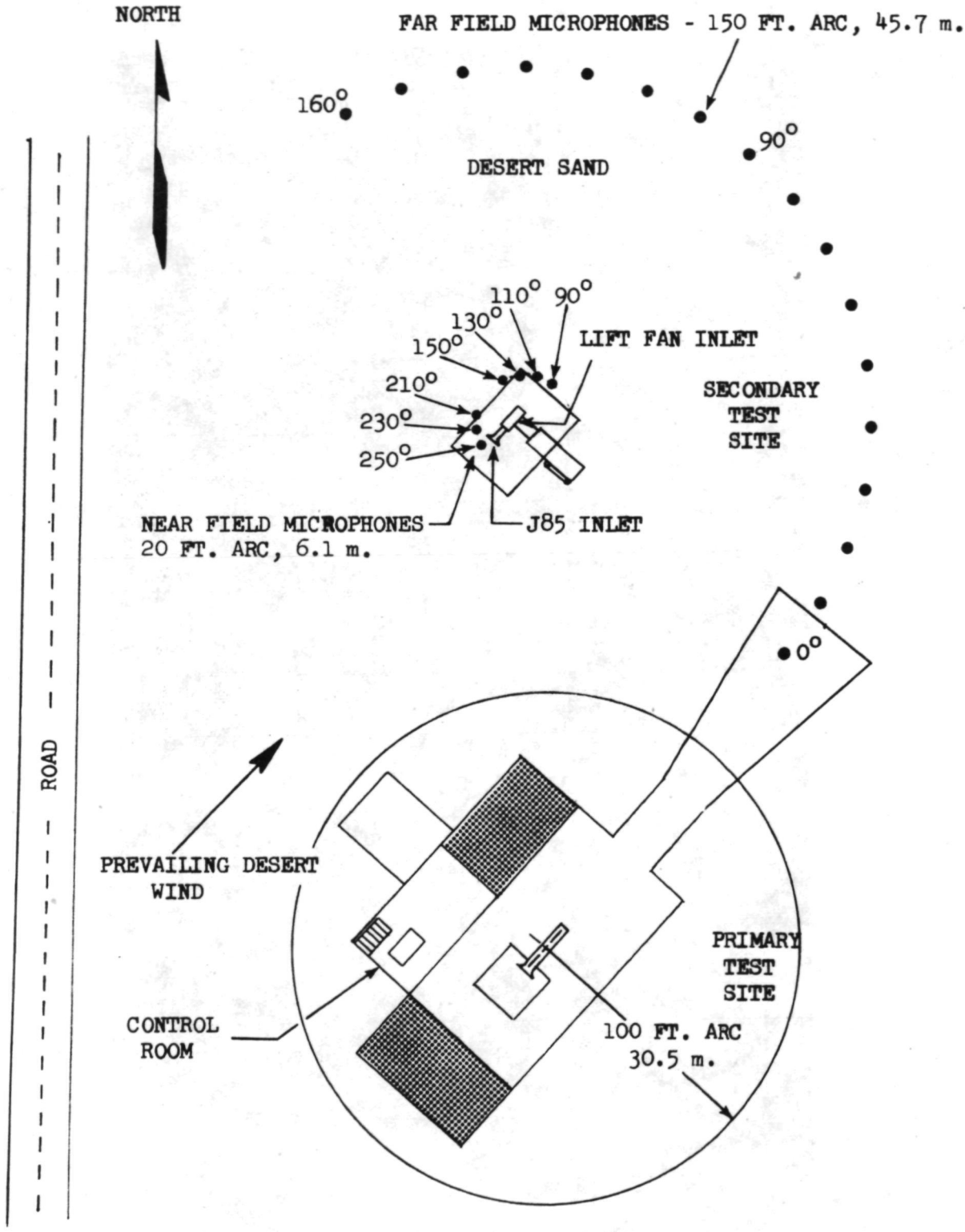

FIGURE 5 SKETCH OF MICROPHONE ORIENTATION AT EDWARDS FLIGHT TEST CENTER

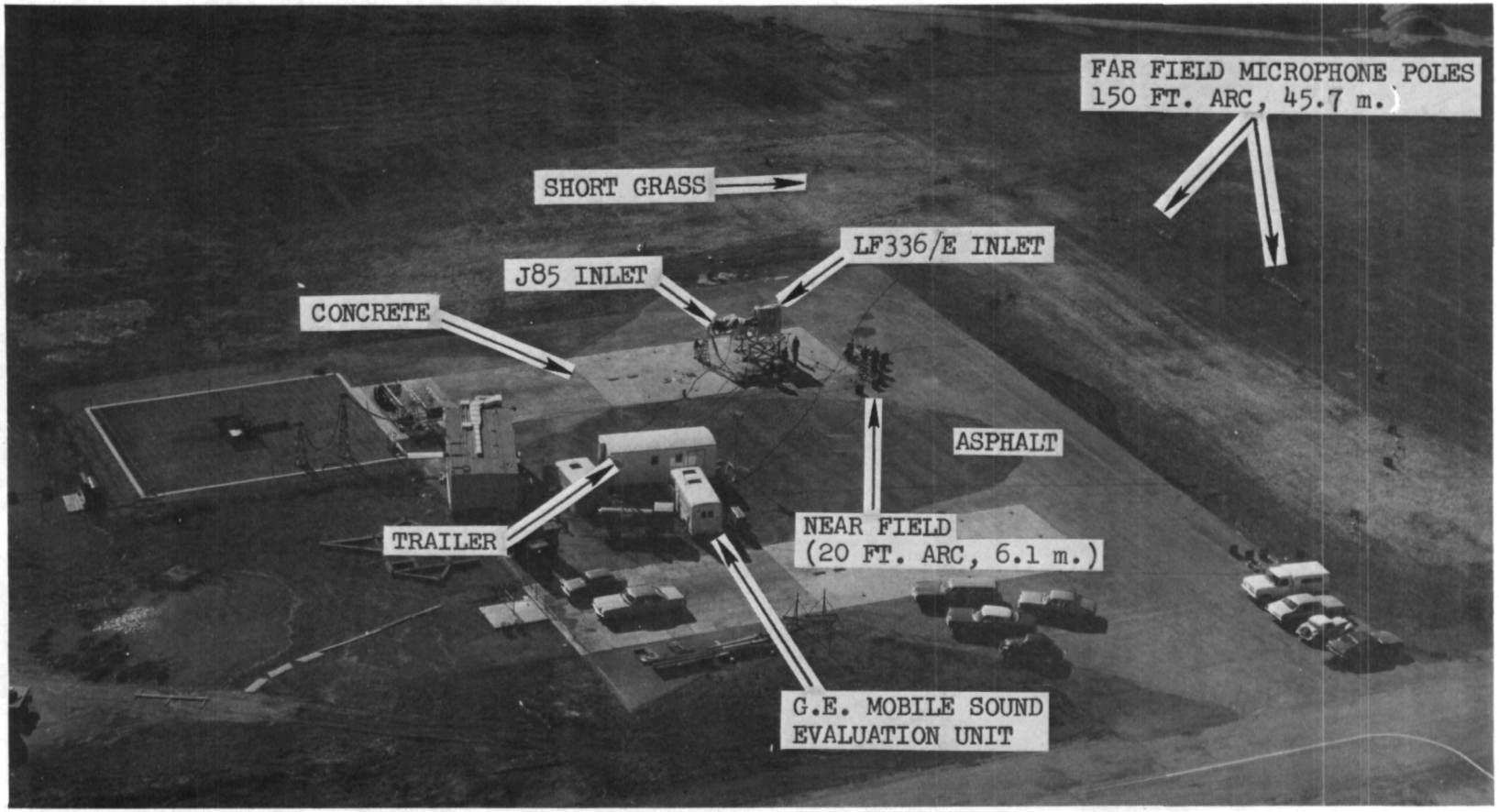

FIGURE 6 AERIAL PHOTOGRAPH OF NASA AMES OUTDOOR TEST SITE

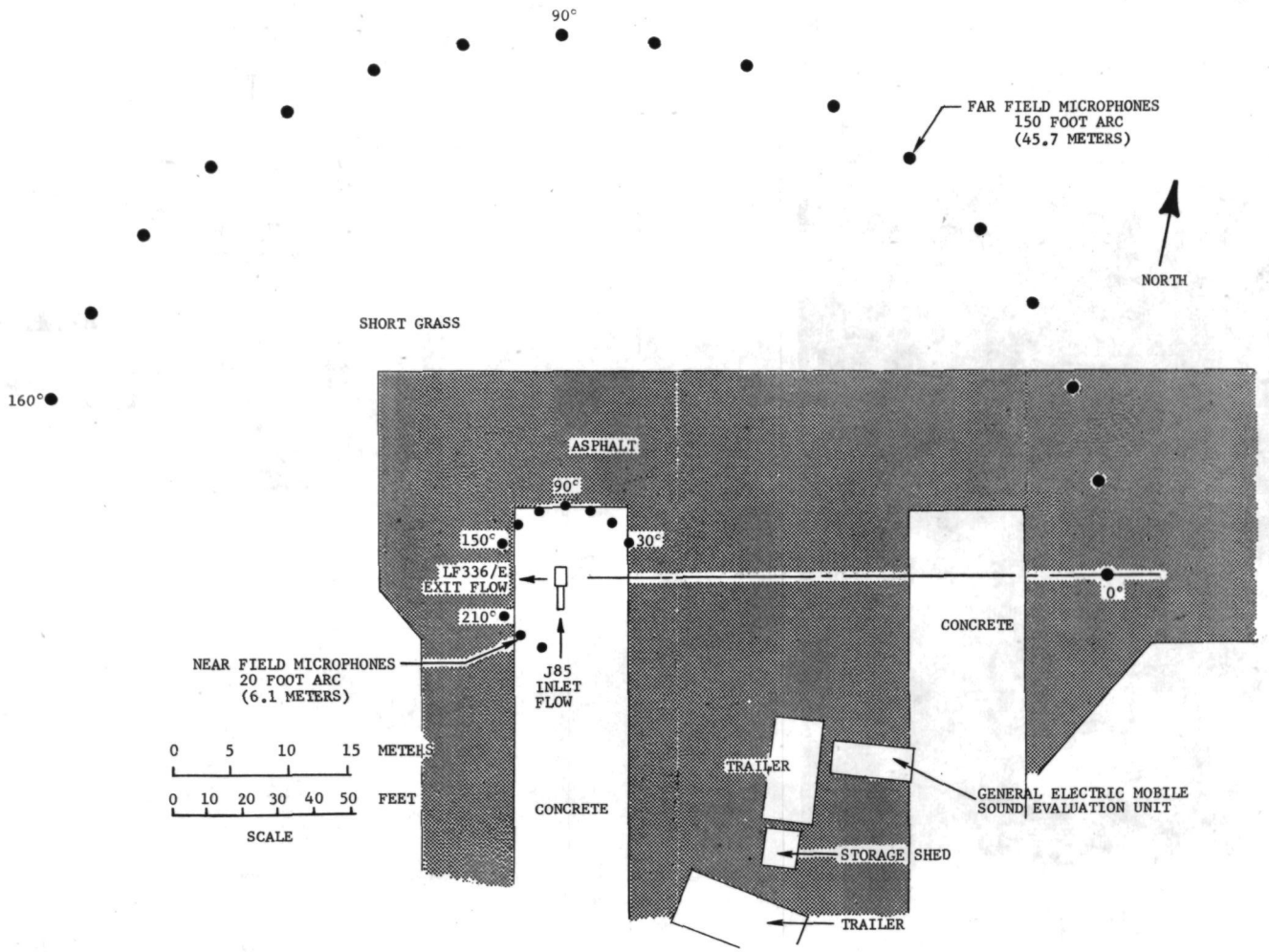

FIGURE 7 SKETCH OF MICROPHONE ORIENTATION AT NASA AMES OUTDOOR TEST SITE

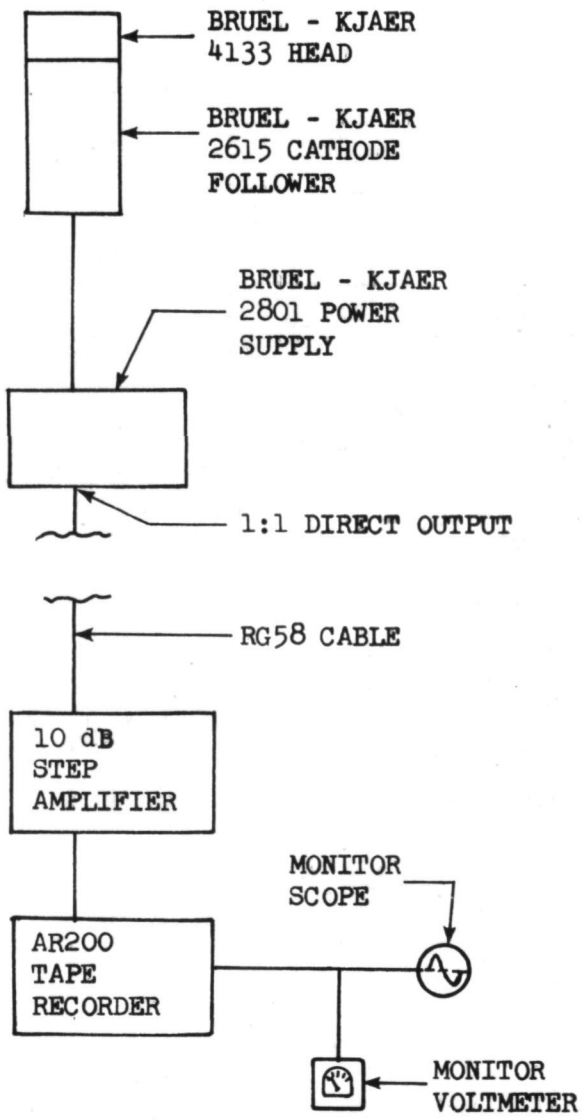

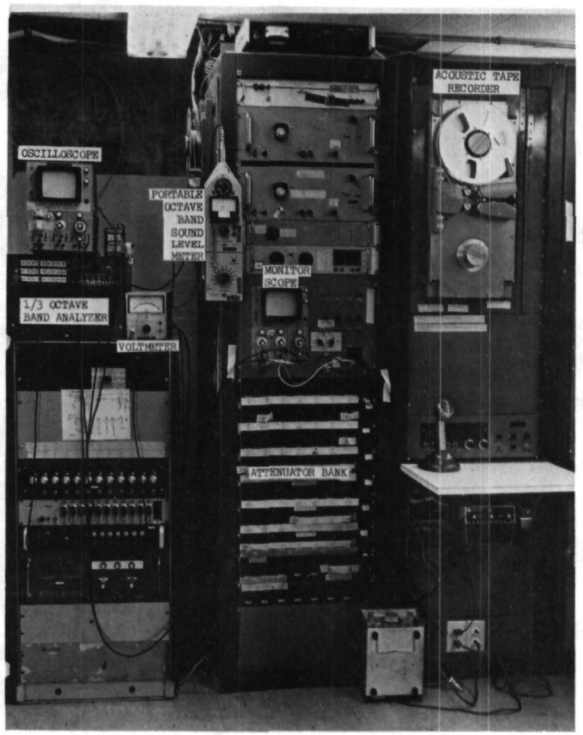

FIGURE 8 ACOUSTIC DATA ACQUISITION AT EDWARDS FLIGHT TEST CENTER

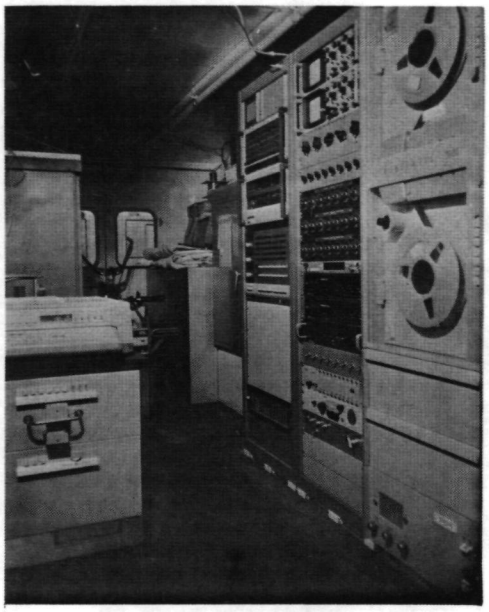

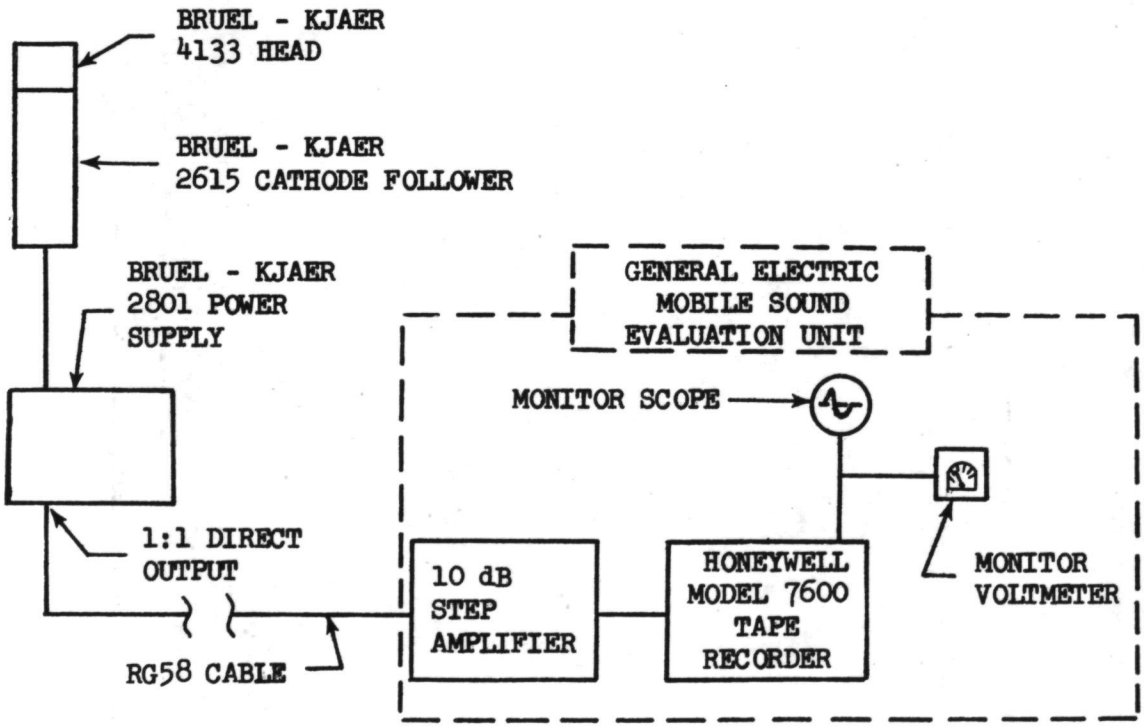

FIGURE 9 ACOUSTIC DATA ACQUISITION AT NASA AMES OUTDOOR SITE

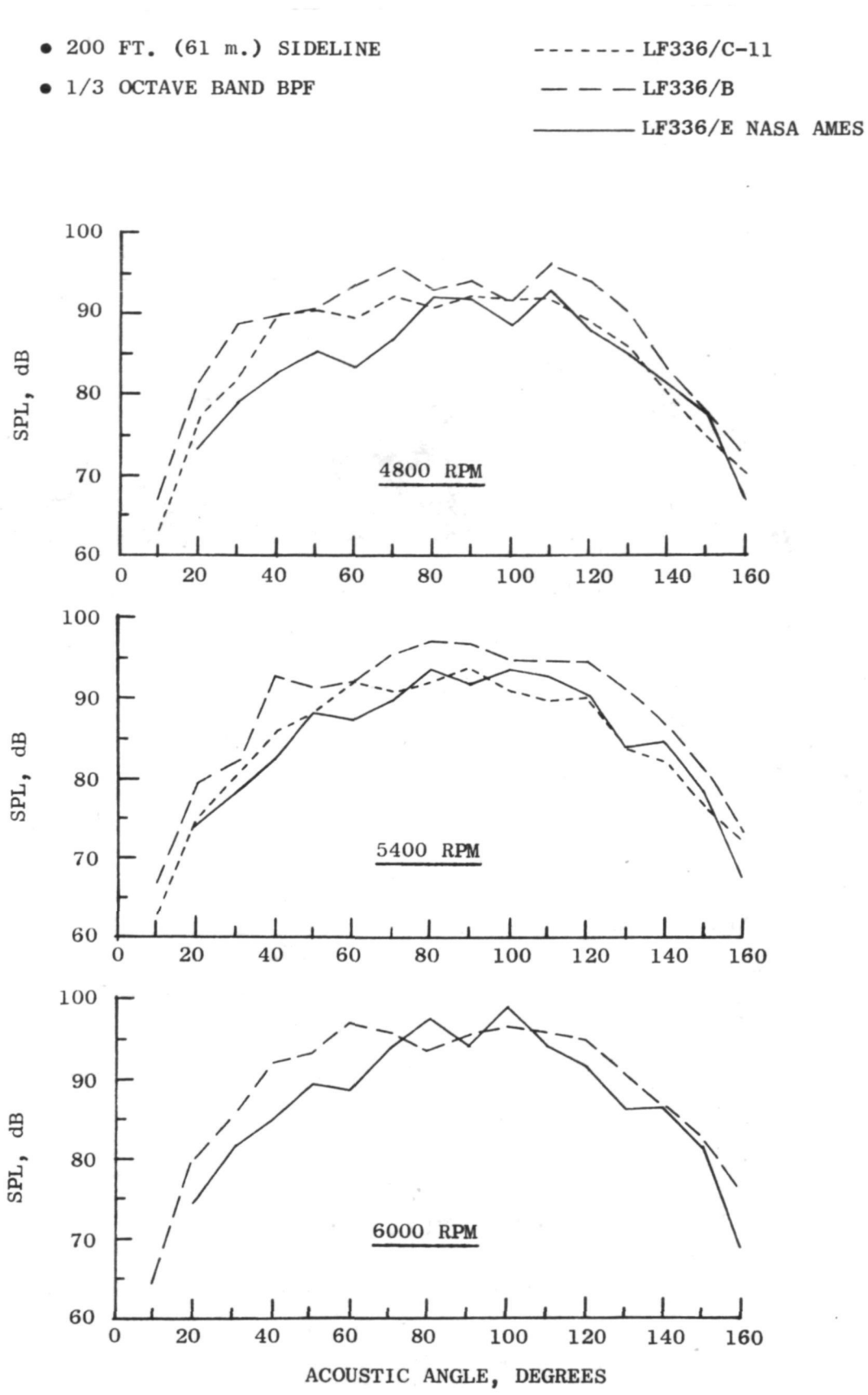

FIGURE 10 LF336/C-11, LF336/B, AND LF336/E 1/3 OCTAVE BAND BPF DIRECTIVITY PATTERNS AT CONSTANT TIP SPEED

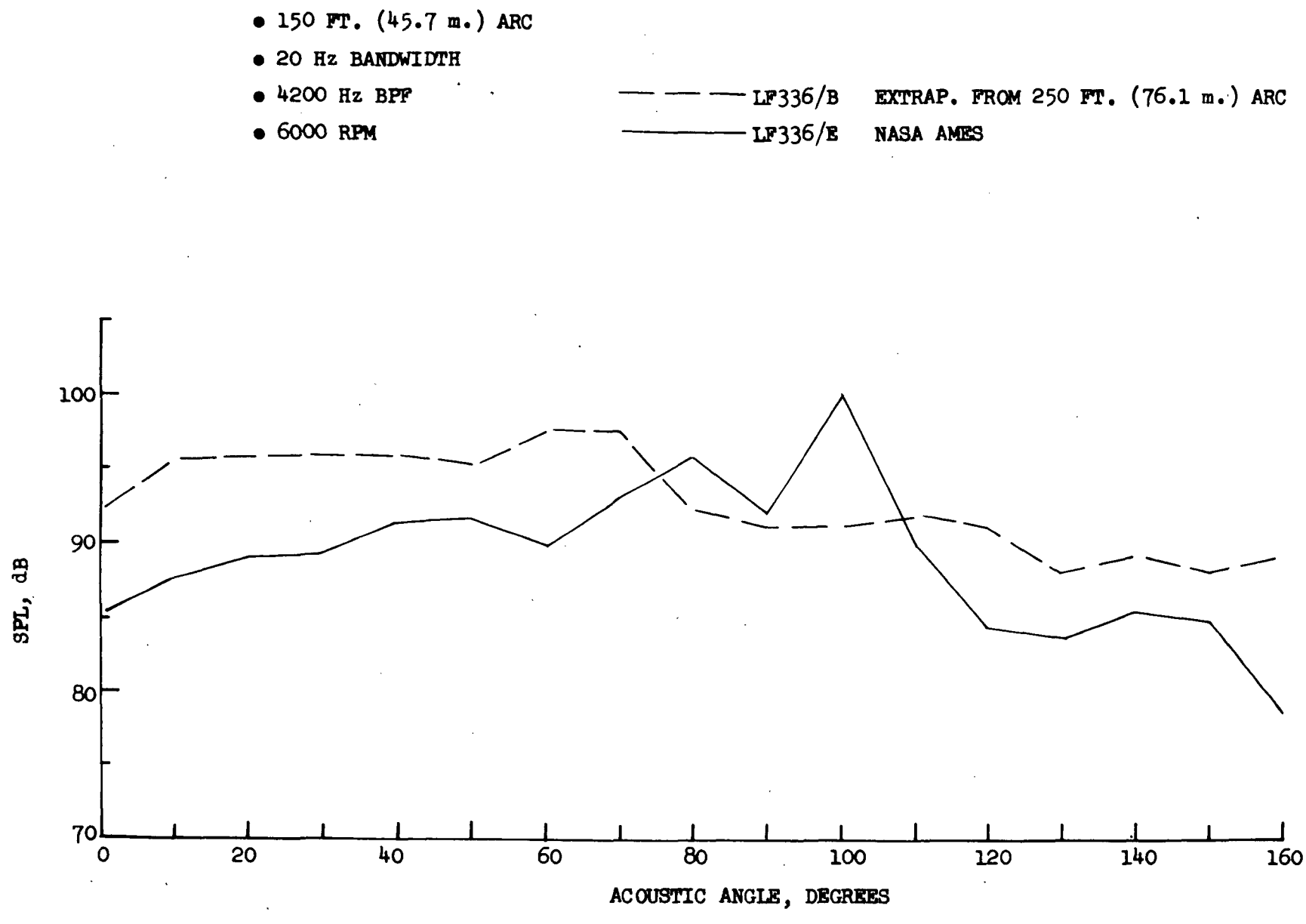

FIGURE 11 LF336/B AND LF336/E NARROWBAND BPF DIRECTIVITY PATTERNS AT CONSTANT TIP SPEED

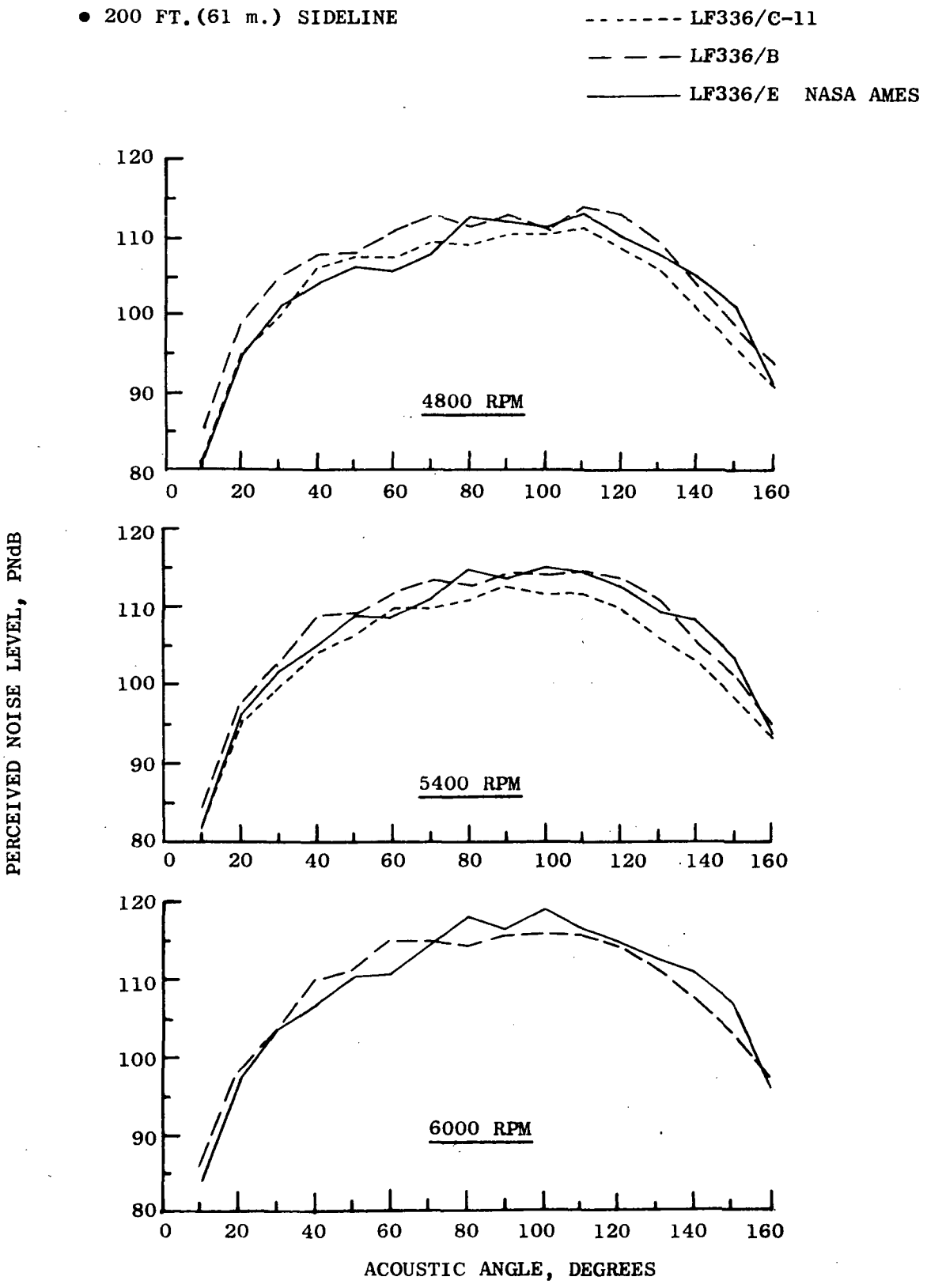

FIGURE 12 LF336/C-11, LF336/B, AND LF336/E PNL DIRECTIVITY PATTERNS AT CONSTANT TIP SPEED

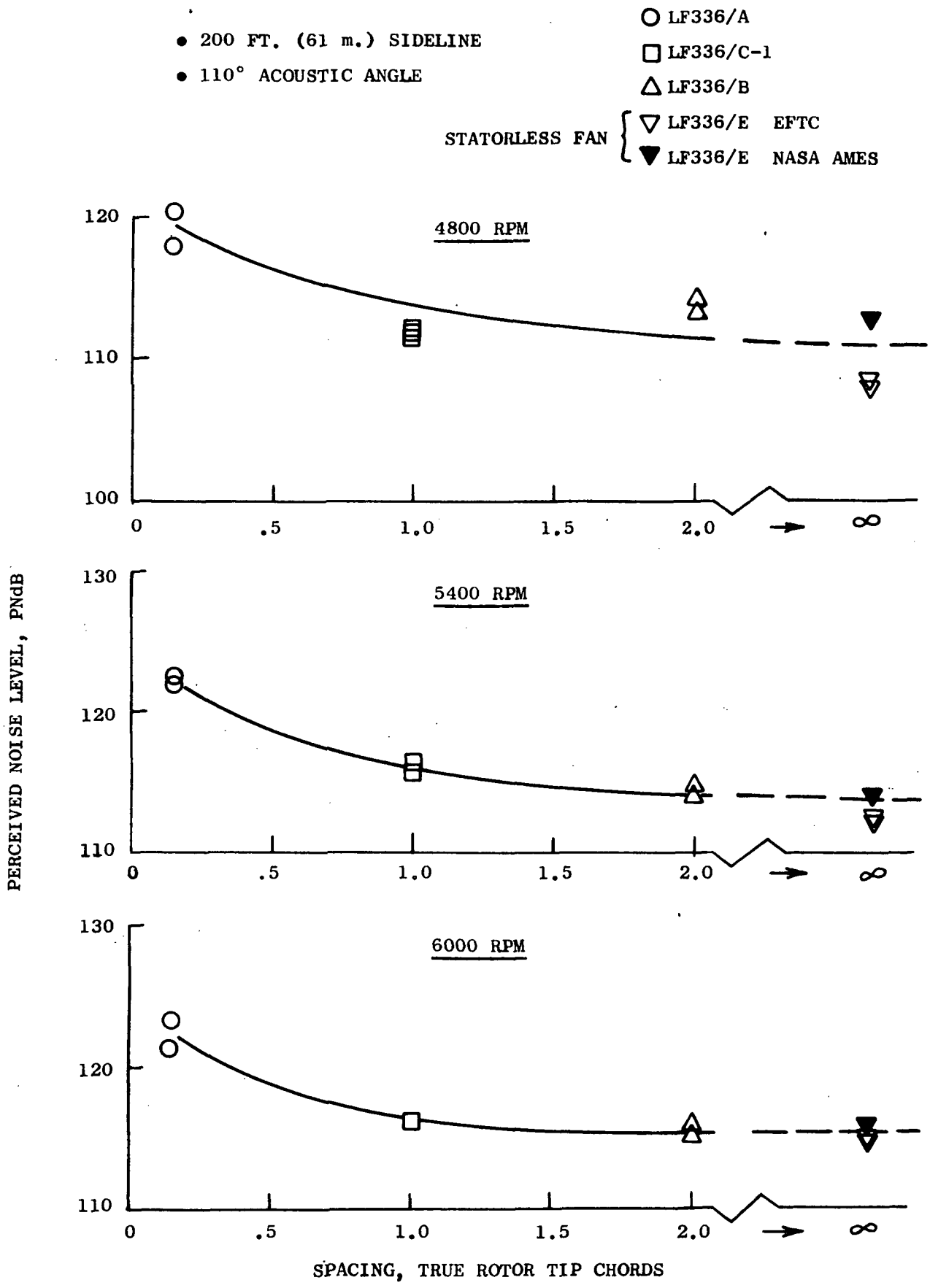

FIGURE 13 EFFECT OF ROTOR - STATOR SPACING ON PNL

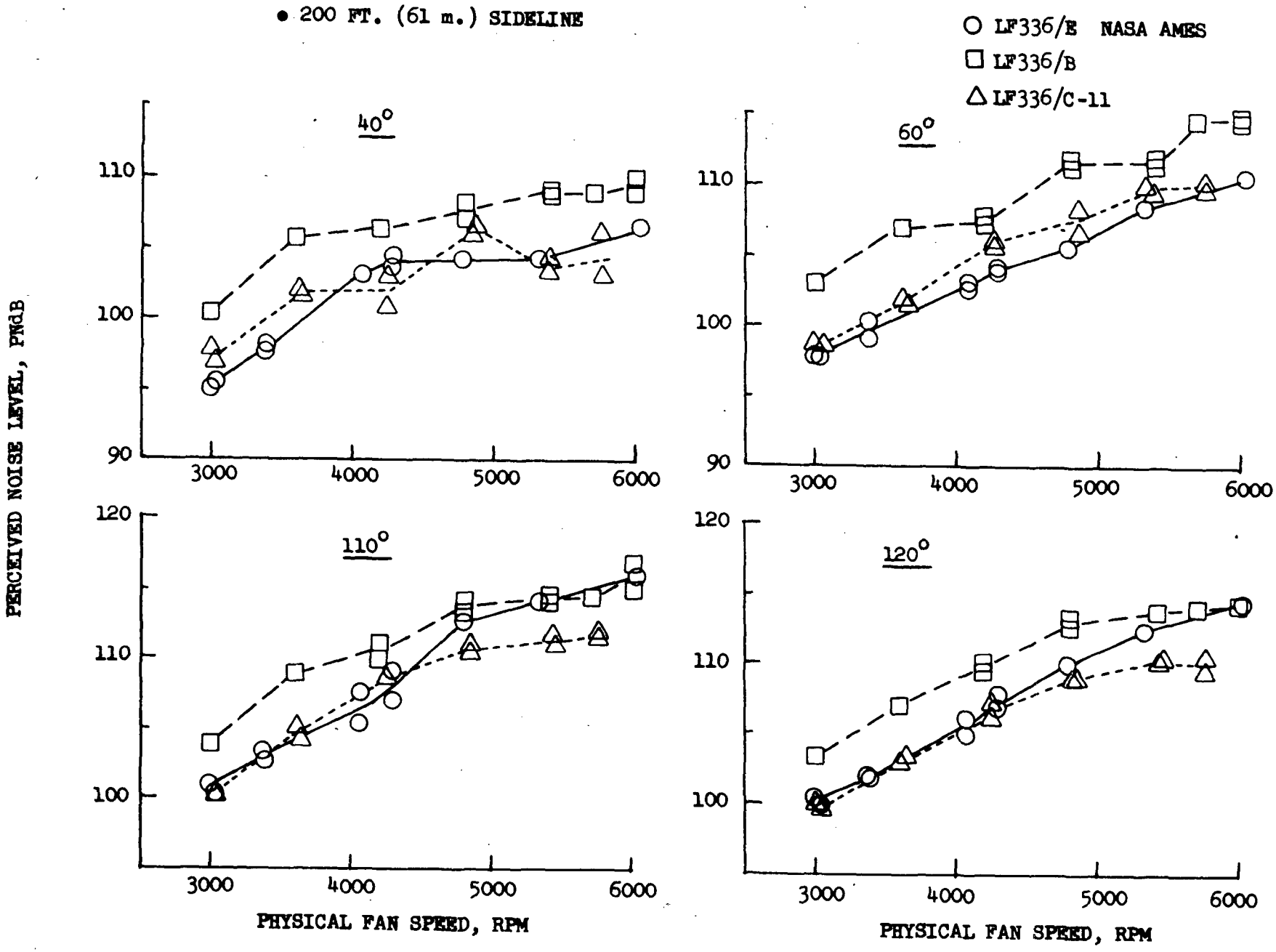

FIGURE 14 LF336/C-11, LF336/B, AND LF336/E PNL'S AS A FUNCTION OF FAN SPEED AT 40°, 60°, 110°, AND 120°

● EFTC TEST SITE

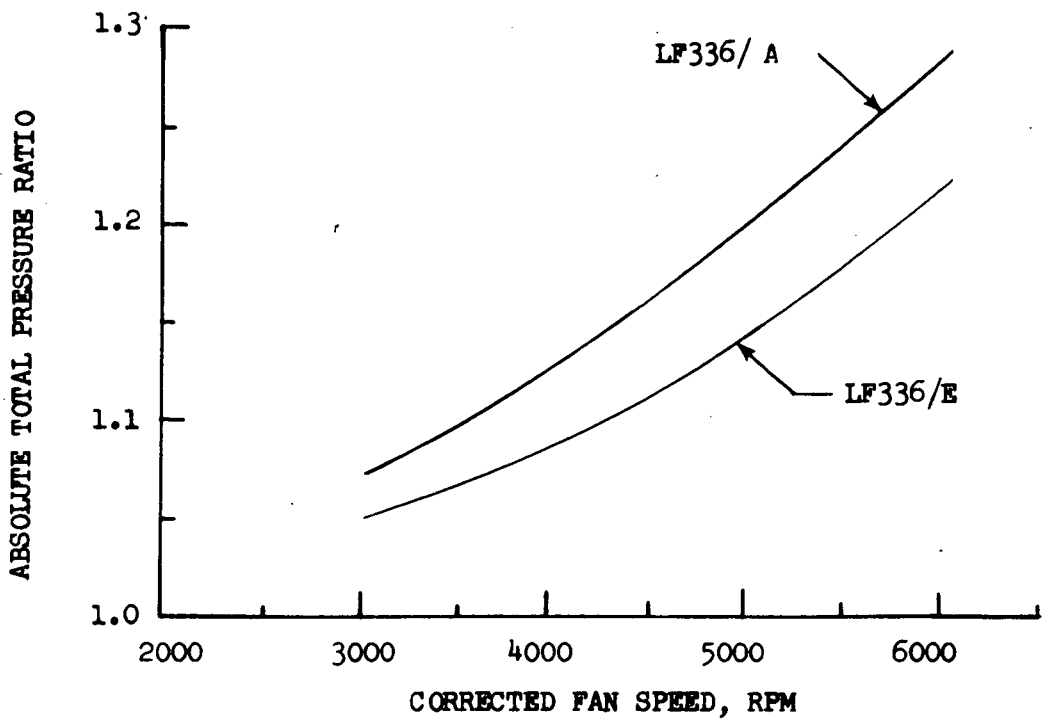

FIGURE 15 LF336/A AND LF336/E ABSOLUTE TOTAL PRESSURE RATIOS AS A FUNCTION OF FAN SPEED

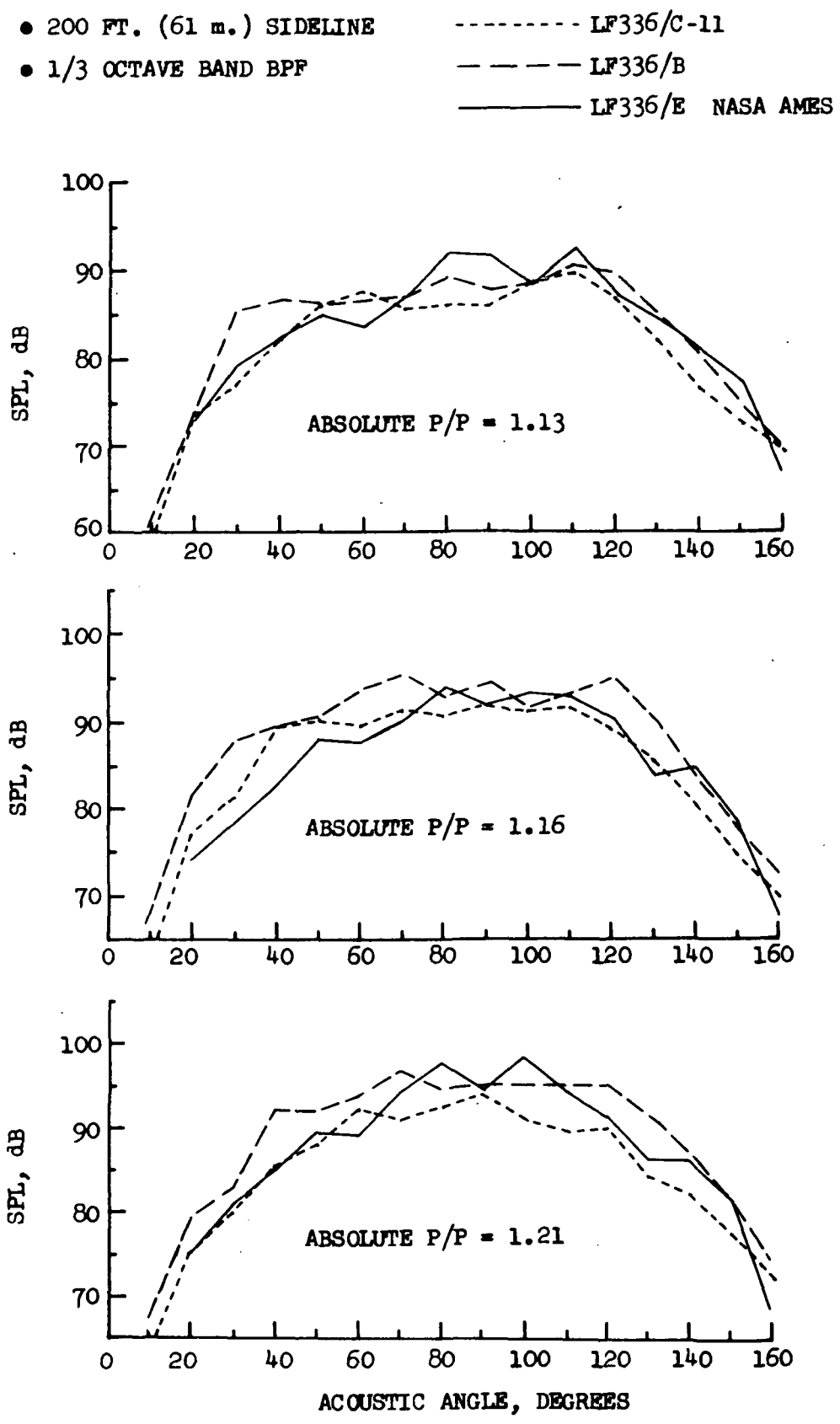

FIGURE 16 LF336/C-11, LF336/B, AND LF336/E 1/3 OCTAVE BAND BPF DIRECTIVITY PATTERNS AT CONSTANT ABSOLUTE PRESSURE RATIOS

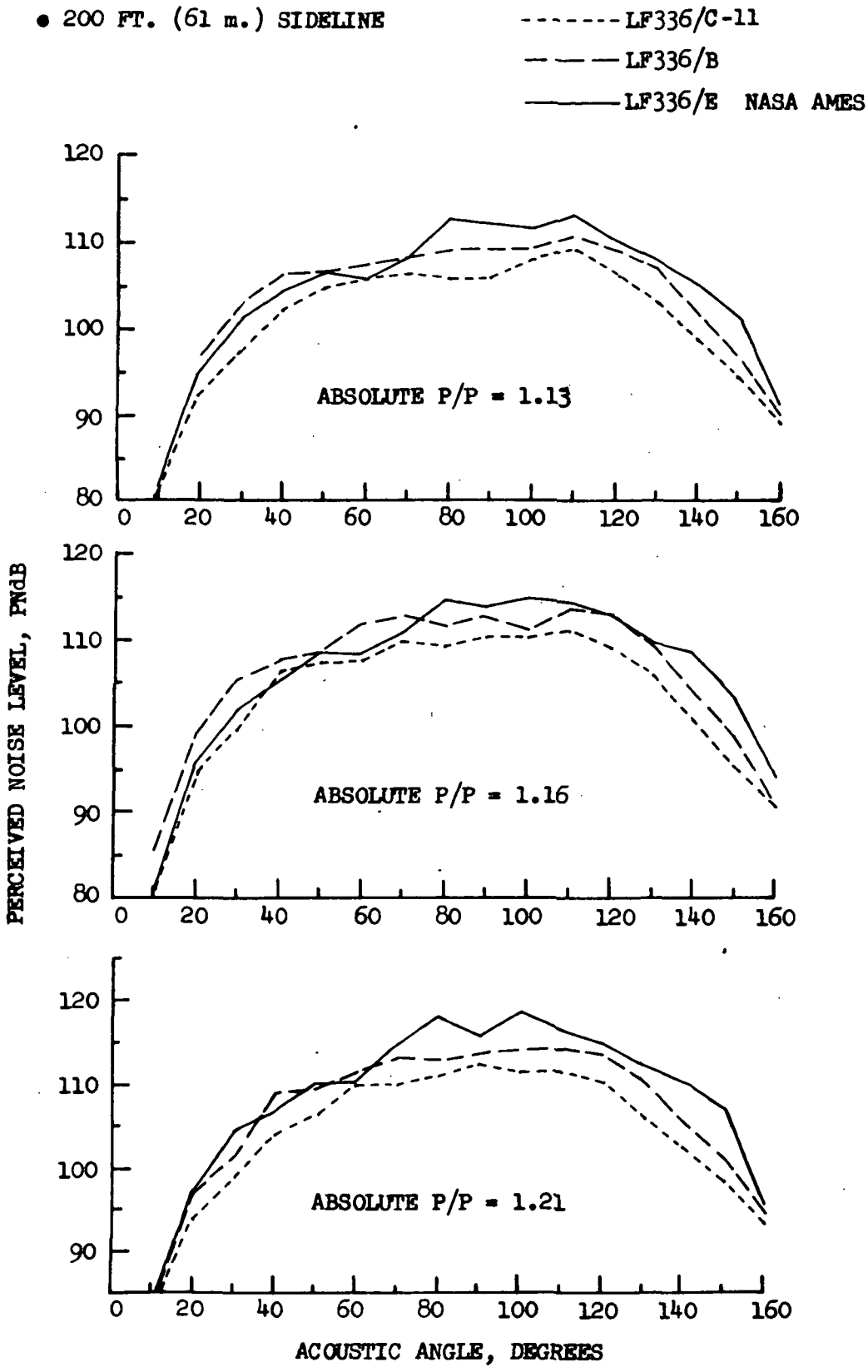

FIGURE 17 LF336/C-11, LF336/B, AND LF336/E PNL DIRECTIVITY PATTERNS AT CONSTANT ABSOLUTE PRESSURE RATIOS

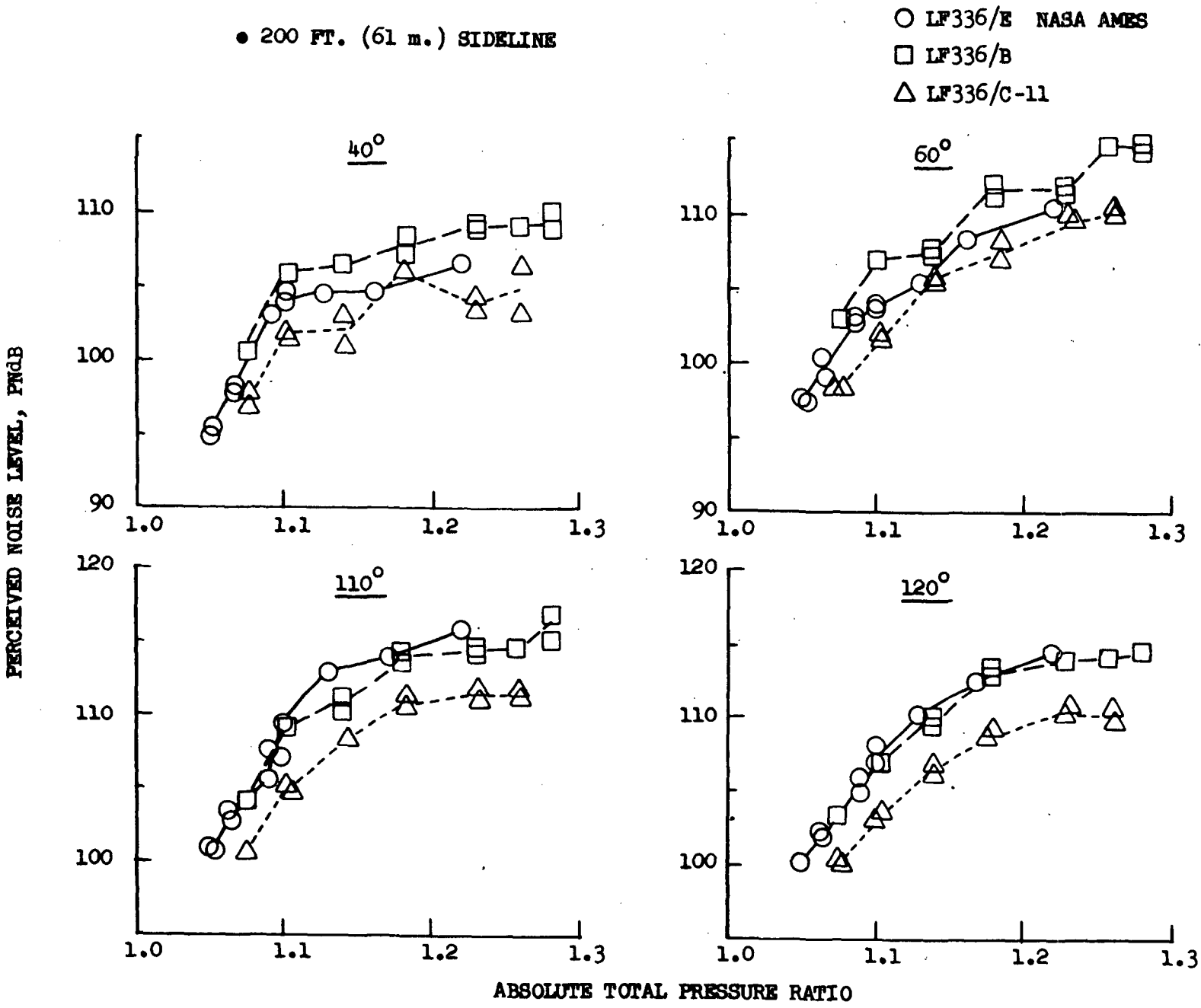

FIGURE 18 LF336/C-11, LF336/B, AND LF336/E PNL'S AS A FUNCTION OF ABSOLUTE PRESSURE RATIOS AT 40°, 60°, 110°, AND 120°

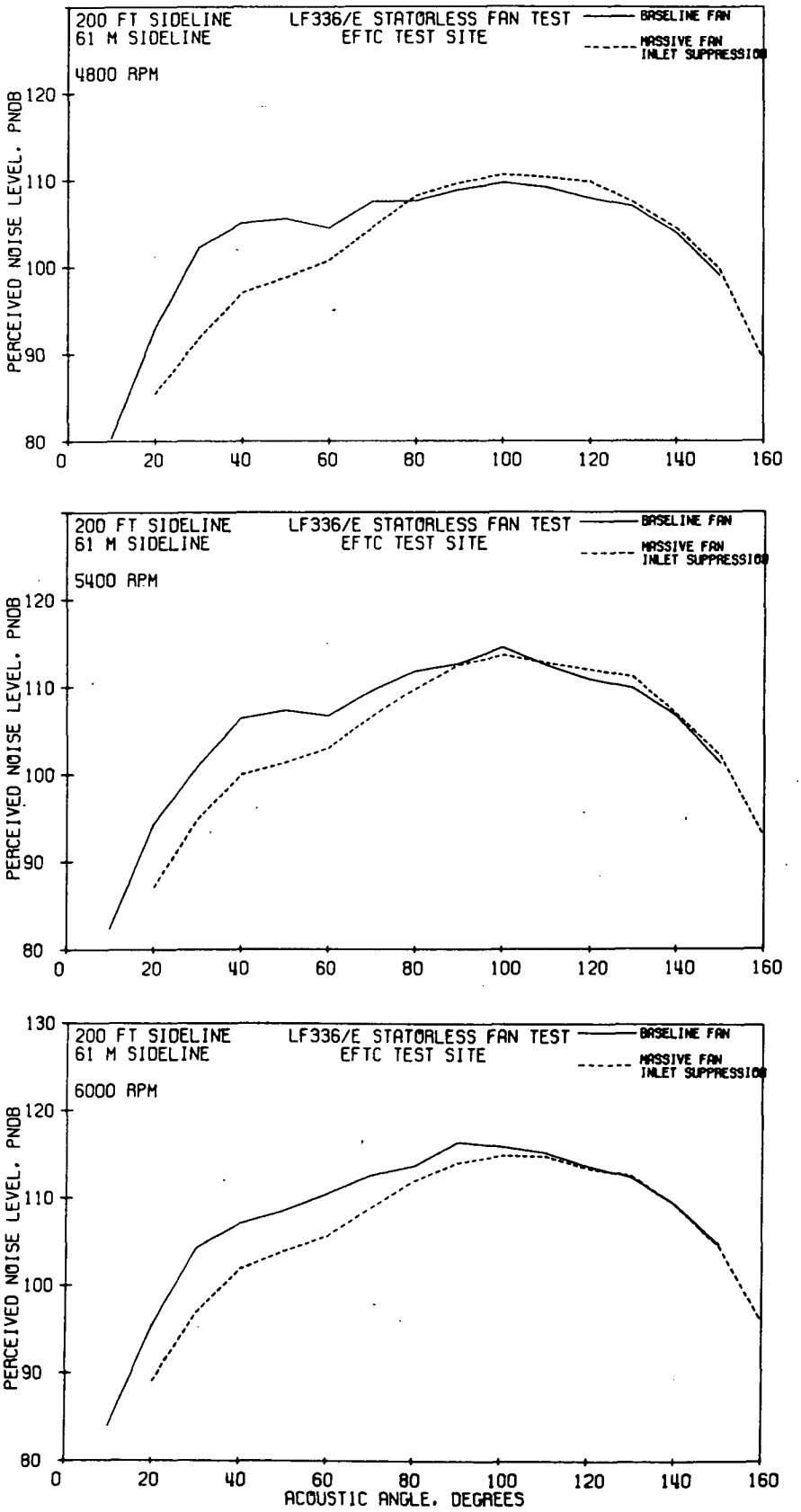

FIGURE 19 EFFECT OF MASSIVE FAN INLET SUPPRESSION ON PNL DIRECTIVITY PATTERNS AT 4800, 5400, AND 6000 RPM

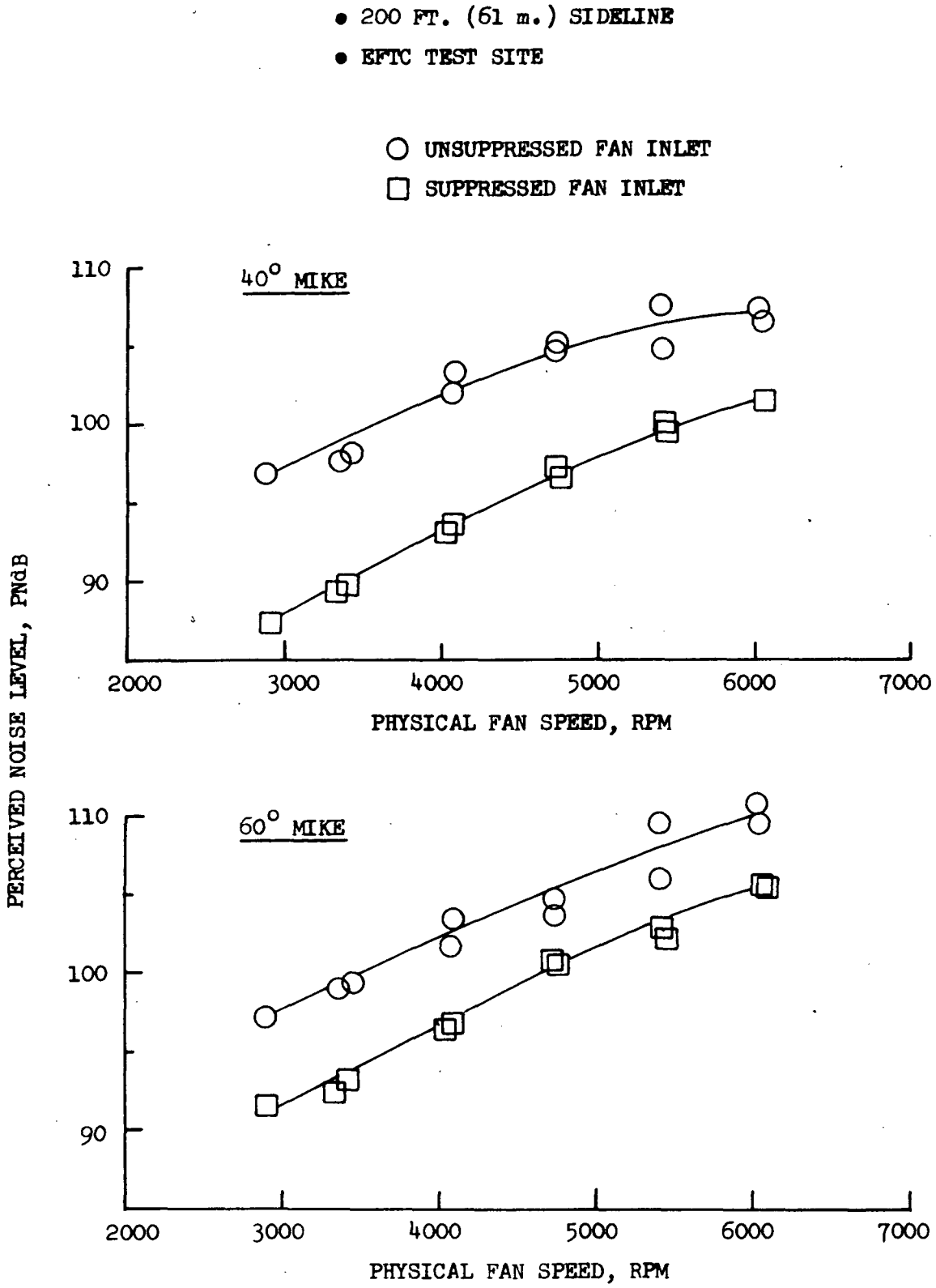

FIGURE 20 EFFECT OF MASSIVE FAN INLET SUPPRESSION ON 40° AND 60° PNL AS A FUNCTION OF FAN SPEED

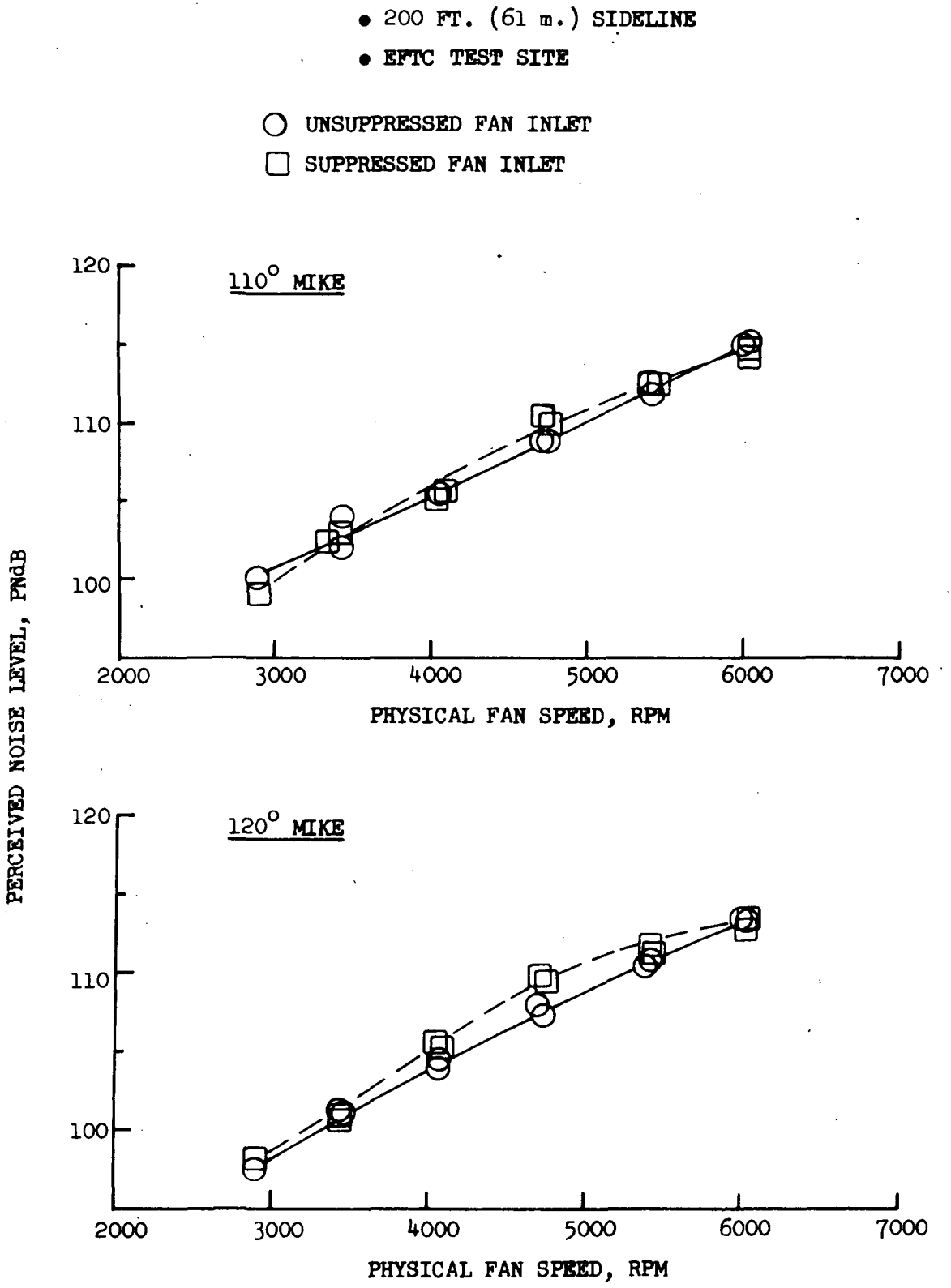

FIGURE 21 EFFECT OF MASSIVE FAN INLET SUPPRESSION ON 110° AND 120° PNL AS A FUNCTION OF FAN SPEED

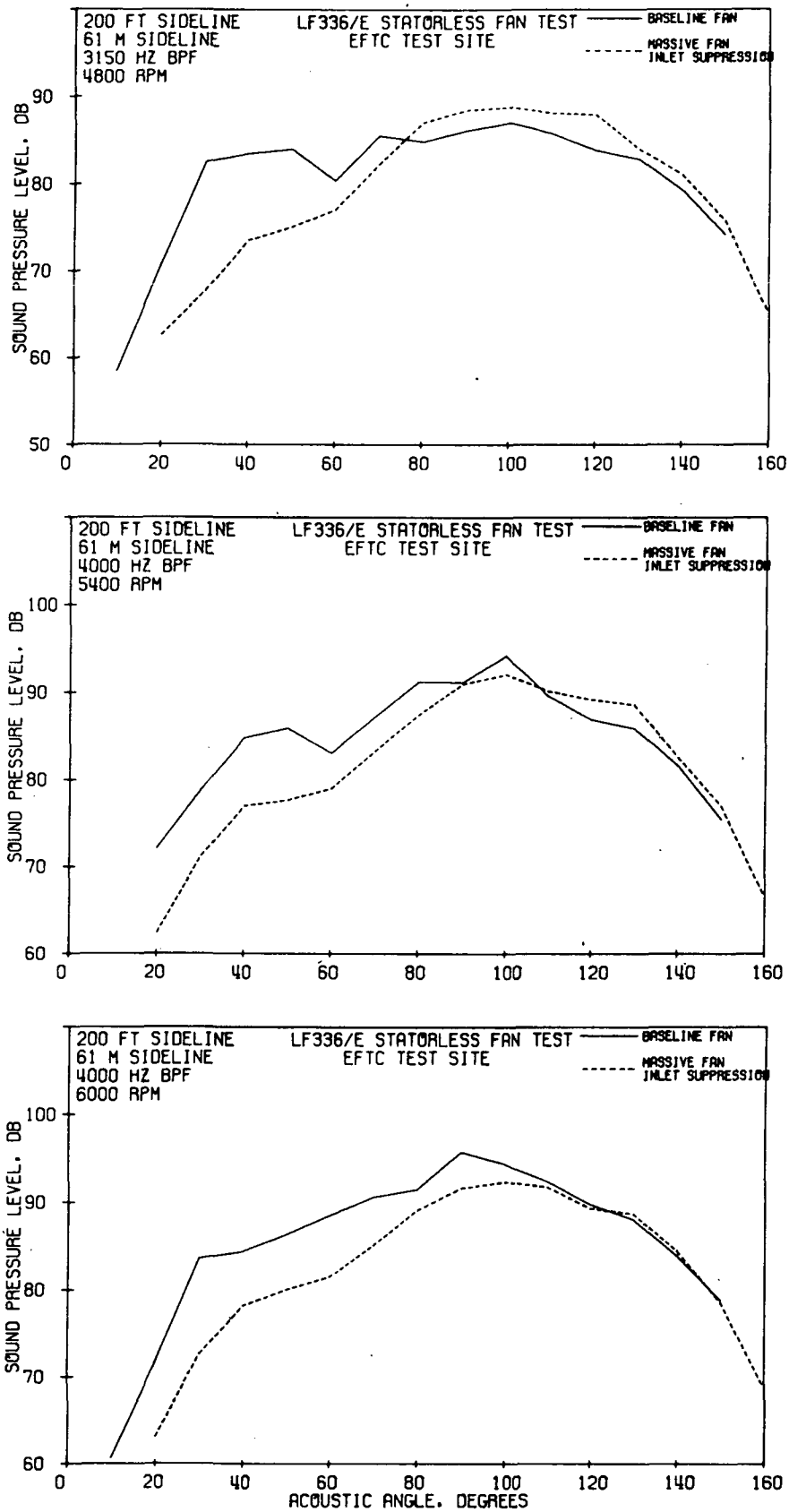

FIGURE 22 EFFECT OF MASSIVE FAN INLET SUPPRESSION ON 1/3 OCTAVE BAND BPF DIRECTIVITY PATTERNS AT 4800, 5400, AND 6000 RPM

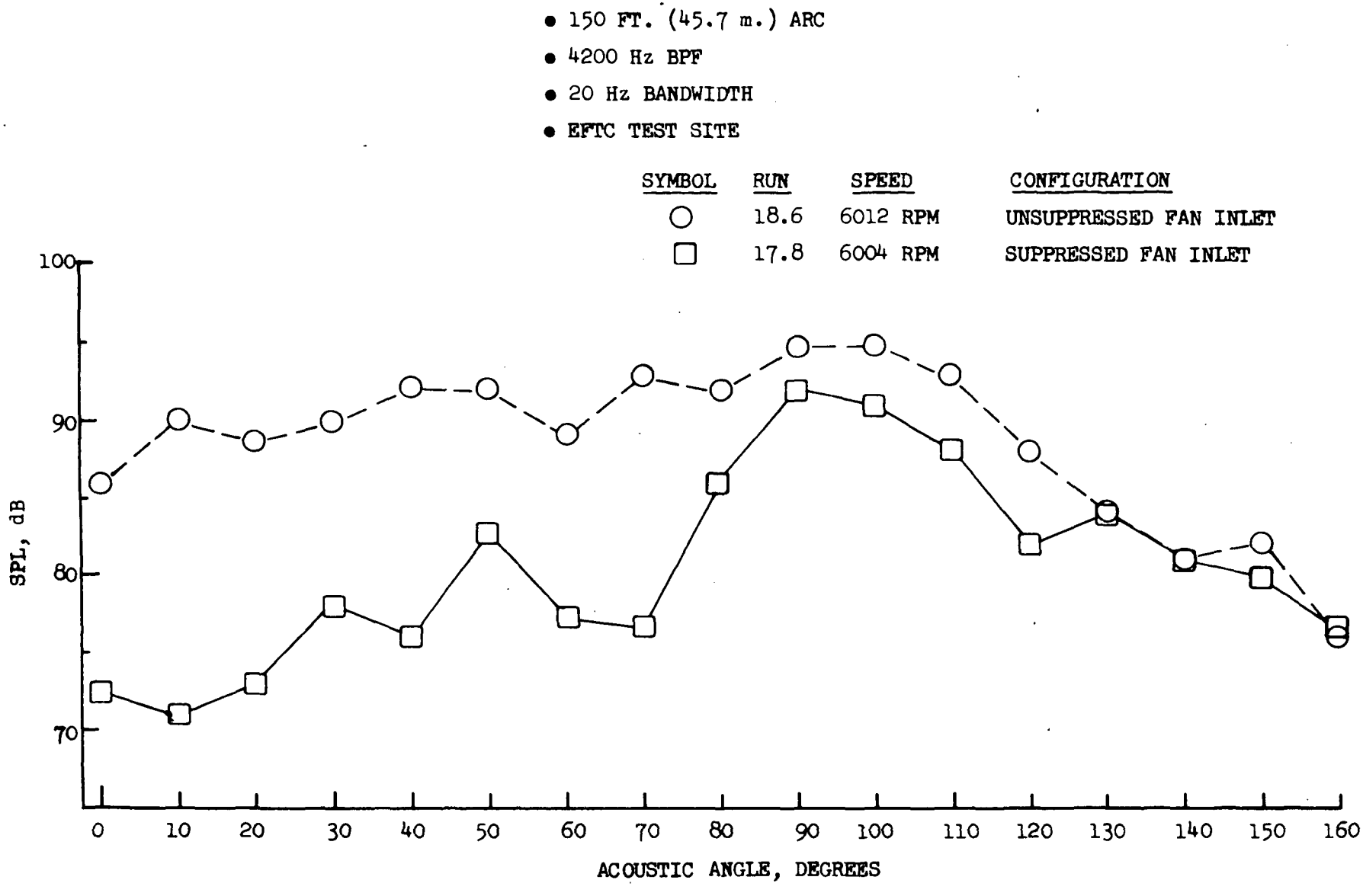

FIGURE 23 EFFECT OF MASSIVE FAN INLET SUPPRESSION ON NARROWBAND BPF DIRECTIVITY PATTERN AT 6000 RPM

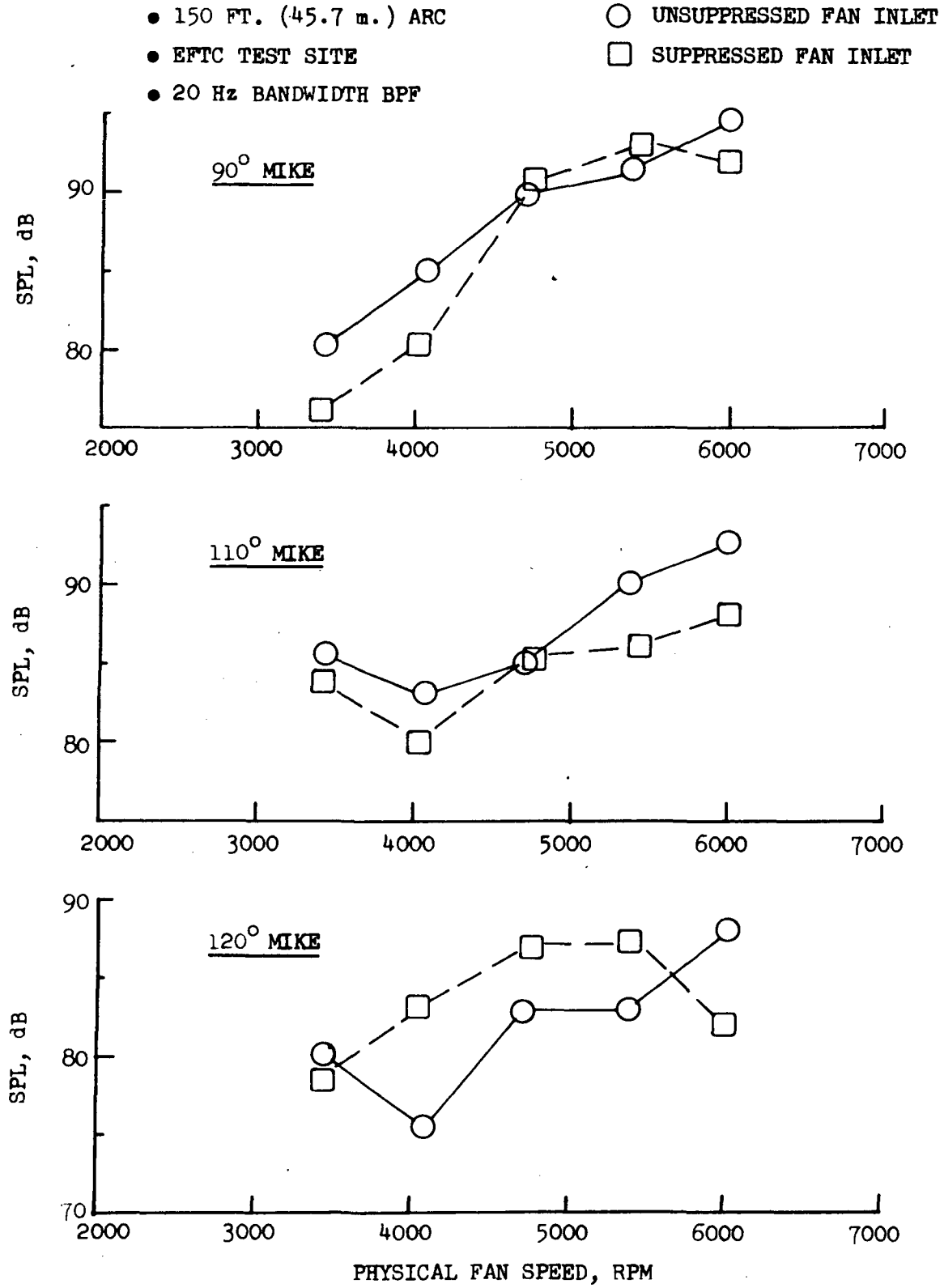

FIGURE 24 EFFECT OF MASSIVE FAN INLET SUPPRESSION ON NARROWBAND BPF AT 90°, 110°, AND 120° AS A FUNCTION OF FAN SPEED

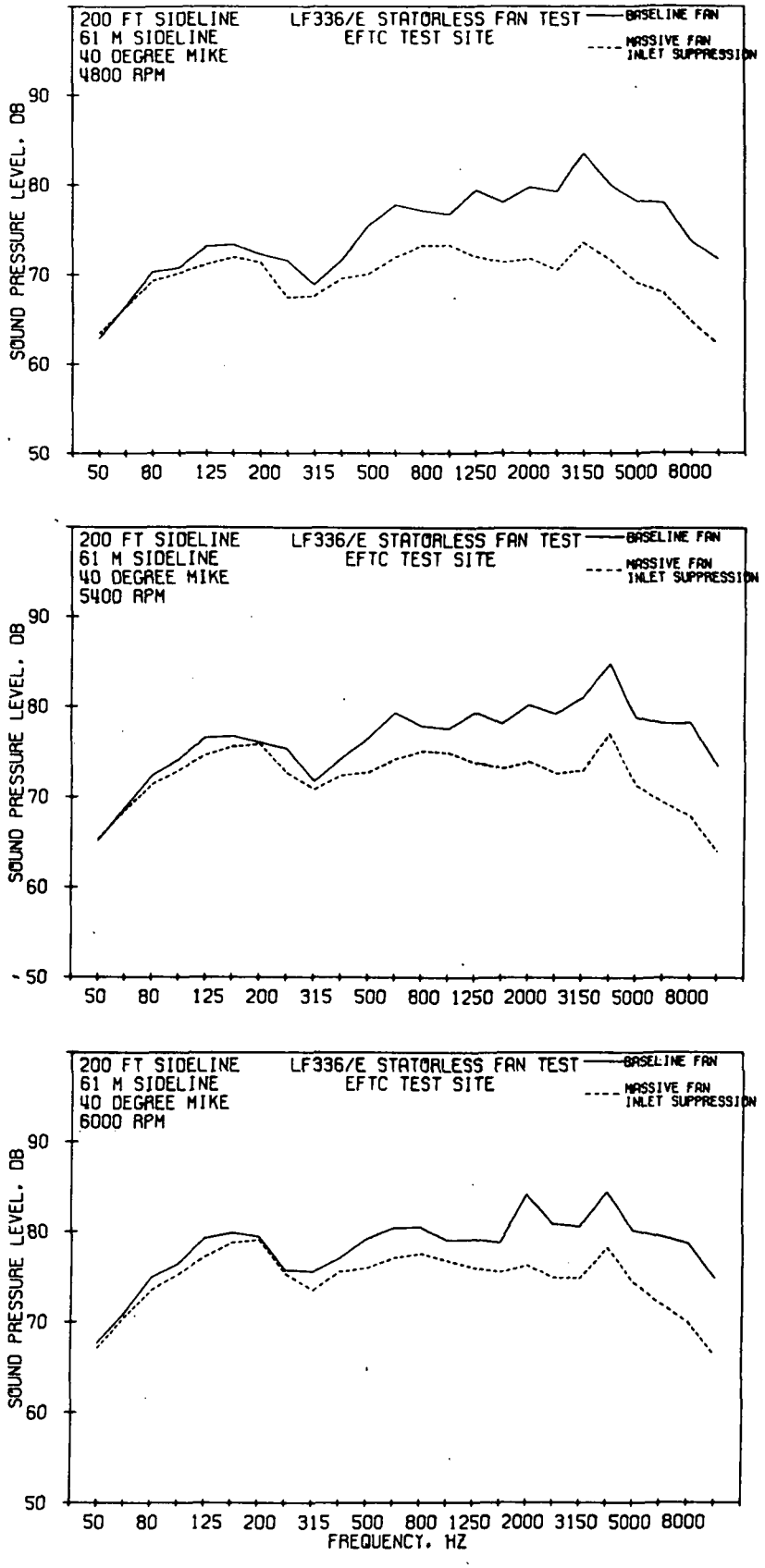

FIGURE 25 EFFECT OF MASSIVE FAN INLET SUPPRESSION ON 40° 1/3 OCTAVE BAND SPECTRA AT 4800, 5400, AND 6000 RPM

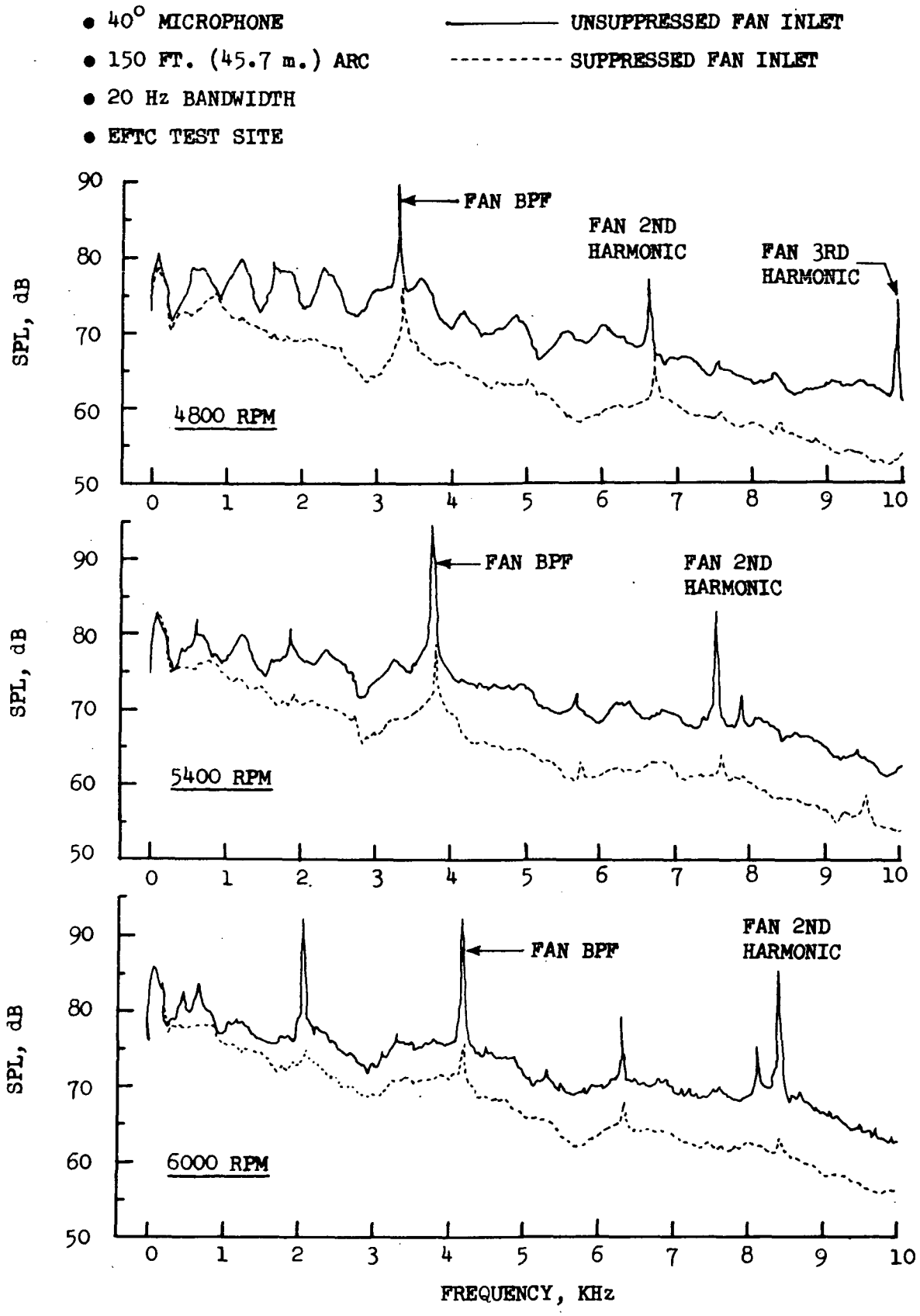

FIGURE 26 EFFECT OF MASSIVE FAN INLET SUPPRESSION ON 40° NARROWBAND SPECTRA AT 4800, 5400, AND 6000 RPM

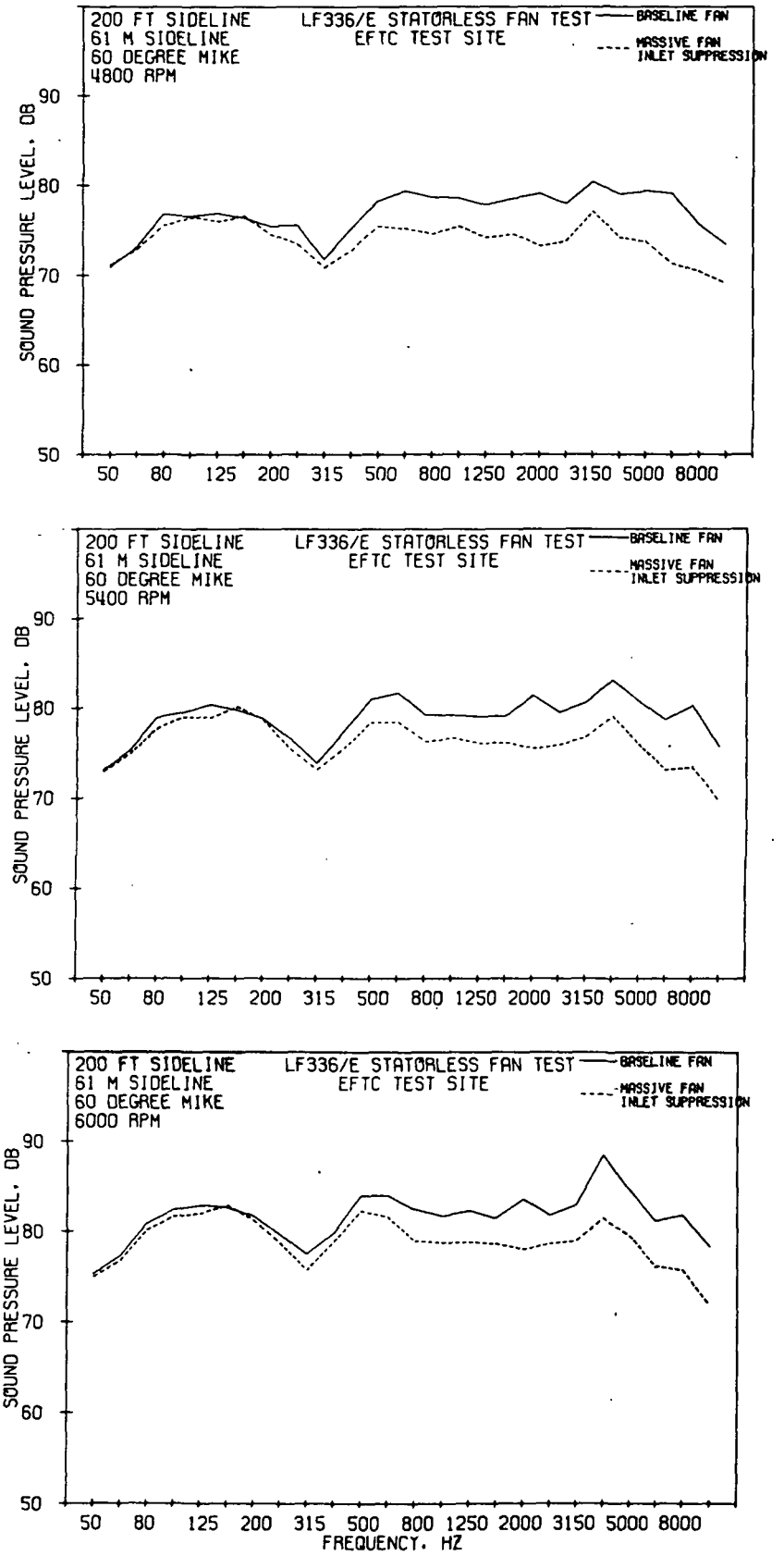

FIGURE 27 EFFECT OF MASSIVE FAN INLET SUPPRESSION ON 60° 1/3 OCTAVE BAND SPECTRA AT 4800, 5400, AND 6000 RPM

- 60° MICROPHONE
- 150 FT. (45.7 m.) ARC
- 20 Hz BANDWIDTH
- EFTC TEST SITE

———— UNSUPPRESSED FAN INLET

---------- SUPPRESSED FAN INLET

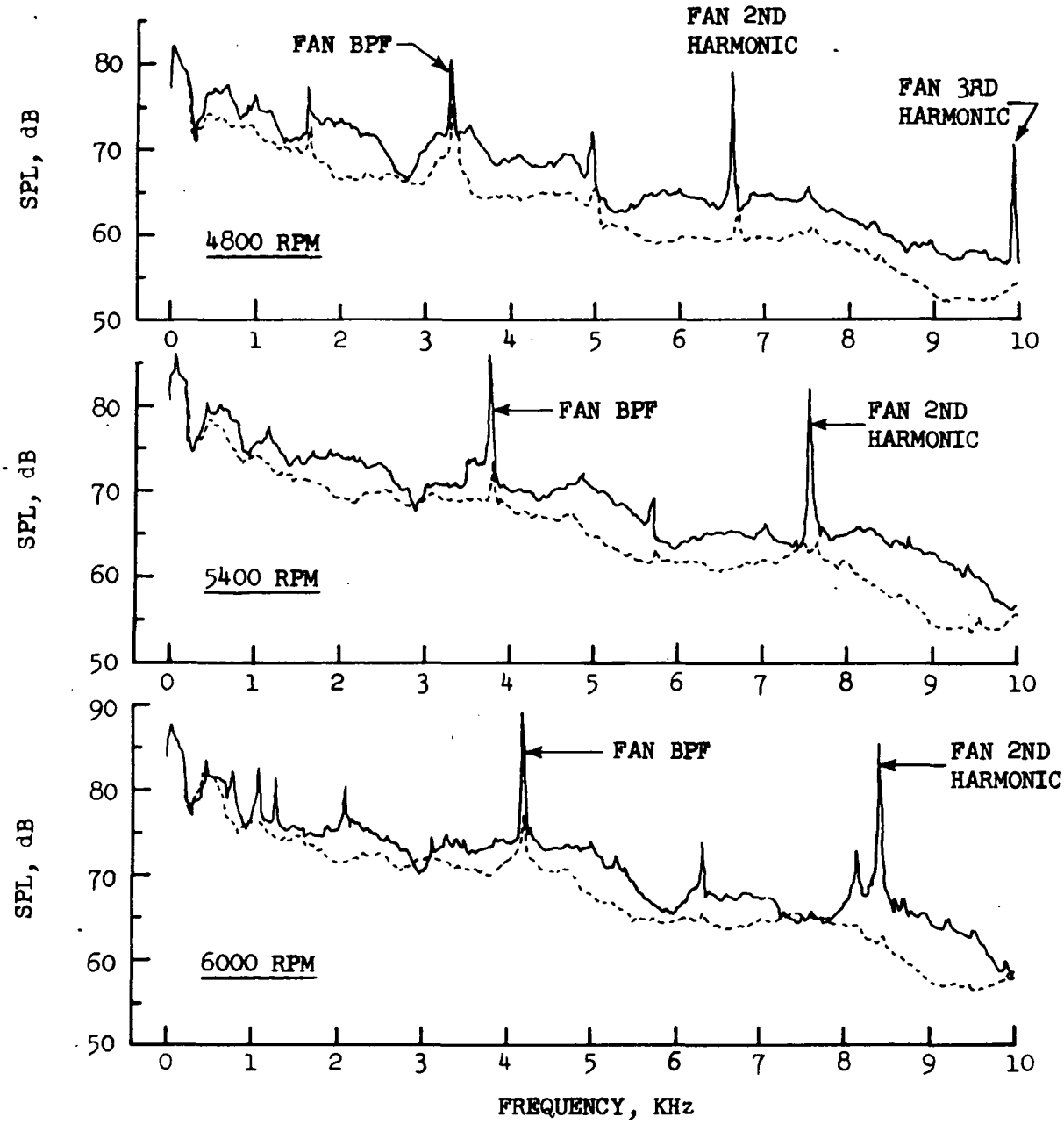

FIGURE 28 EFFECT OF MASSIVE FAN INLET SUPPRESSION ON 60° NARROWBAND SPECTRA AT 4800, 5400, AND 6000 RPM

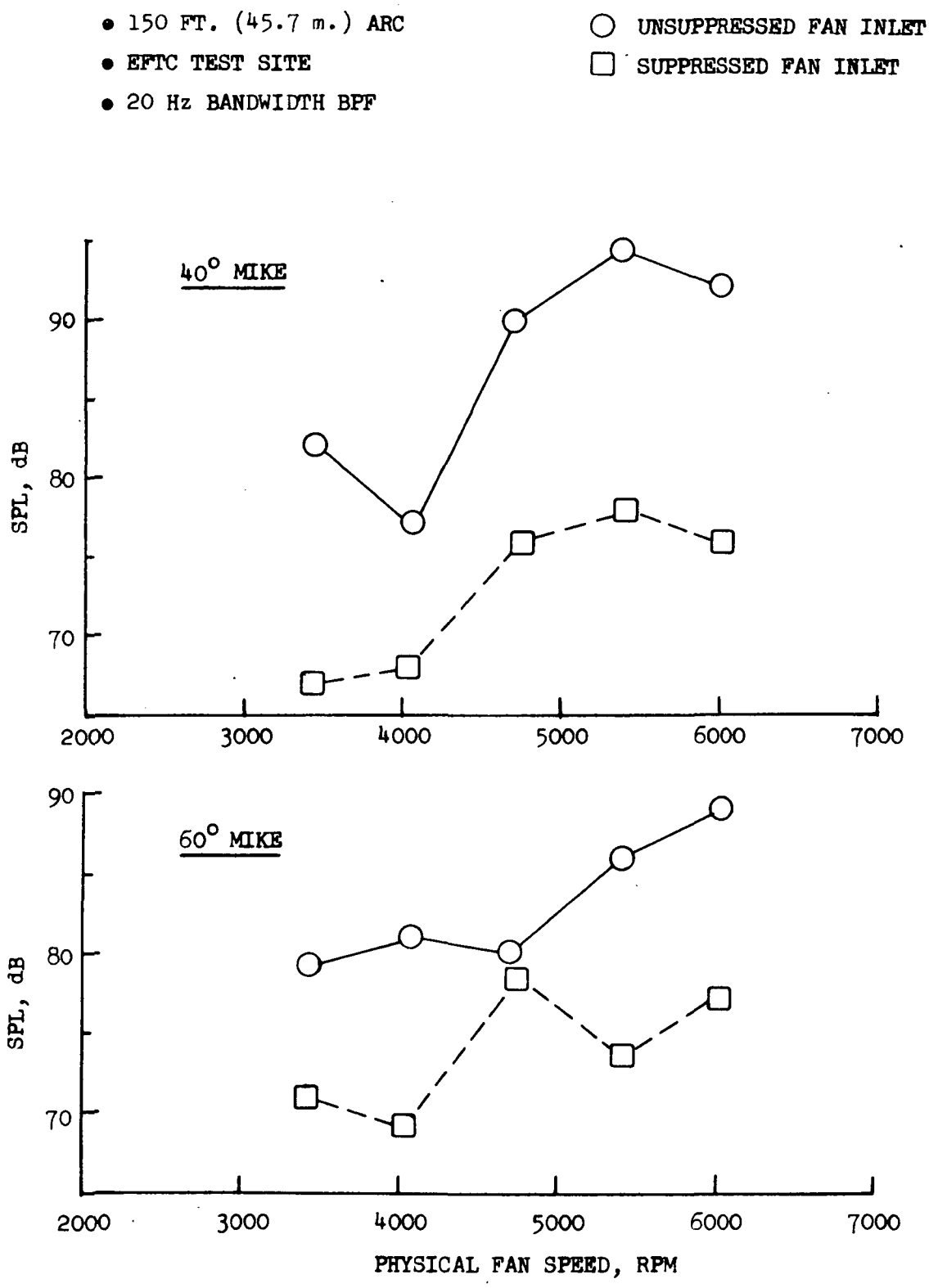

FIGURE 29 EFFECT OF MASSIVE FAN INLET SUPPRESSION ON 40° AND 60° NARROWBAND BPF AS A FUNCTION OF FAN SPEED

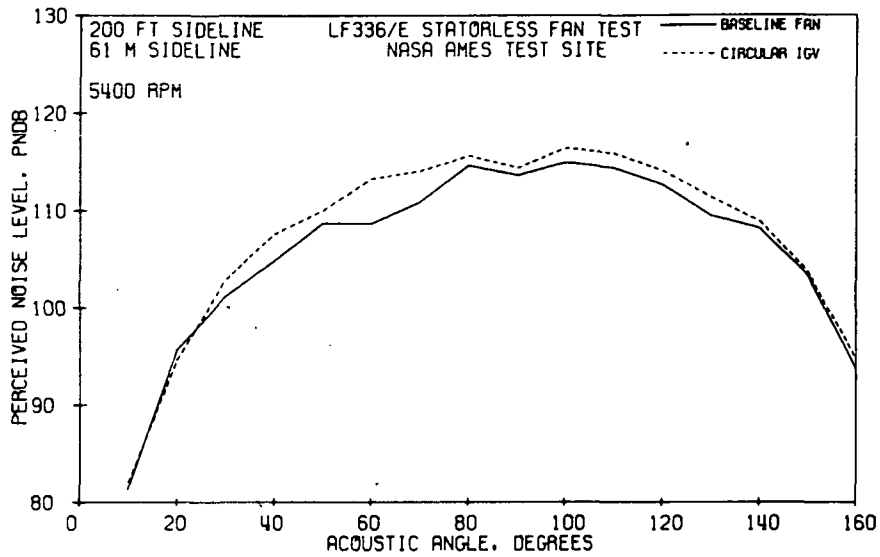

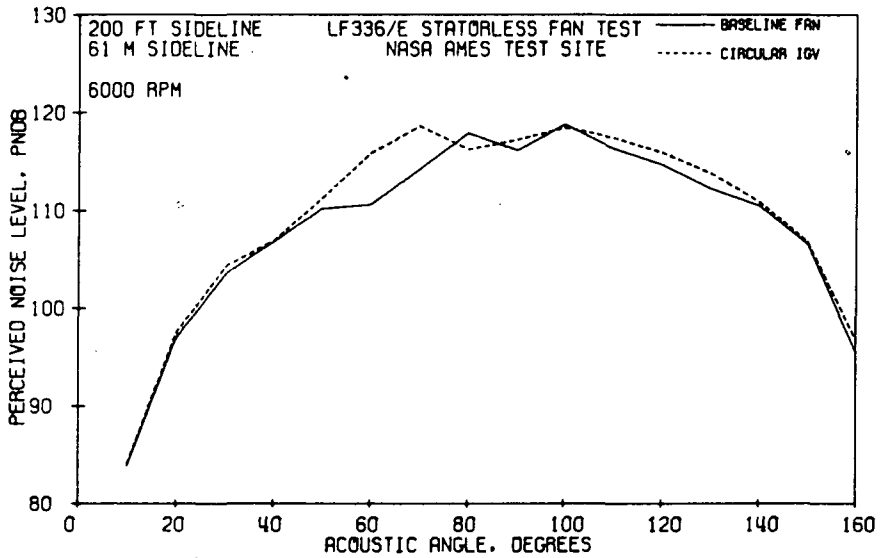

FIGURE 30 EFFECT OF CIRCULAR IGV ON PNL DIRECTIVITY PATTERNS AT 5400 AND 6000 RPM

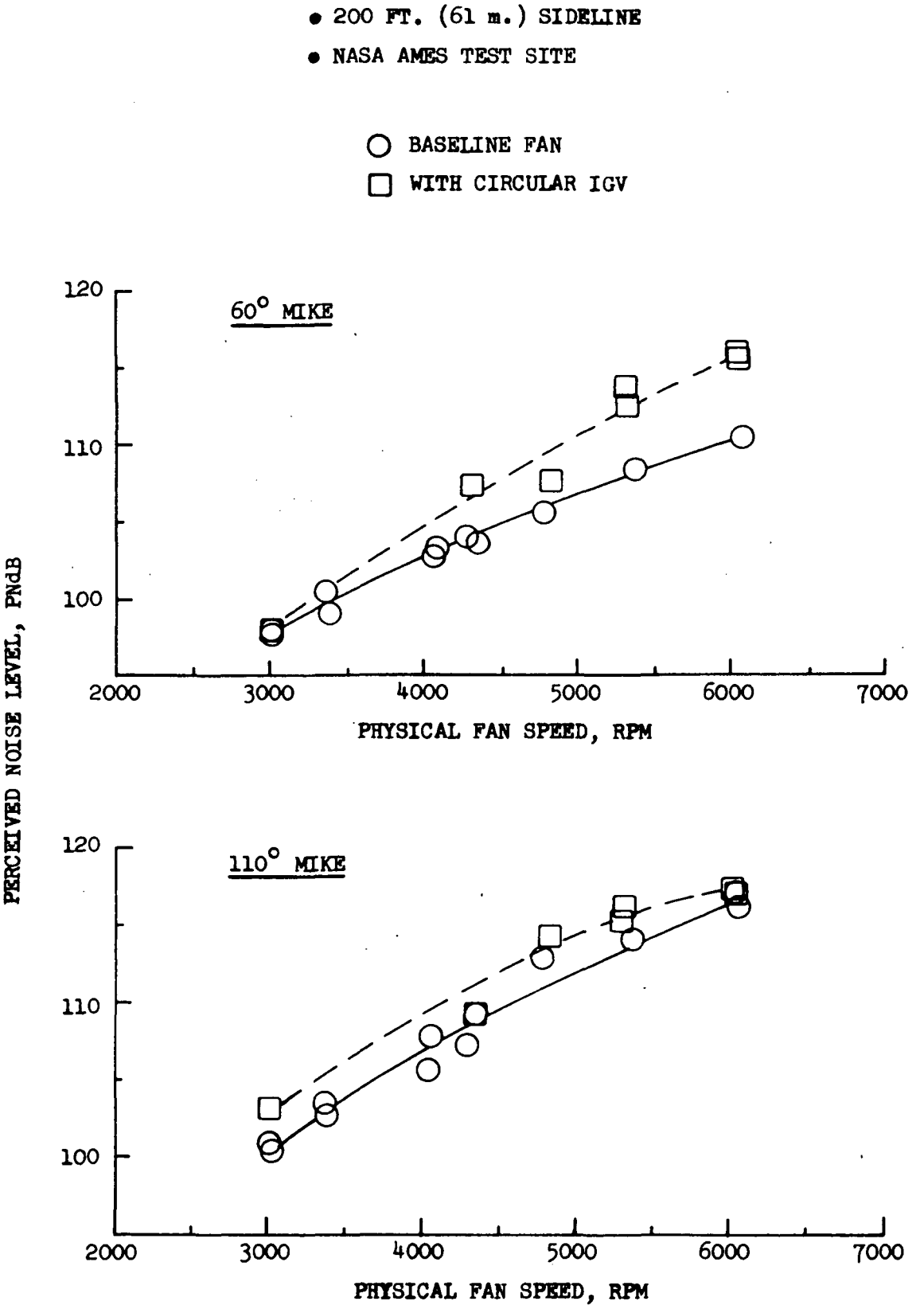

FIGURE 31 EFFECT OF CIRCULAR IGV ON 60° AND 110° PNL AS A FUNCTION OF FAN SPEED

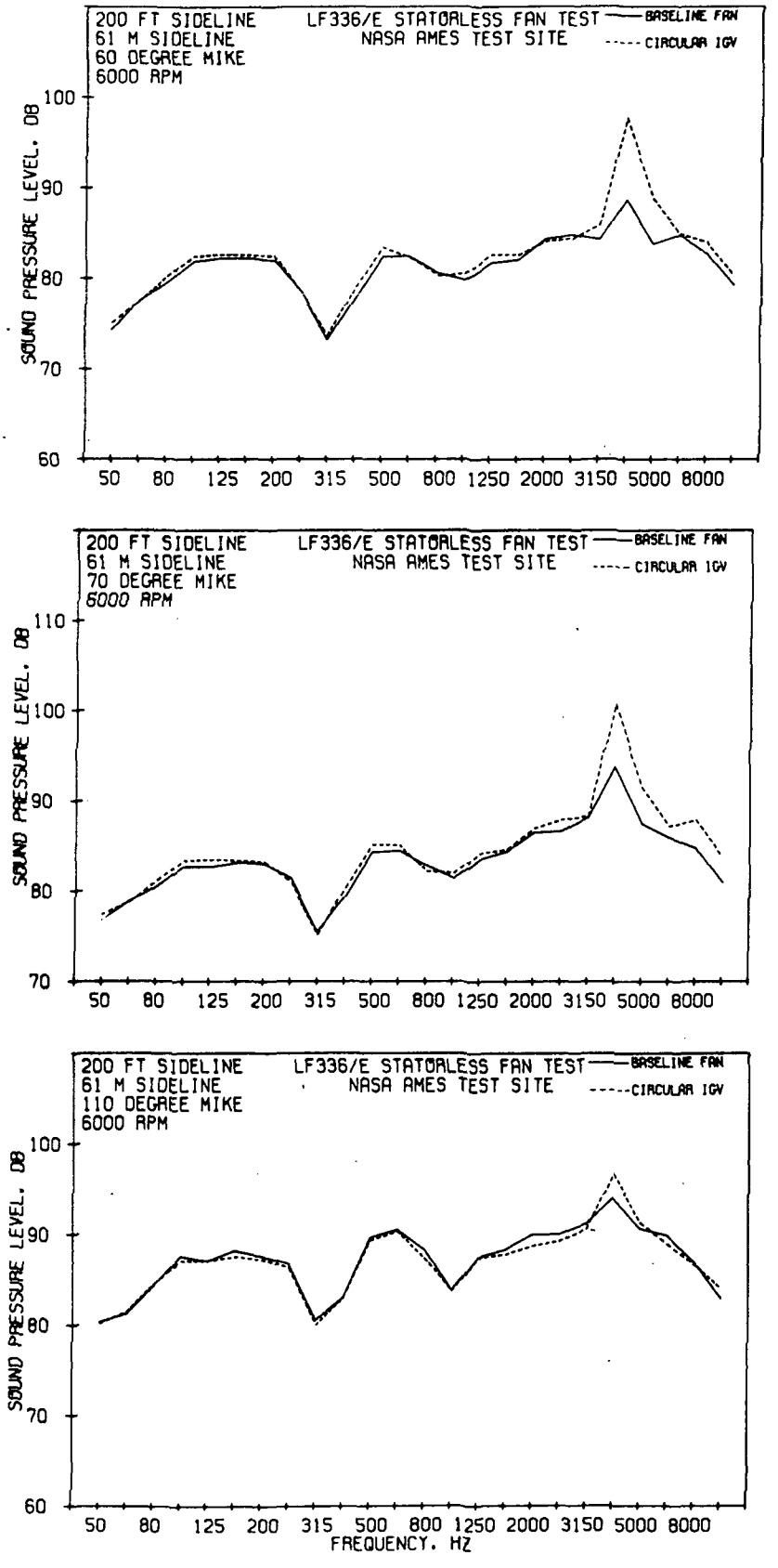

FIGURE 32 EFFECT OF CIRCULAR IGV ON 60°, 70°, AND 110° 1/3 OCTAVE BAND SPECTRA AT 6000 RPM

- 150 FT. (45.7 m.) ARC
- NASA AMES TEST SITE
- 20 Hz BANDWIDTH
- 6000 RPM

——— BASELINE FAN

- - - - - - - - WITH CIRCULAR IGV

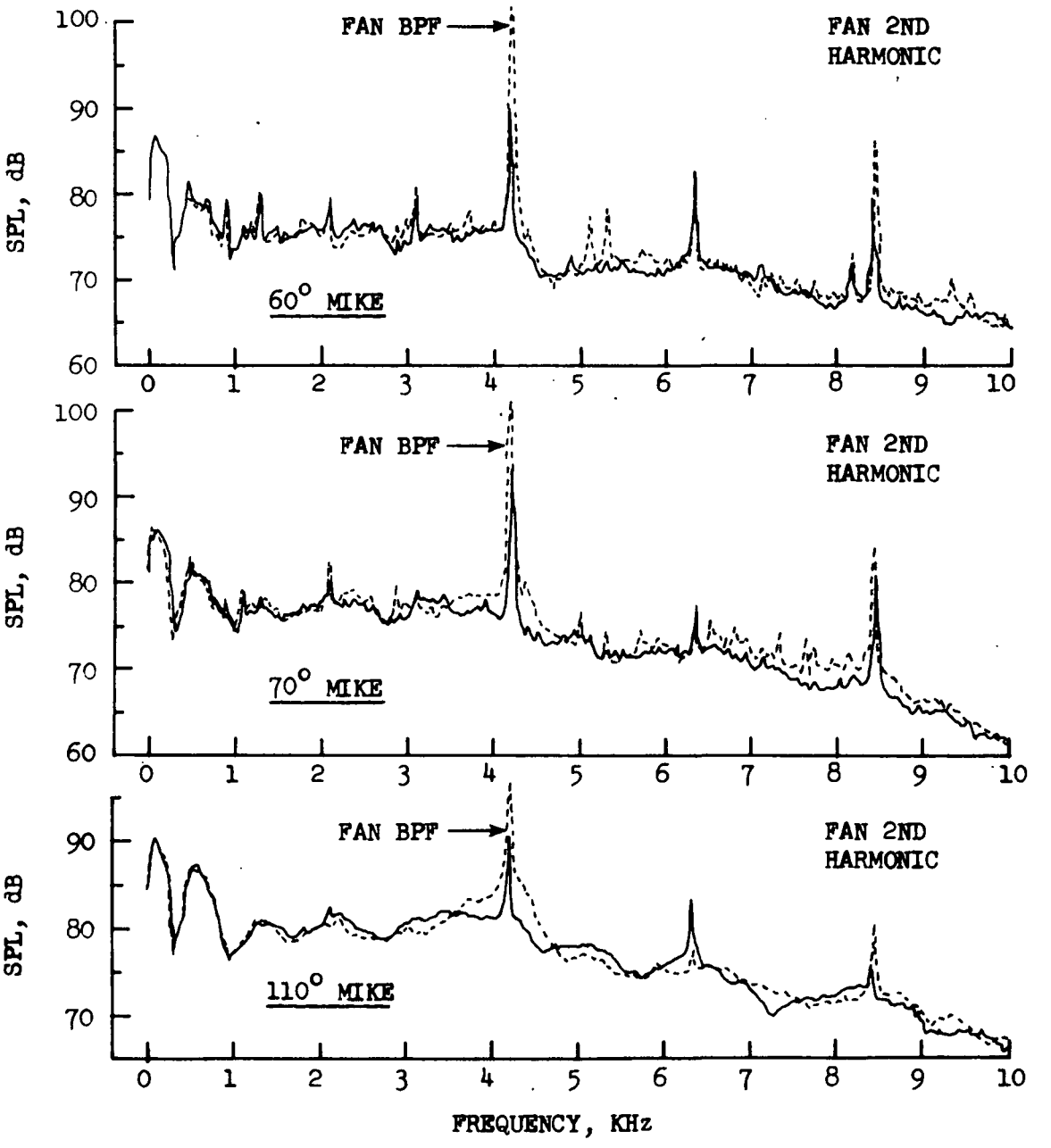

FIGURE 33 EFFECT OF CIRCULAR IGV ON 60°, 70°, AND 110° NARROWBAND SPECTRA AT 6000 RPM

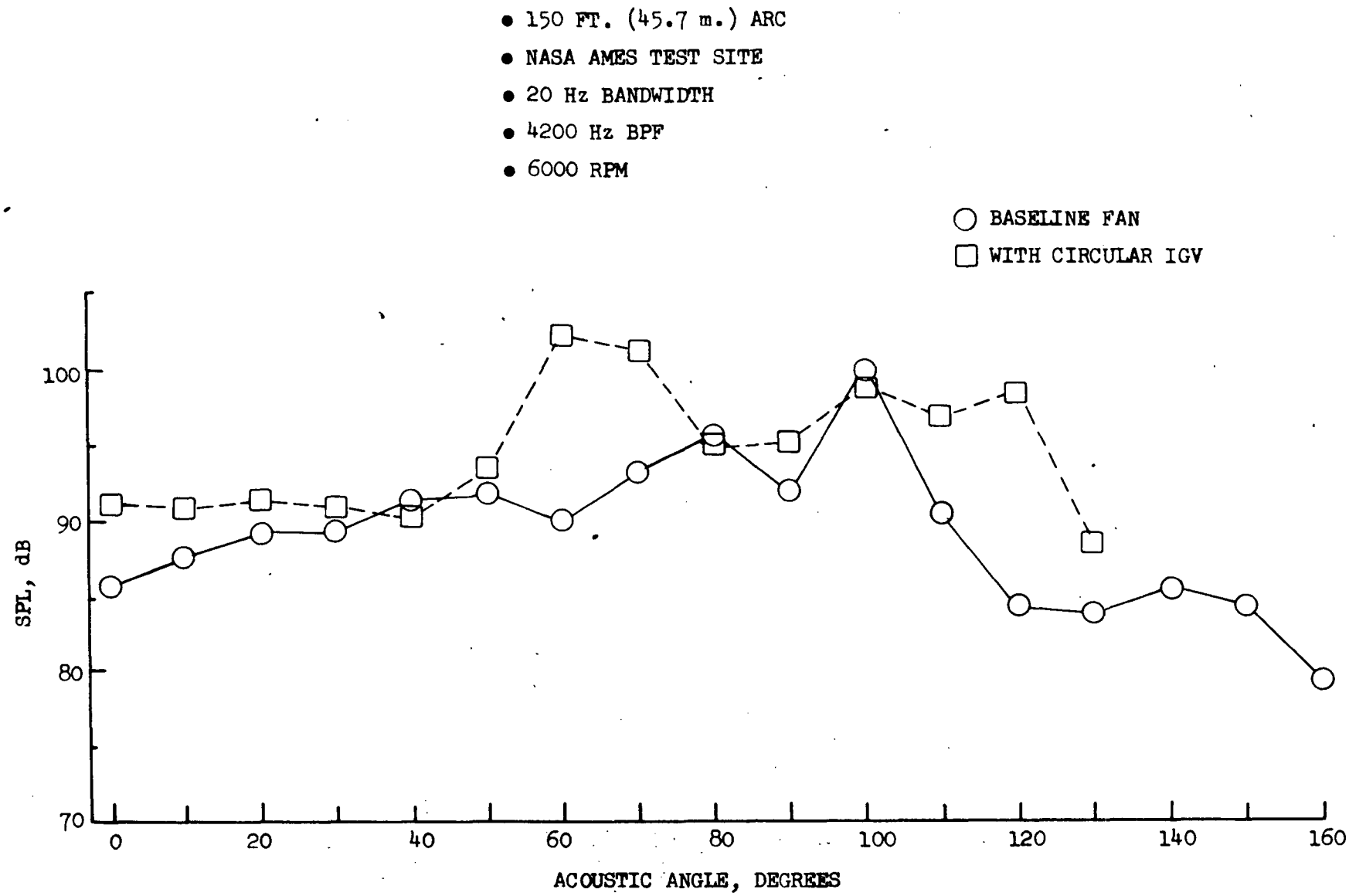

FIGURE 34 EFFECT OF CIRCULAR IGV ON NARROWBAND BPF DIRECTIVITY PATTERN AT 6000 RPM

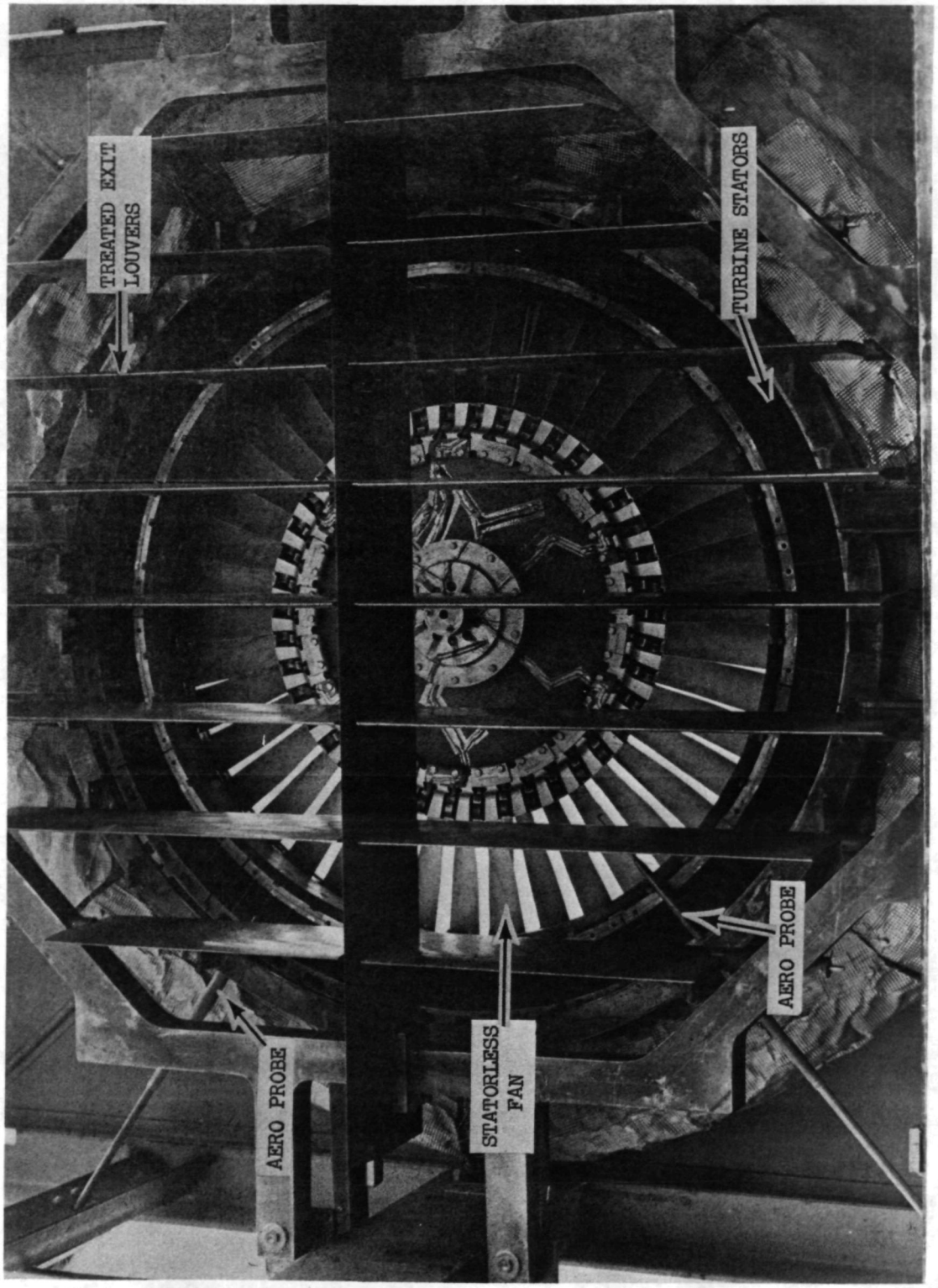

FIGURE 35 PHOTOGRAPH OF LF336/E TREATED EXIT LOUVERS

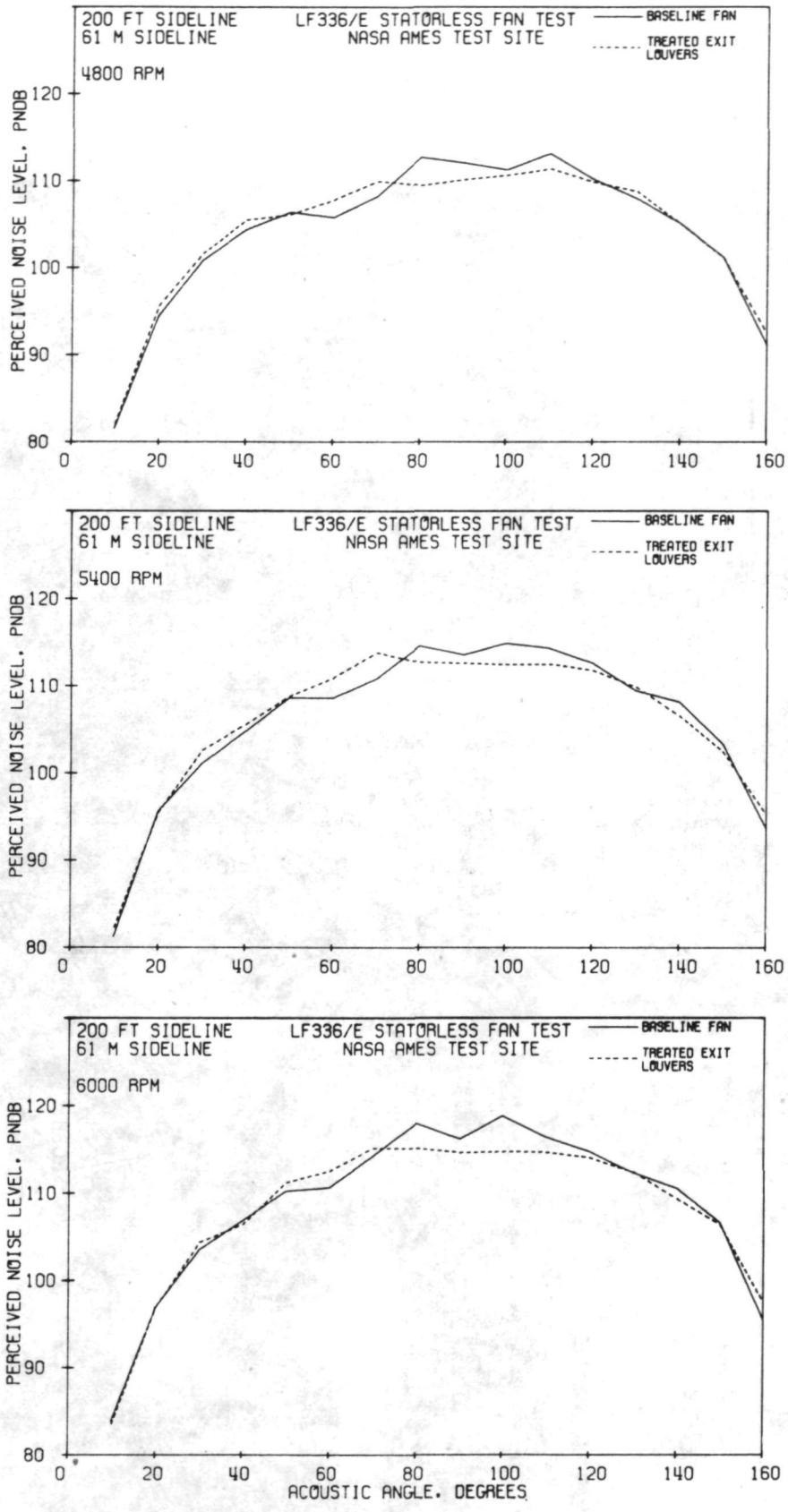

FIGURE 36 EFFECT OF TREATED EXIT LOUVERS ON PNL DIRECTIVITY PATTERNS AT 4800, 5400, AND 6000 RPM

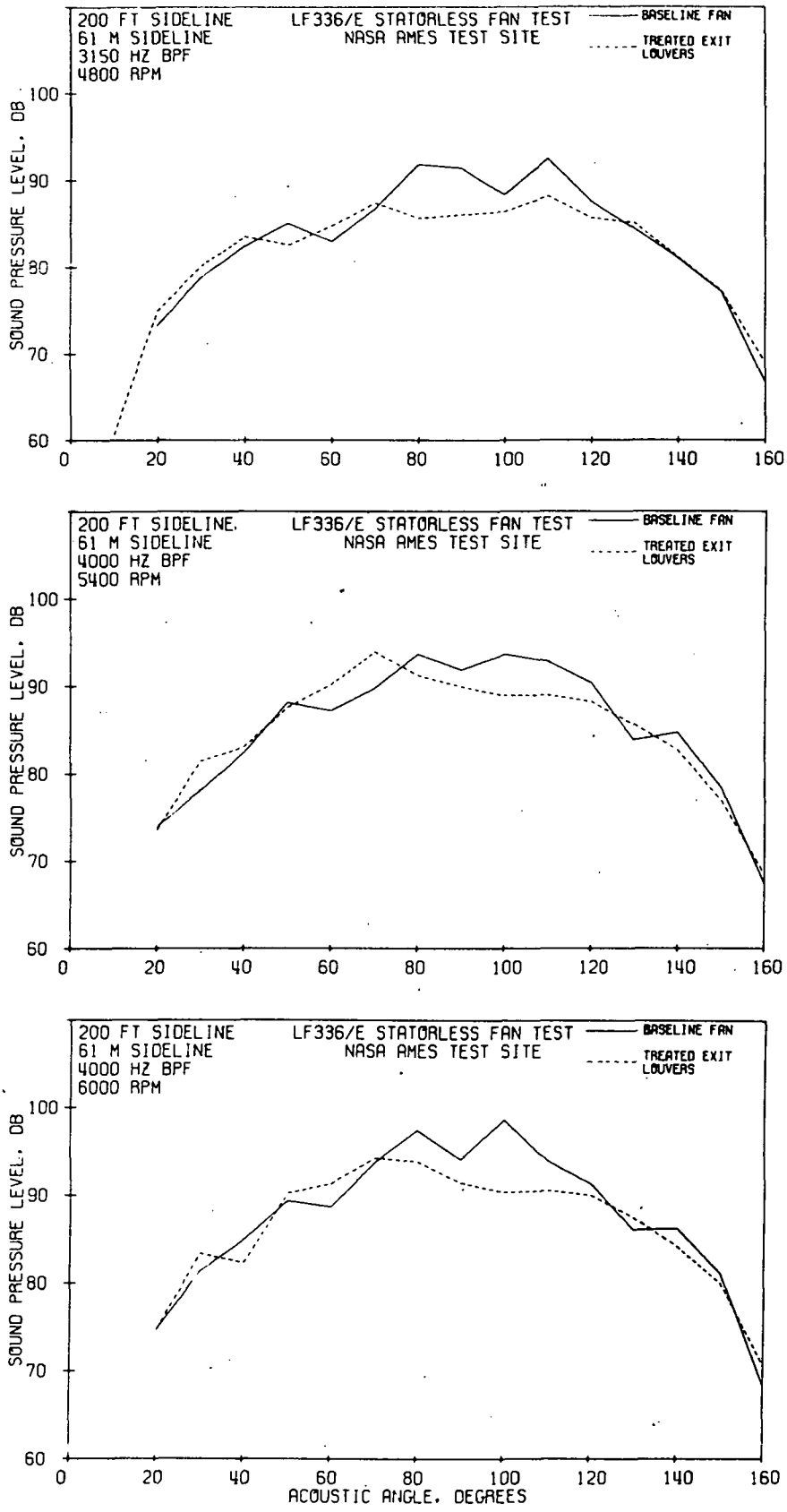

FIGURE 37 EFFECT OF TREATED EXIT LOUVERS ON 1/3 OCTAVE BAND BPF DIRECTIVITY PATTERNS AT 4800, 5400, AND 6000 RPM

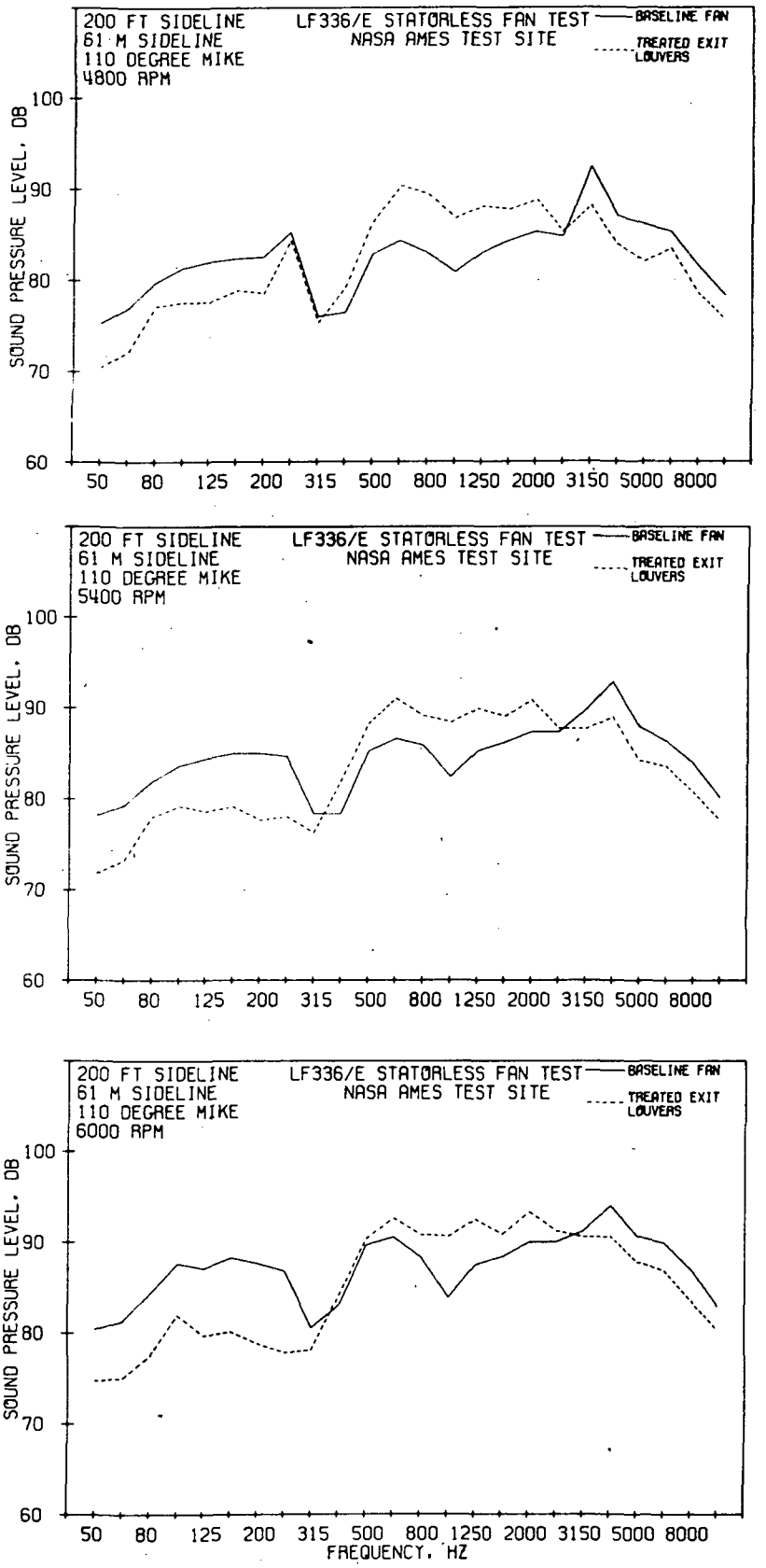

FIGURE 38 EFFECT OF TREATED EXIT LOUVERS ON 110° 1/3 OCTAVE BAND SPECTRA AT 4800, 5400, AND 6000 RPM

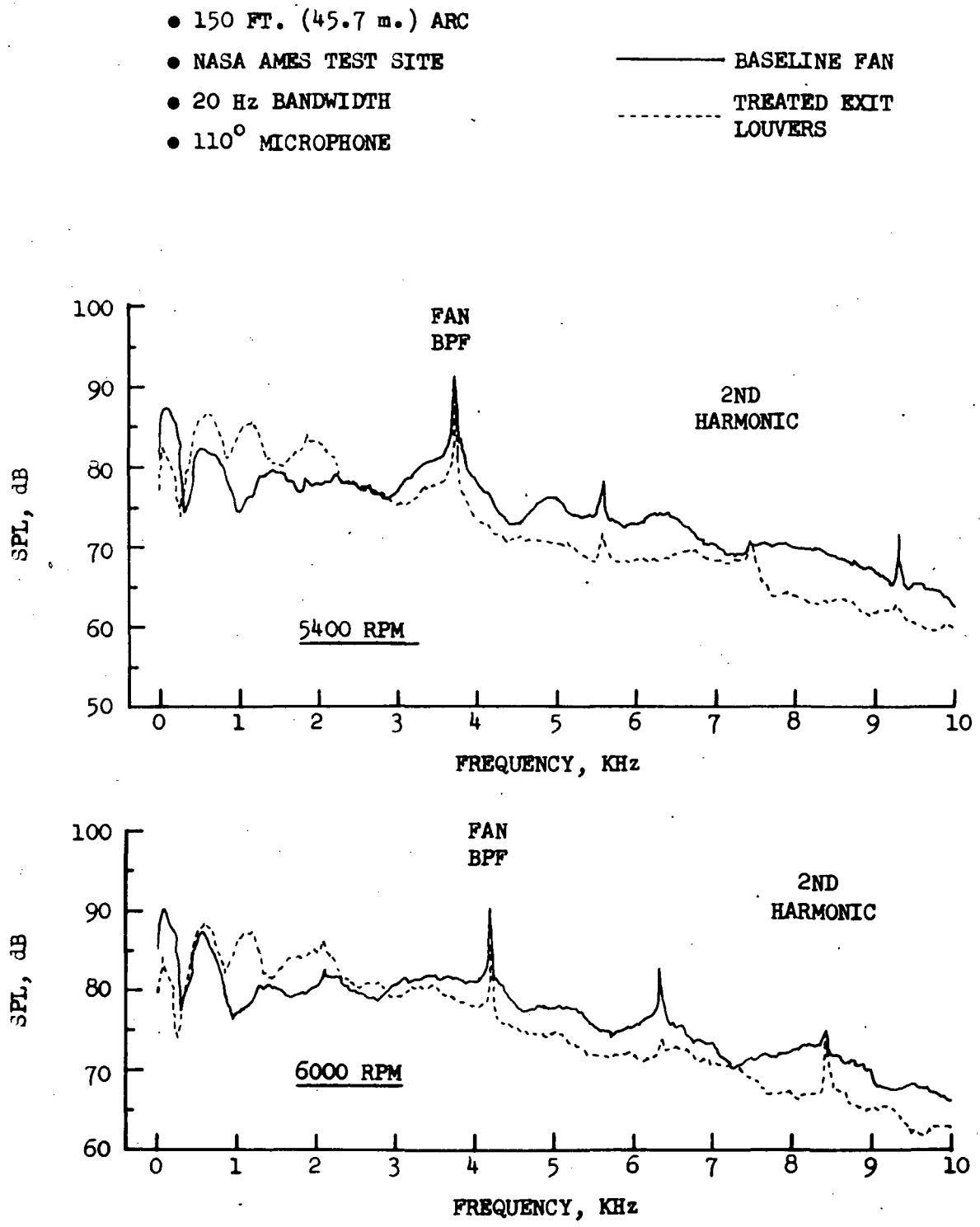

FIGURE 39 EFFECT OF TREATED EXIT LOUVERS ON 110° NARROWBAND SPECTRA AT 5400 AND 6000 RPM

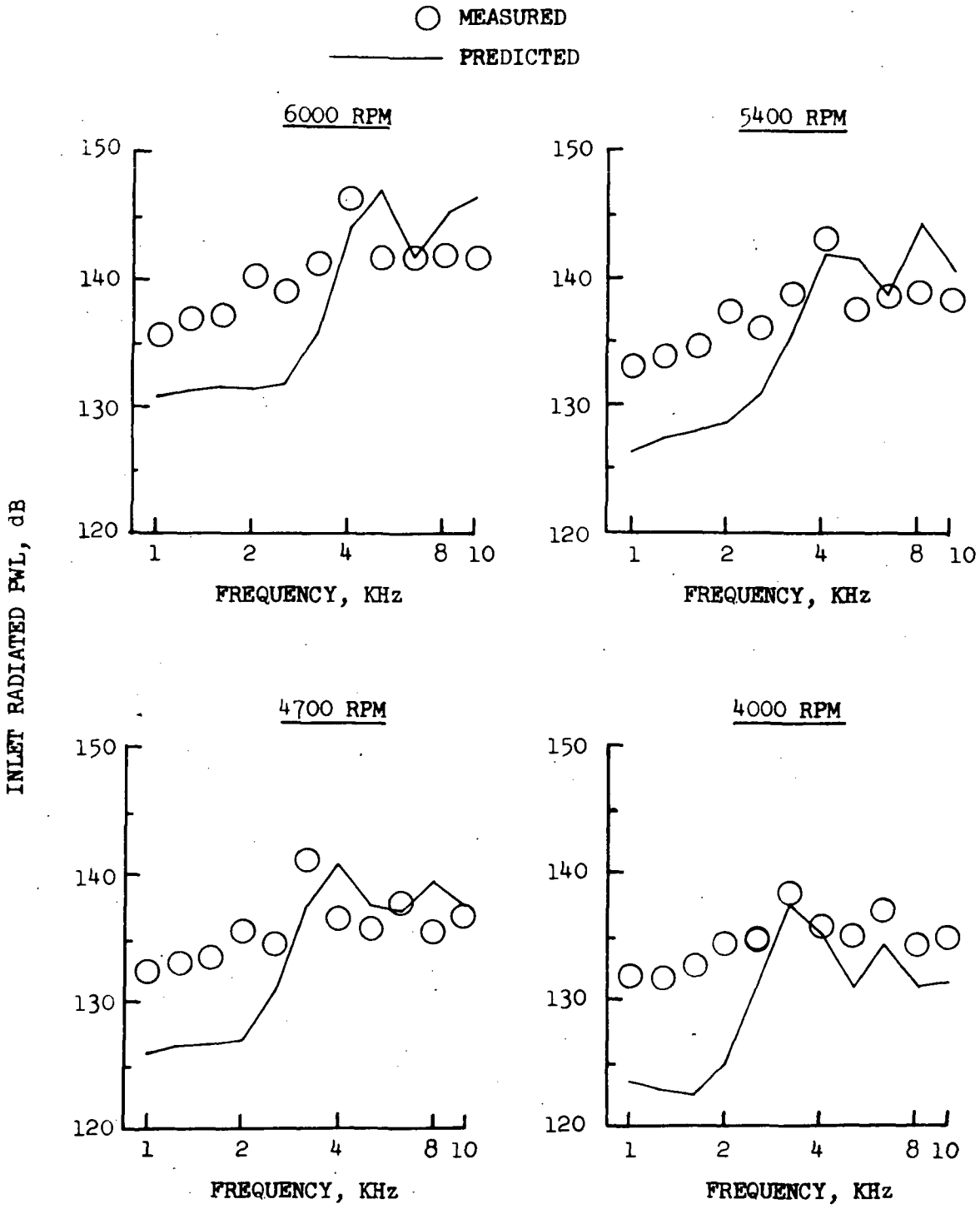

FIGURE 40 COMPARISON OF MEASURED AND PREDICTED INLET RADIATED SOUND POWER LEVELS

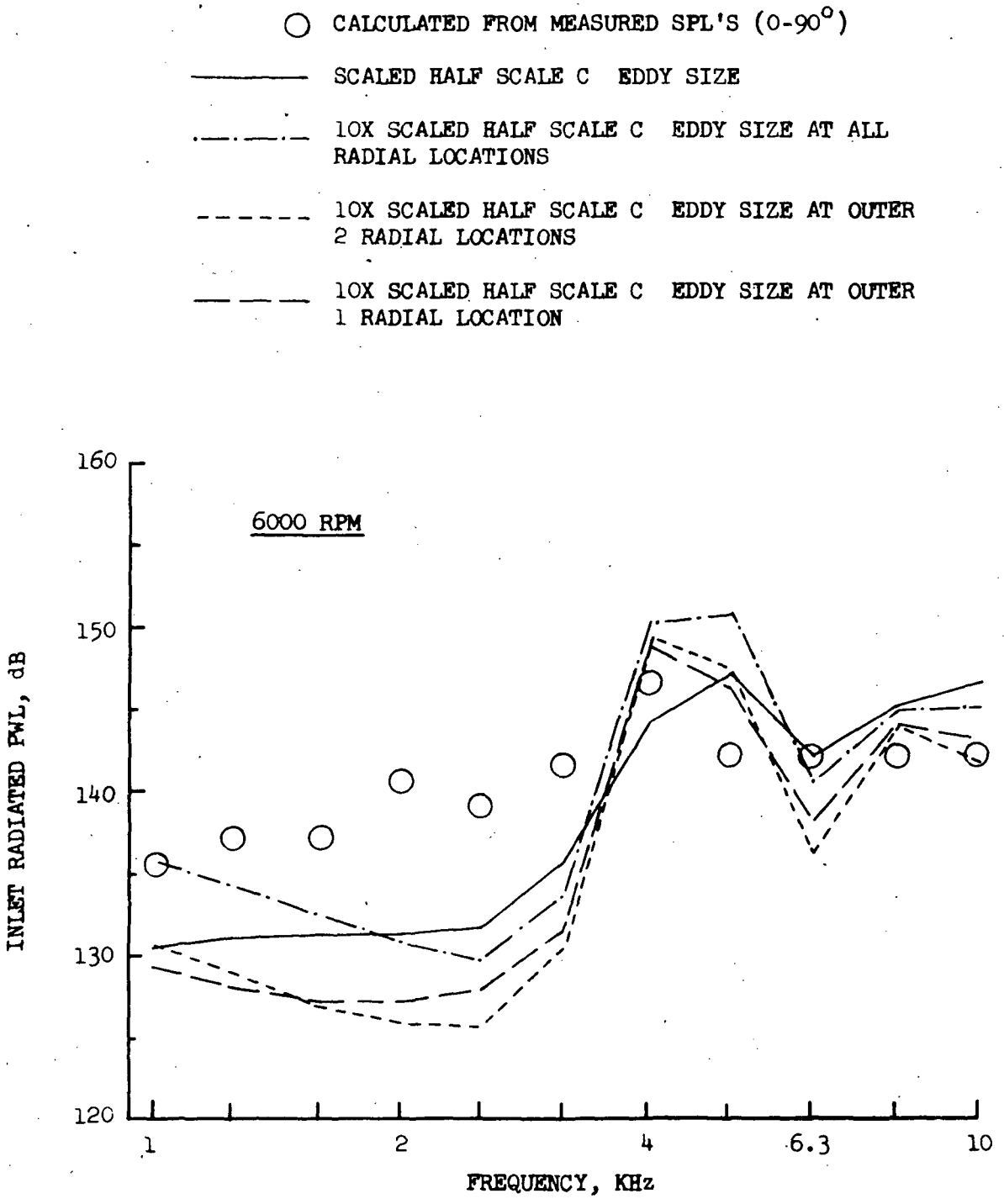

FIGURE 41 COMPARISON OF MEASURED AND PREDICTED INLET RADIATED SOUND POWER LEVELS VARYING EDDY SIZE AT RADIAL LOCATIONS

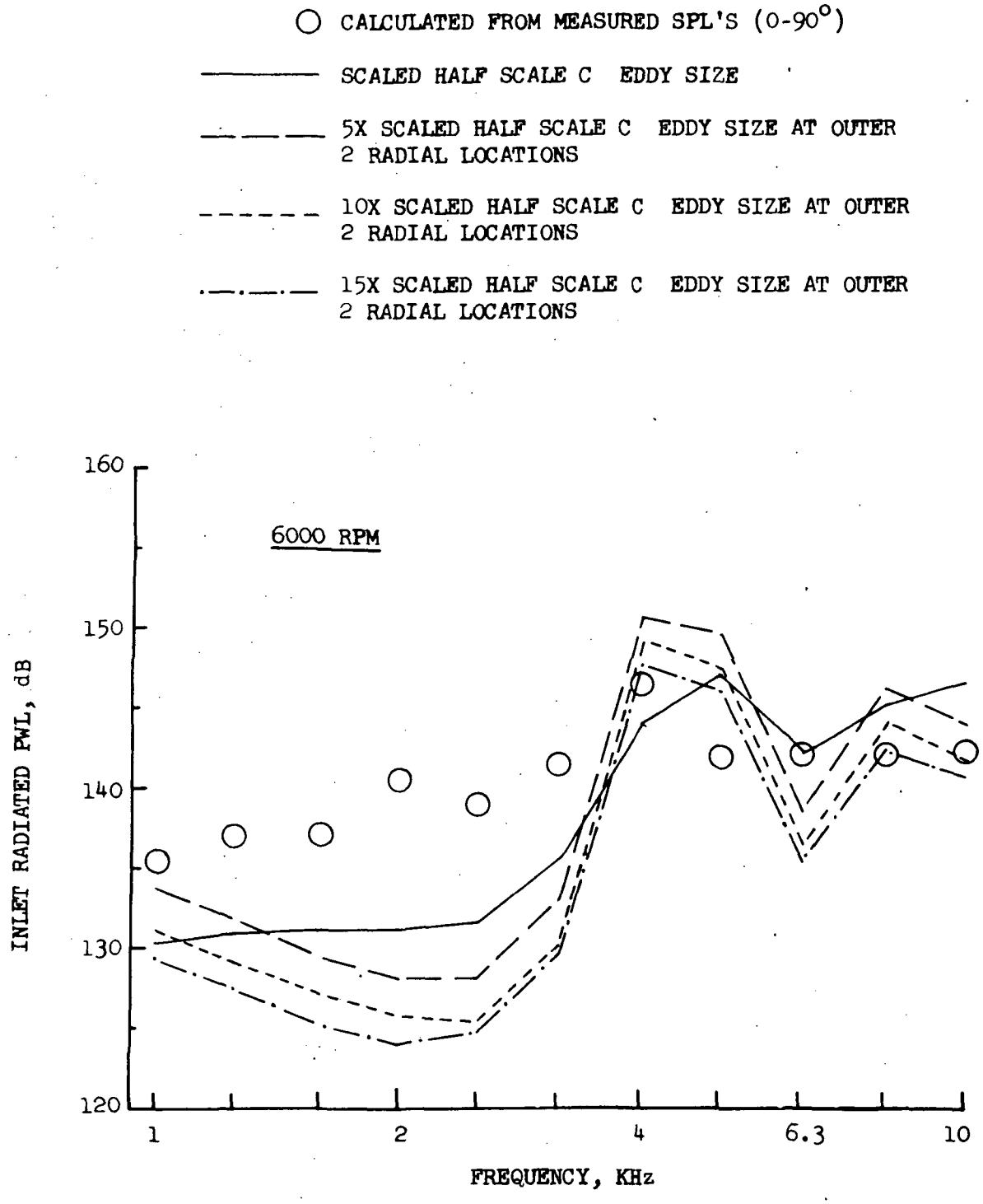

FIGURE 42 COMPARISON OF MEASURED AND PREDICTED INLET RADIATED SOUND POWER LEVELS VARYING EDDY SIZE AT OUTER TWO RADIAL LOCATIONS

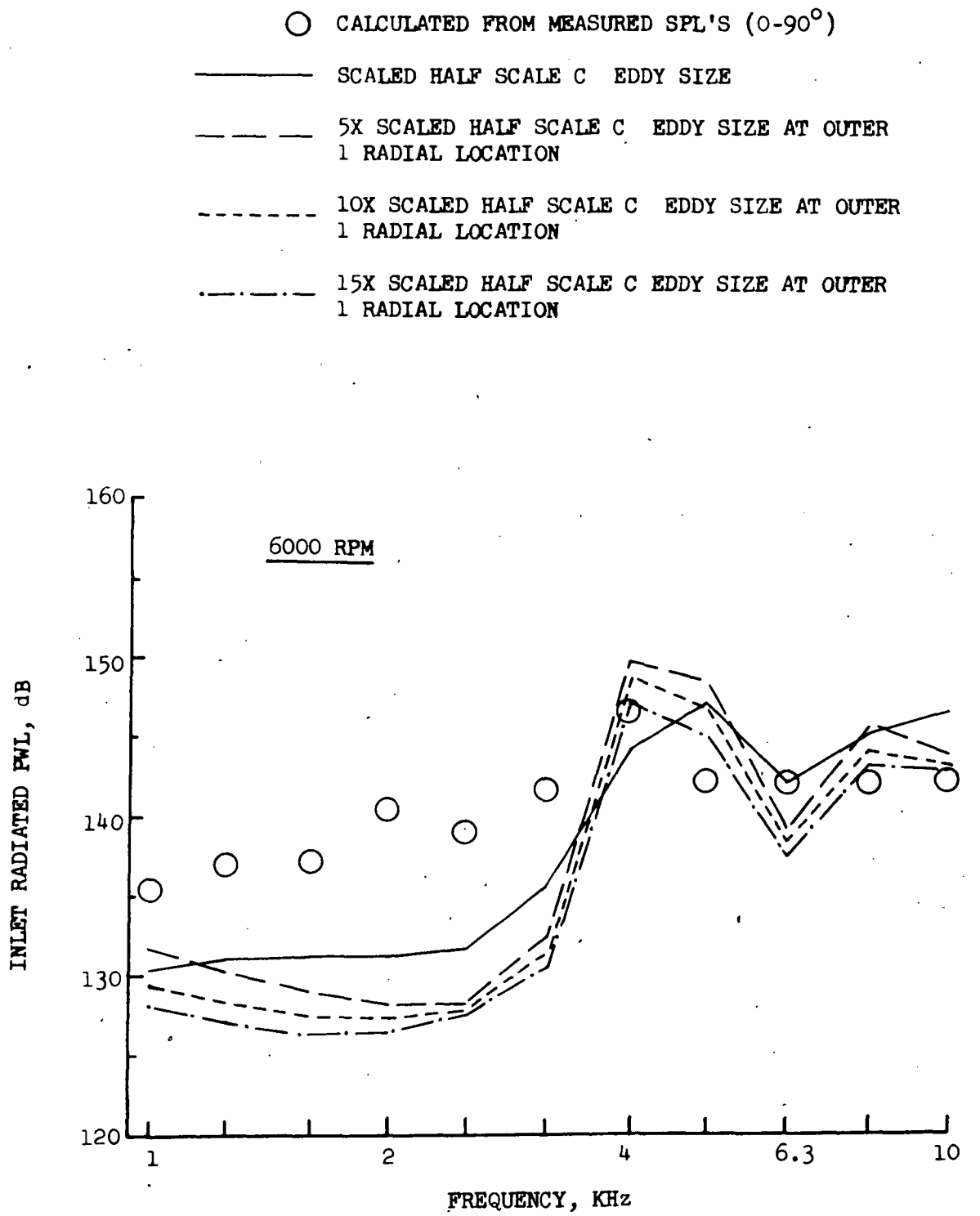

FIGURE 43 COMPARISON OF MEASURED AND PREDICTED INLET RADIATED SOUND POWER LEVELS VARYING EDDY SIZE AT OUTERMOST RADIAL LOCATION

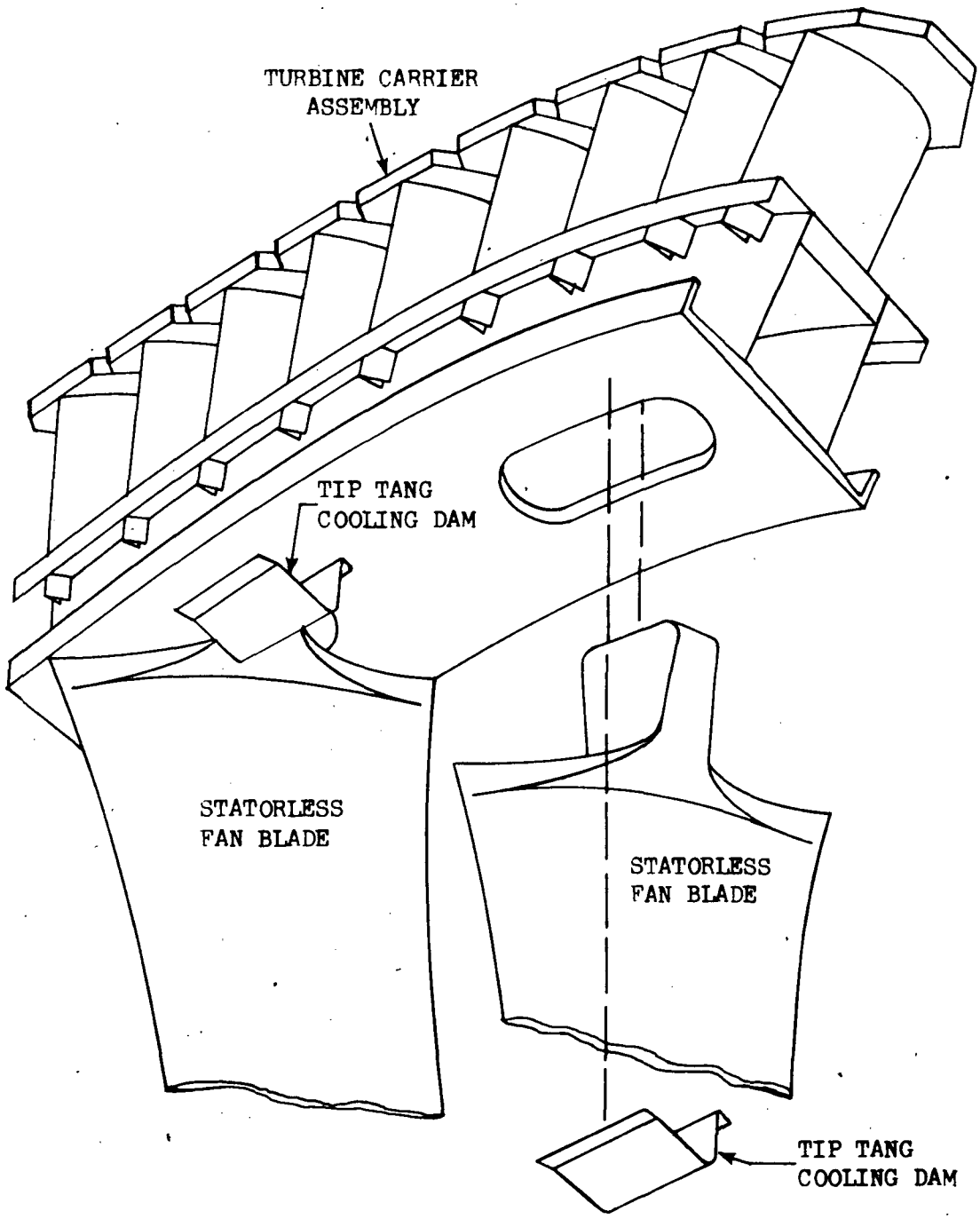

FIGURE 44 LOCATION OF LF336/E STATORLESS FAN TIP TANG COOLING DAMS

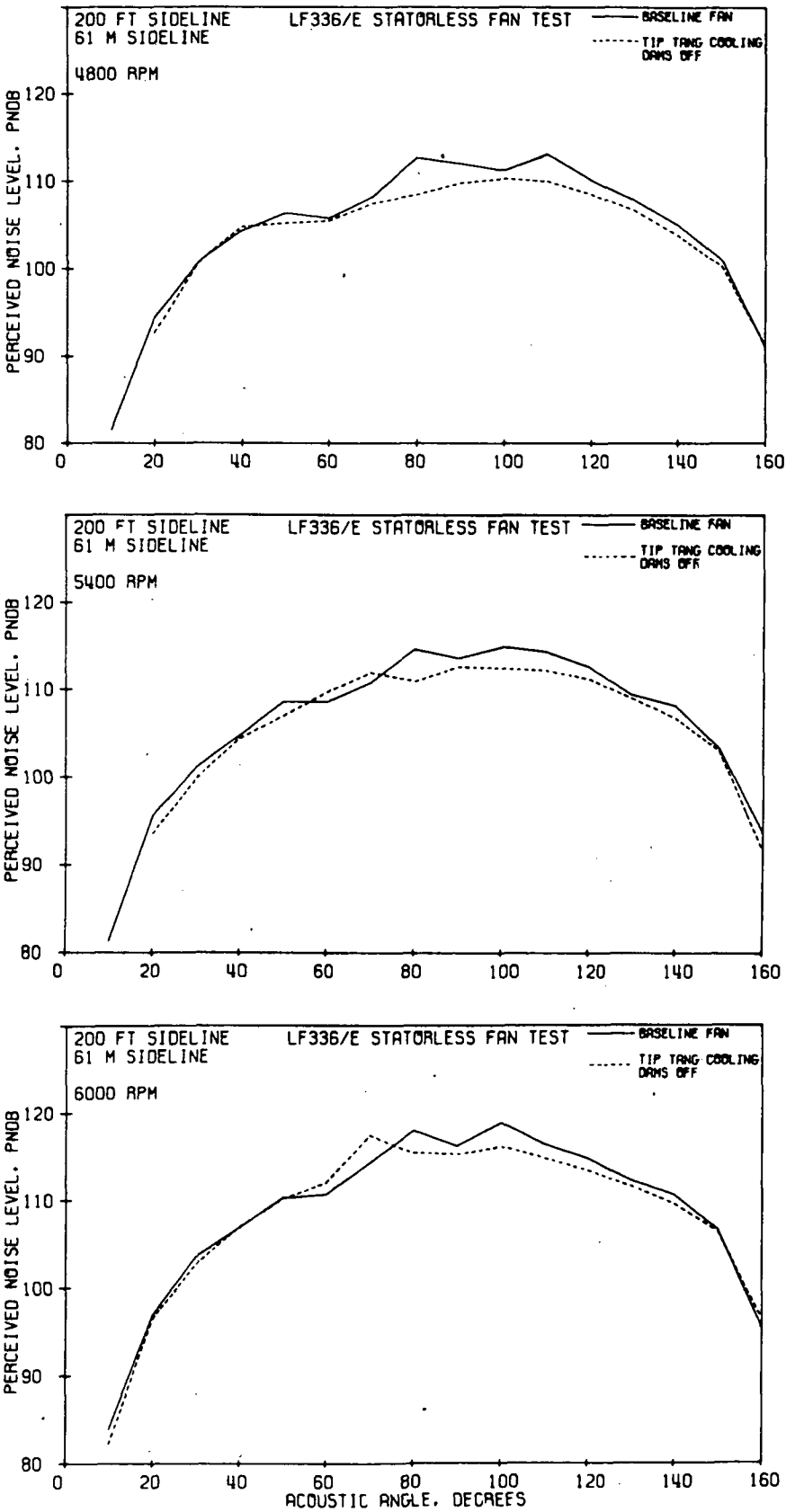

FIGURE 45 EFFECT OF TIP TANG COOLING DAMS ON PNL DIRECTIVITY PATTERNS AT 4800, 5400, AND 6000 RPM

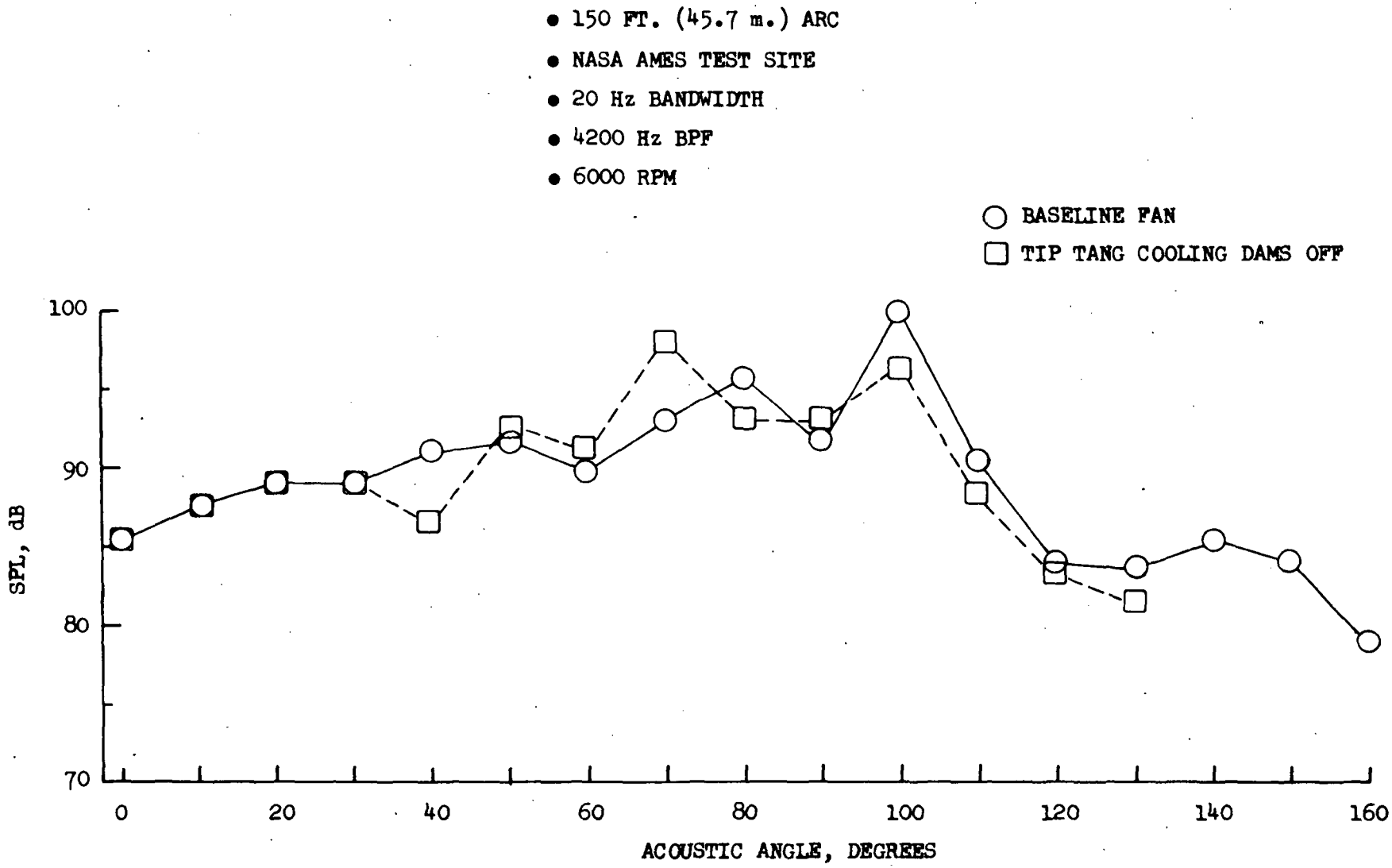

FIGURE 46 EFFECT OF TIP TANG COOLING DAMS ON NARROWBAND BPF DIRECTIVITY PATTERNS AT 6000 RPN

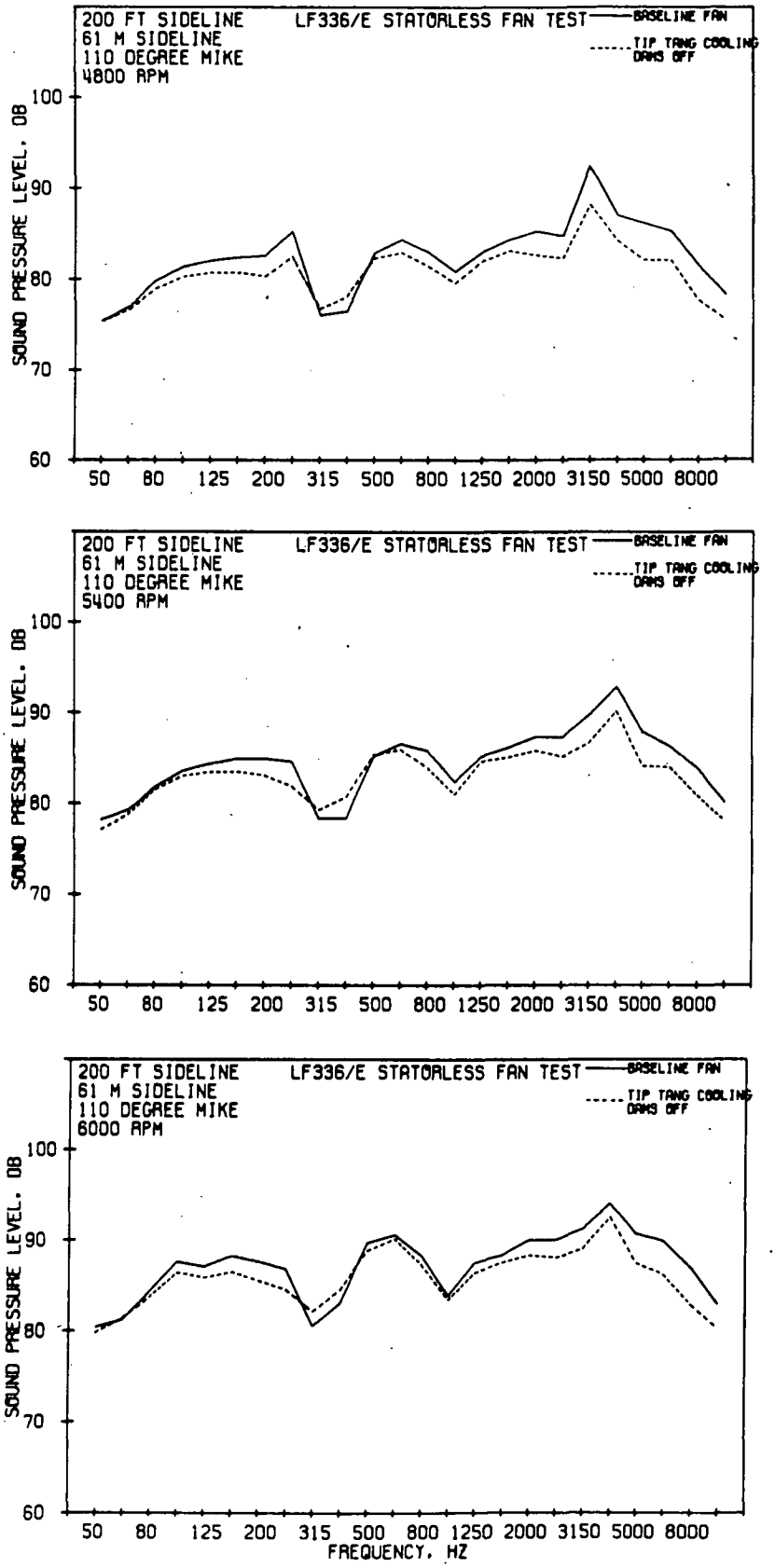

FIGURE 47 EFFECT OF TIP TANG COOLING DAMS ON 110° 1/3 OCTAVE BAND SPECTRA AT 4800, 5400, AND 6000 RPM

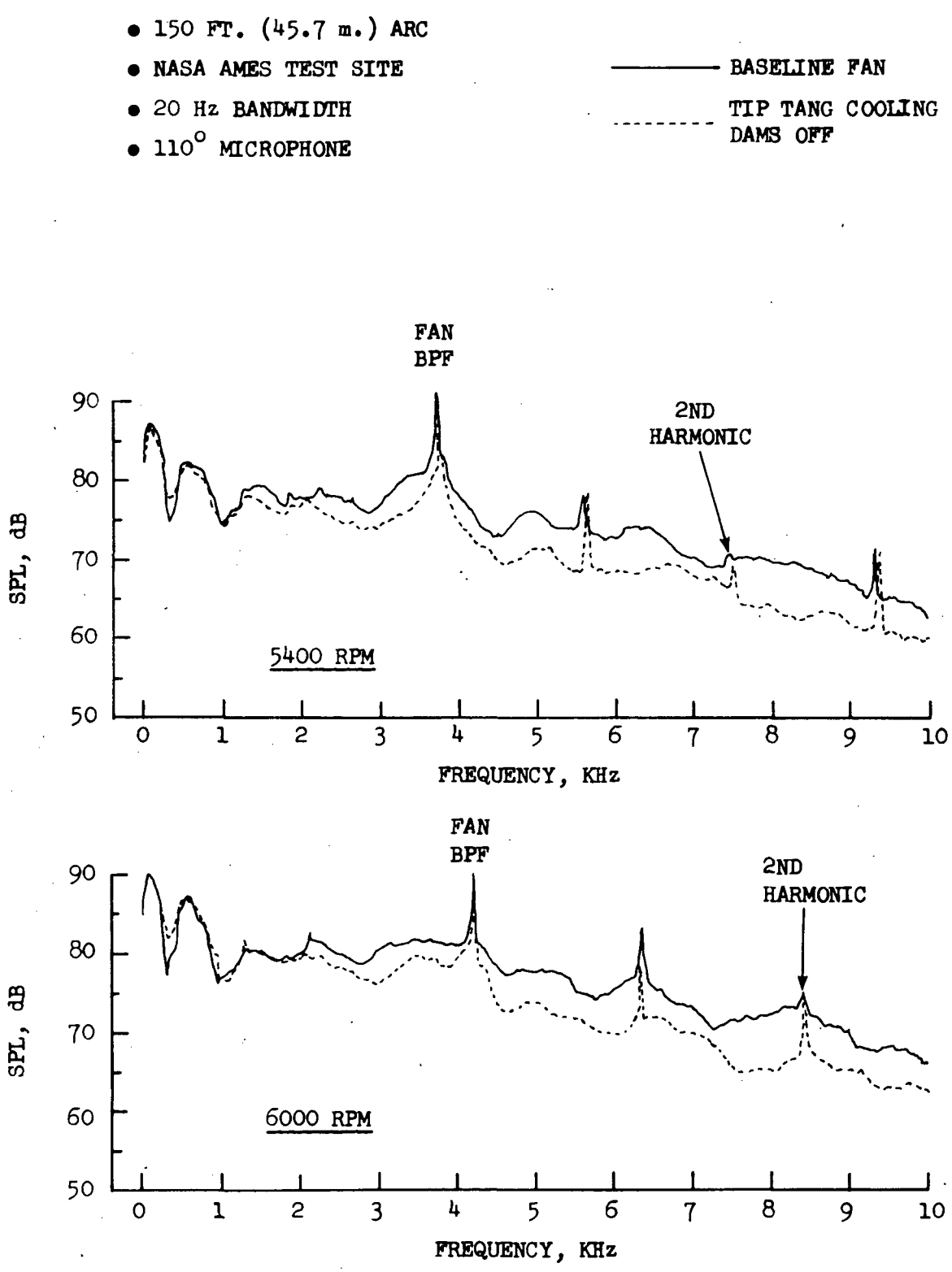

FIGURE 48 EFFECT OF TIP TANG COOLING DAMS ON 110° NARROWBAND SPECTRA

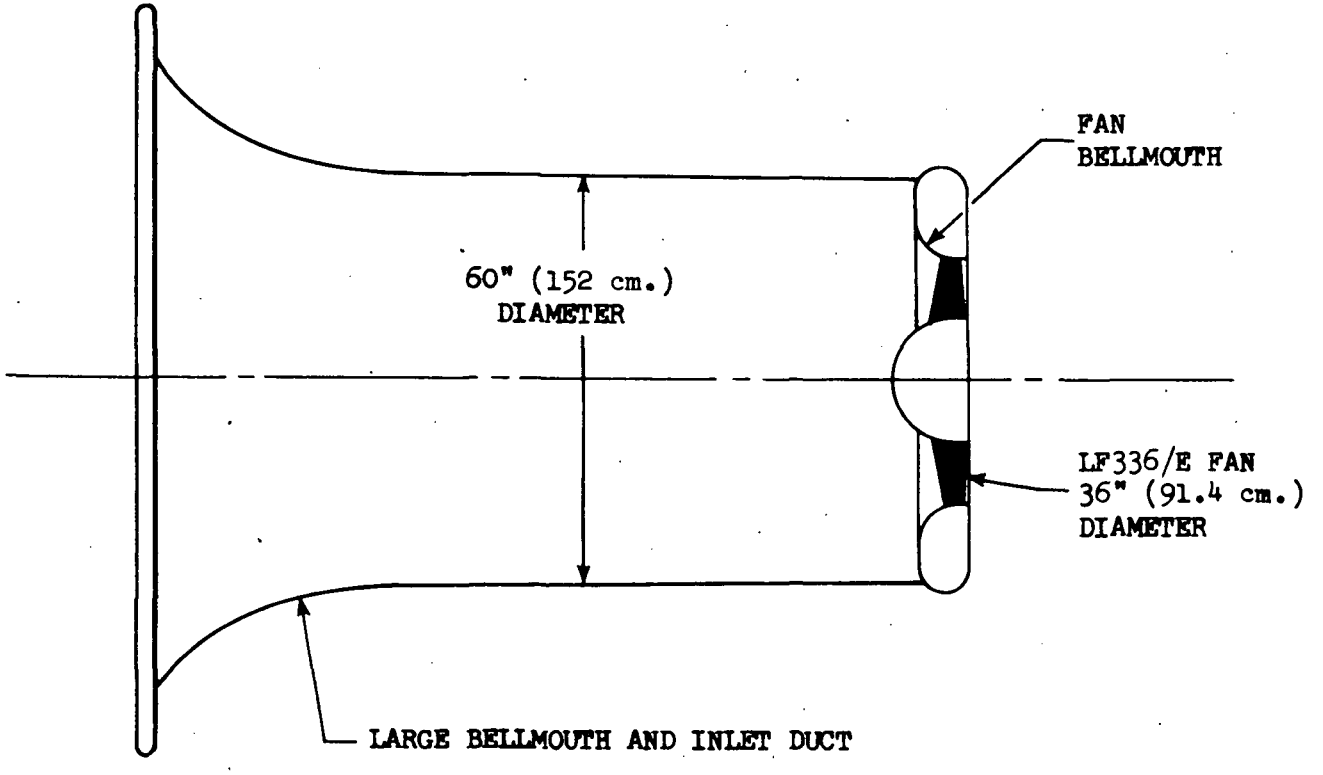

FIGURE 49 SKETCH OF LARGE BELLMOUTH INSTALLED ON THE LF336/E STATORLESS LIFT FAN

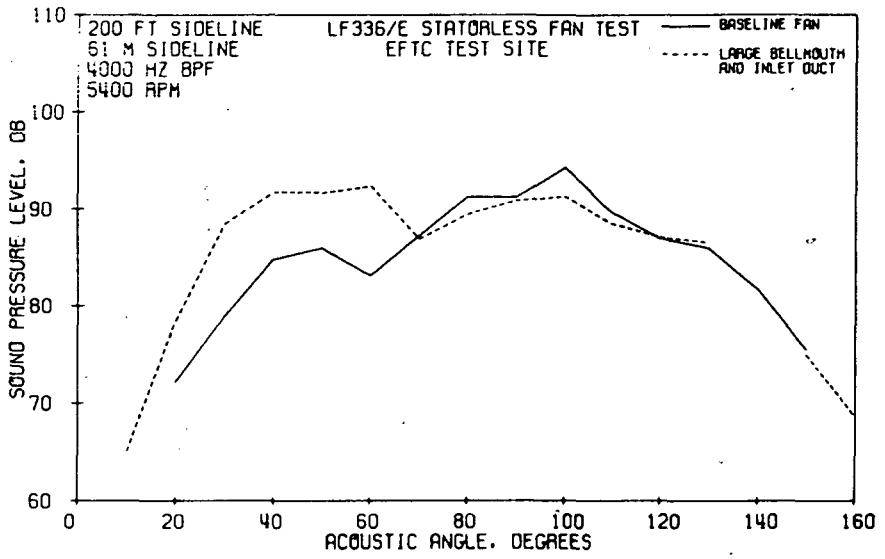

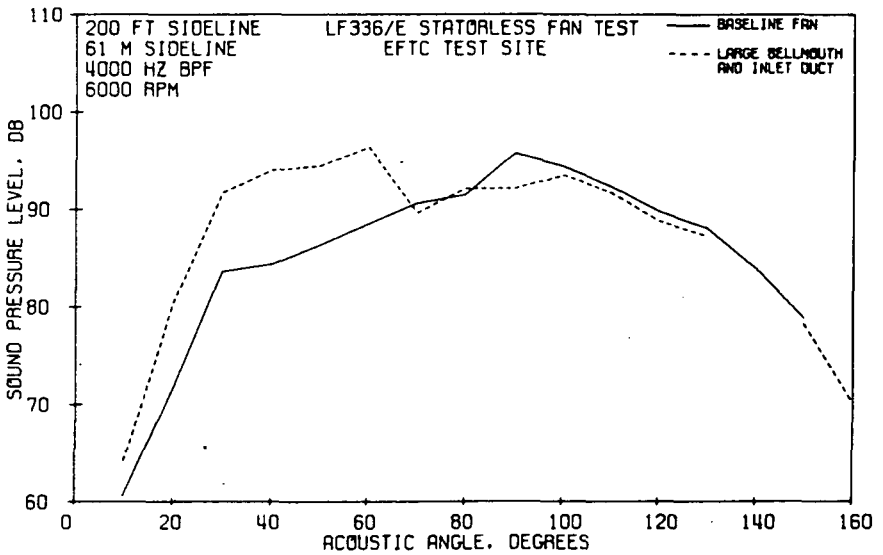

FIGURE 50 EFFECT OF LARGE BELLMOUTH ON 1/3 OCTAVE BAND BPF DIRECTIVITY PATTERNS AT 5400 AND 6000 RPM

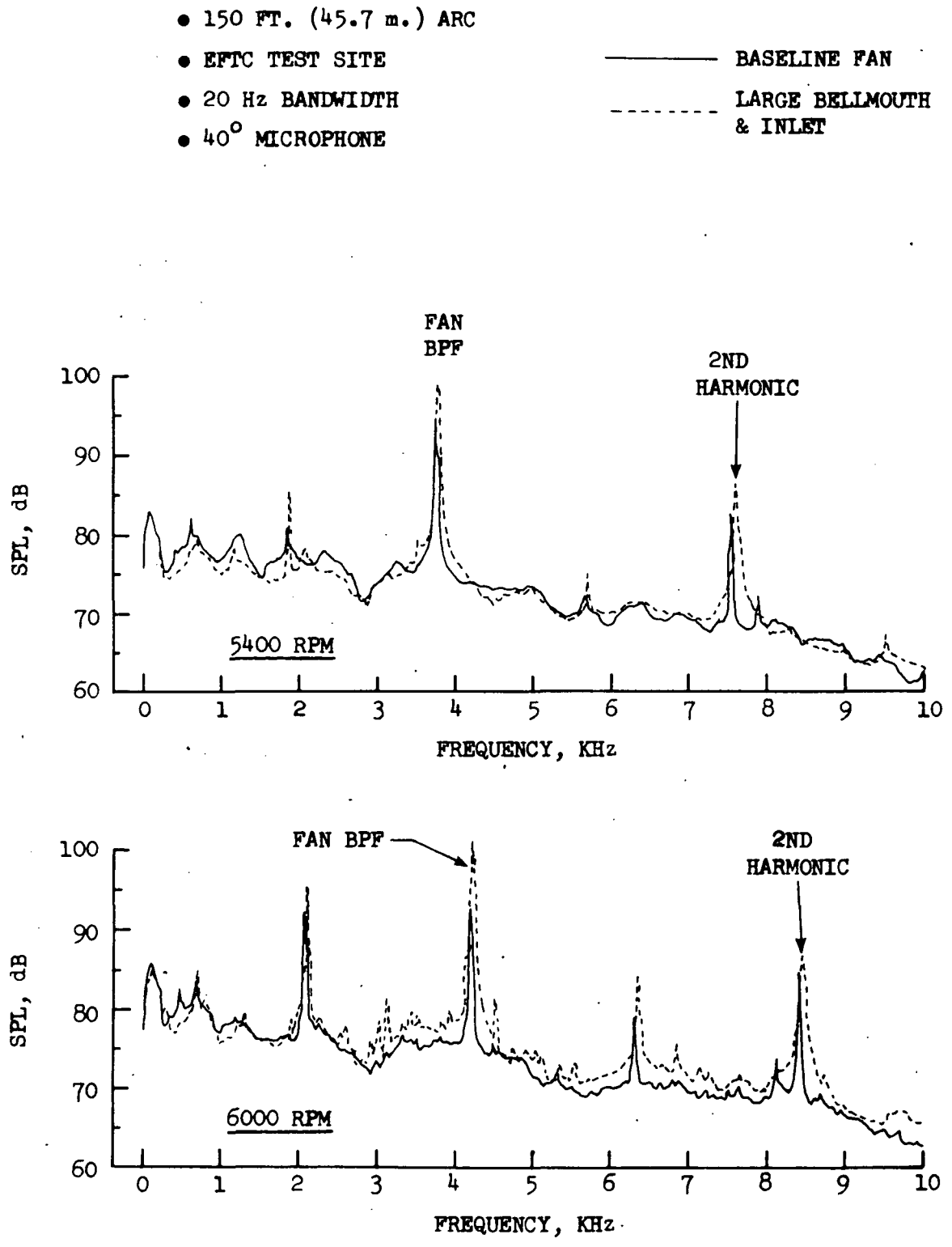

FIGURE 51 EFFECT OF LARGE BELLMOUTH ON 40° NARROWBAND SPECTRA AT 5400 AND 6000 RPM

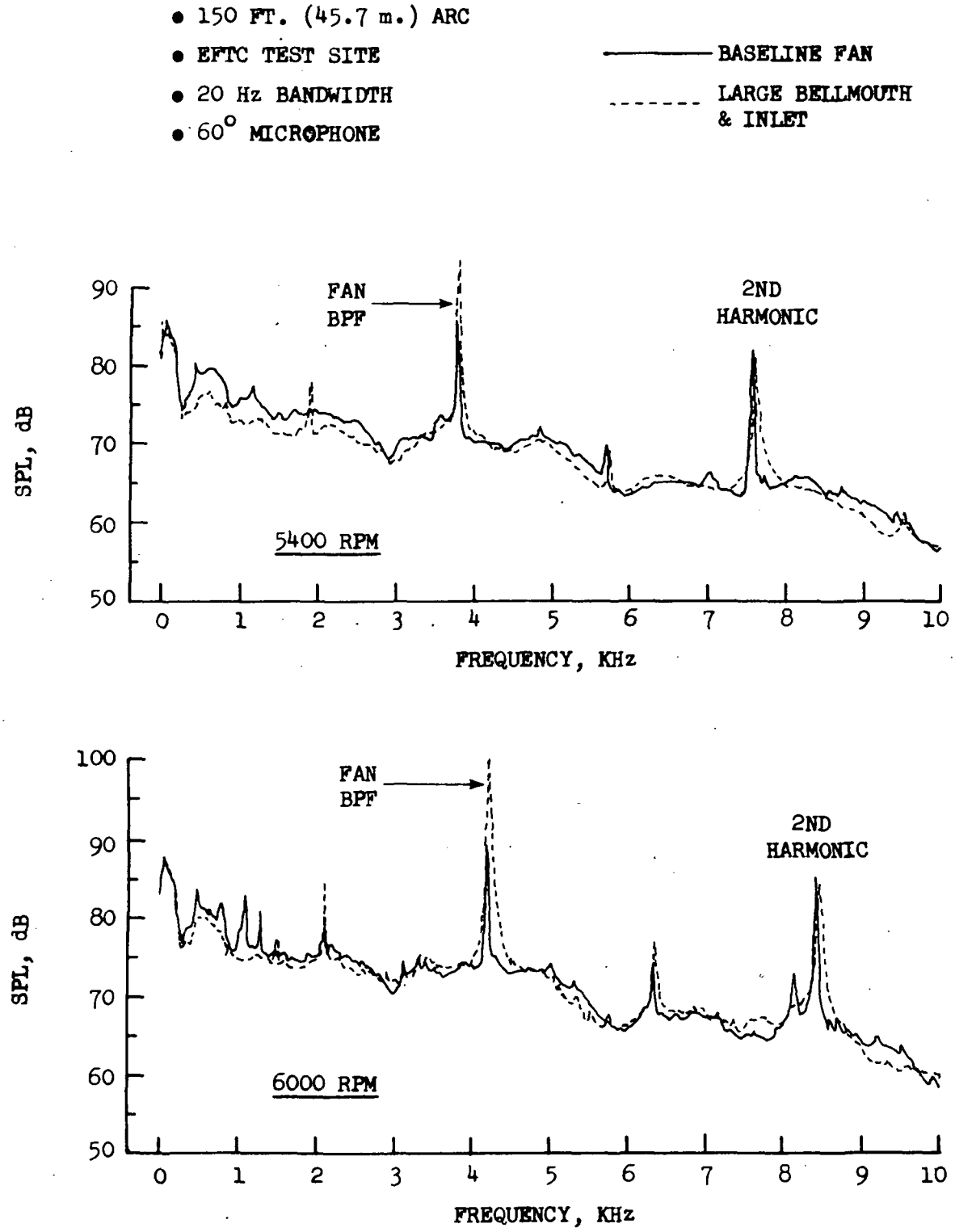

FIGURE 52 EFFECT OF LARGE BELLMOUTH ON 60° NARROWBAND SPECTRA AT 5400 AND 6000 RPM

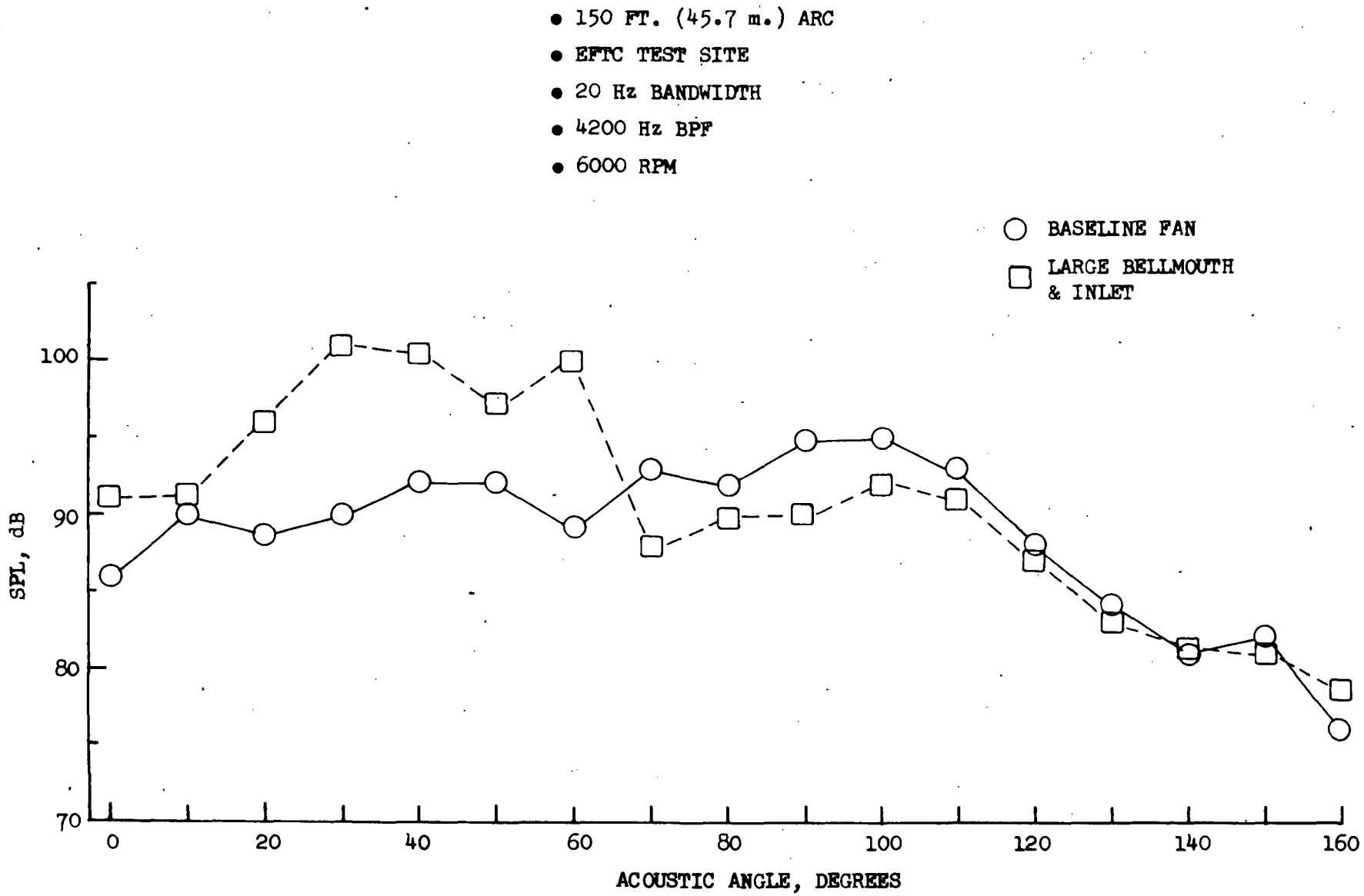

FIGURE 53 EFFECT OF LARGE BELLMOUTH ON NARROWBAND BPF DIRECTIVITY PATTERNS AT 6000 RPM AT EFTC

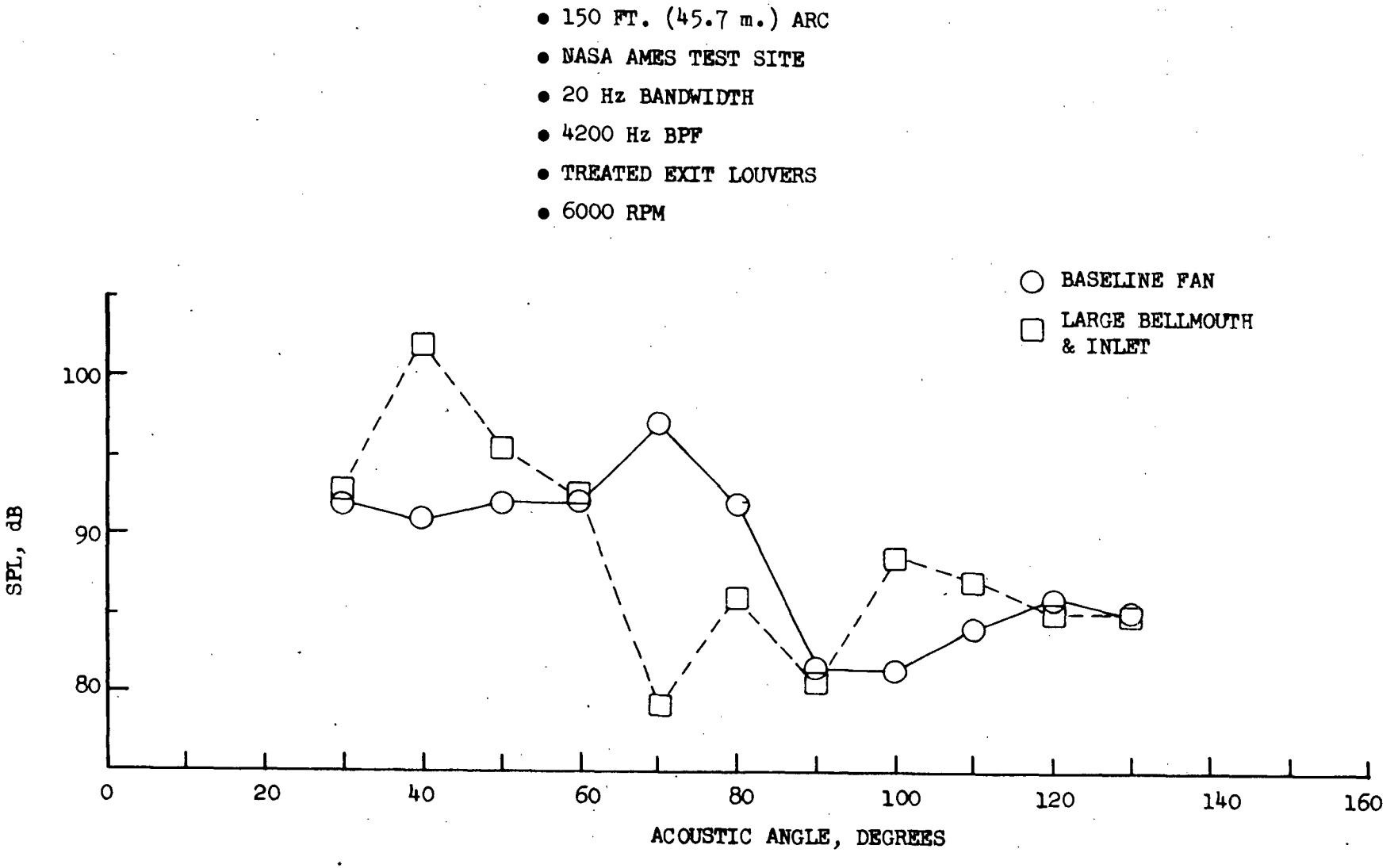

FIGURE 54 EFFECT OF LARGE BELLMOUTH ON NARROWBAND BPF DIRECTIVITY PATTERN AT 6000 RPM AT NASA AMES

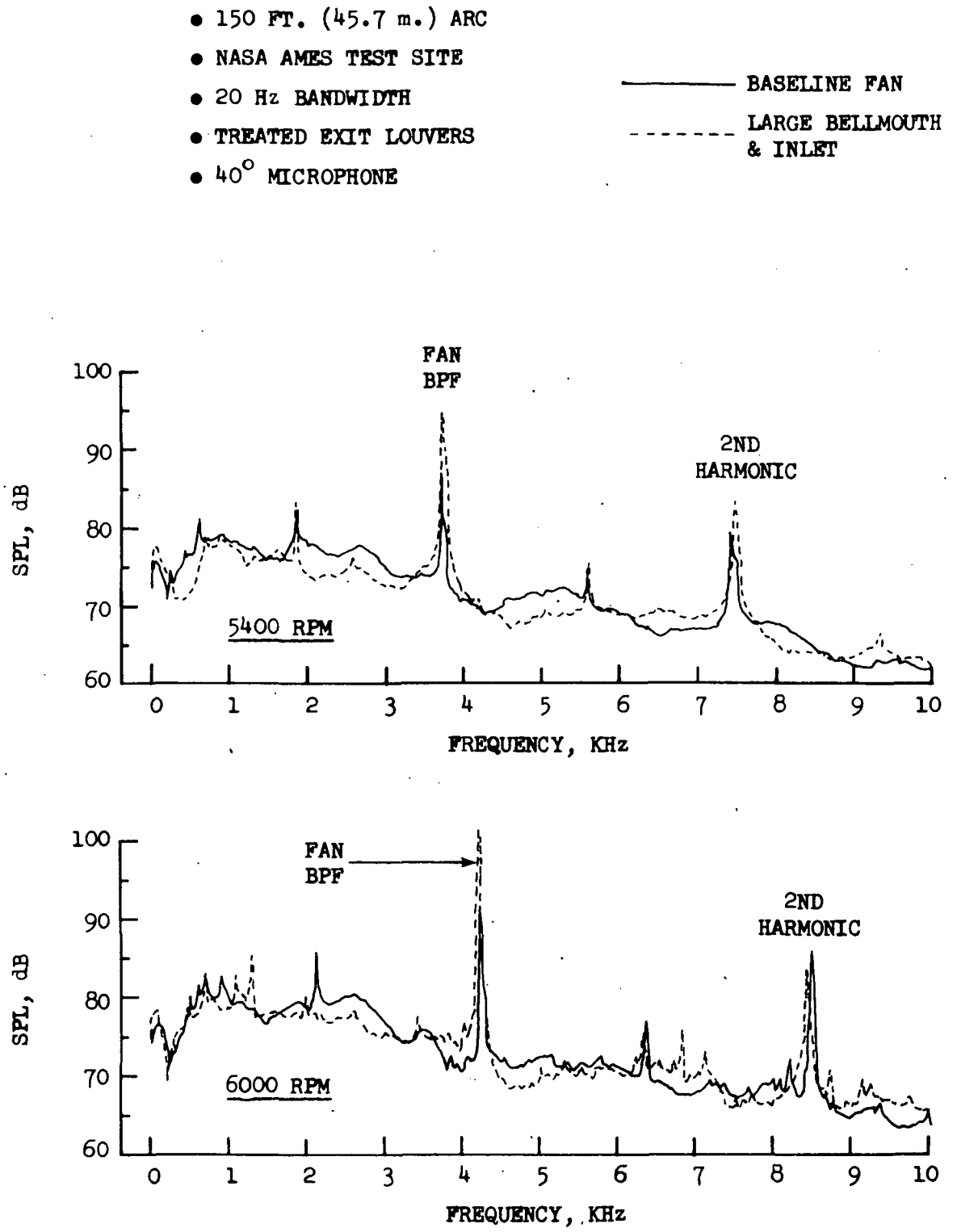

FIGURE 55 EFFECT OF LARGE BELMOUTH ON 40° NARROWBAND SPECTRA AT 5400 AND 6000 RPM AT NASA AMES

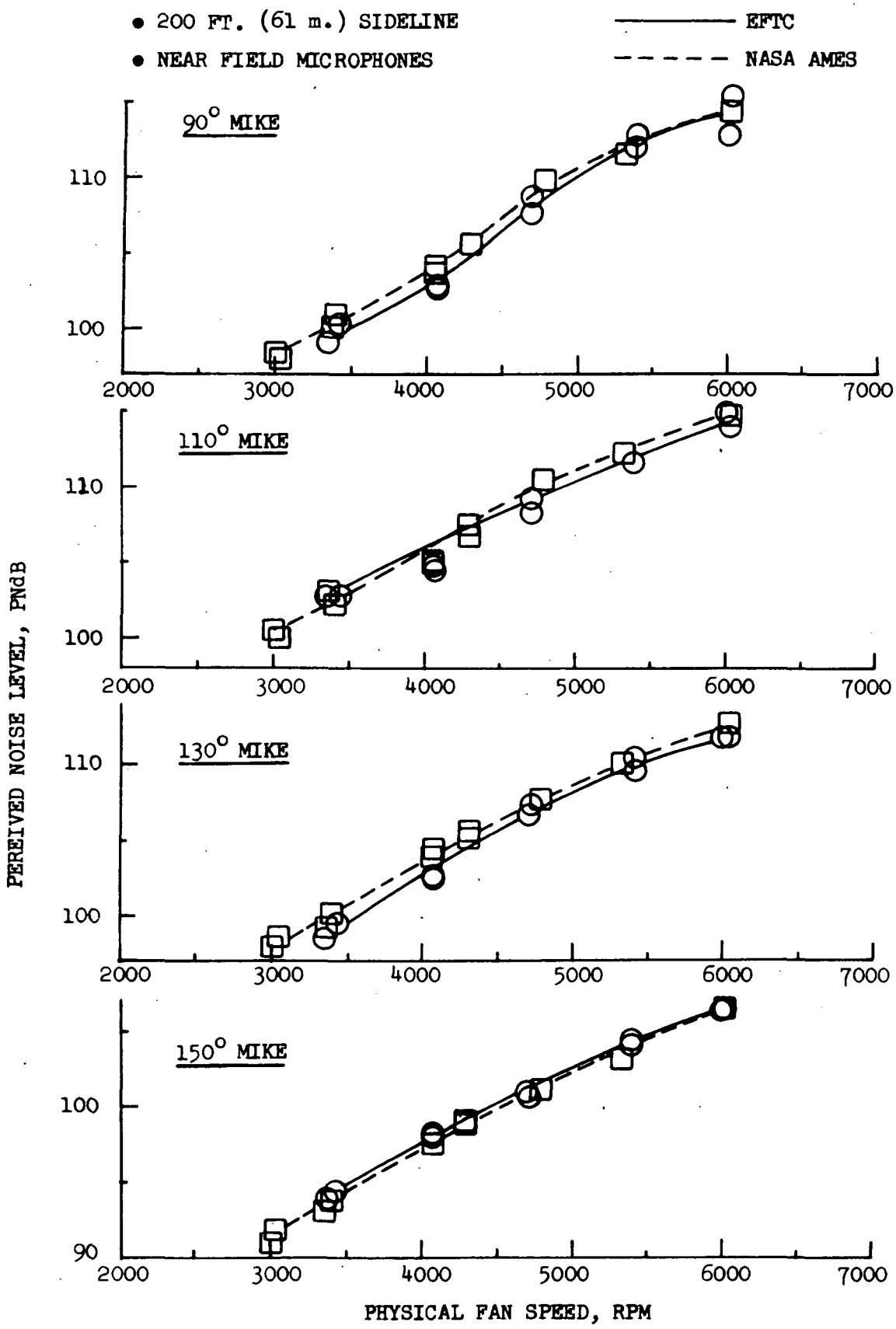

FIGURE 56 COMPARISON OF EFTC AND NASA AMES NEAR FIELD PNL'S AS A FUNCTION OF FAN SPEED

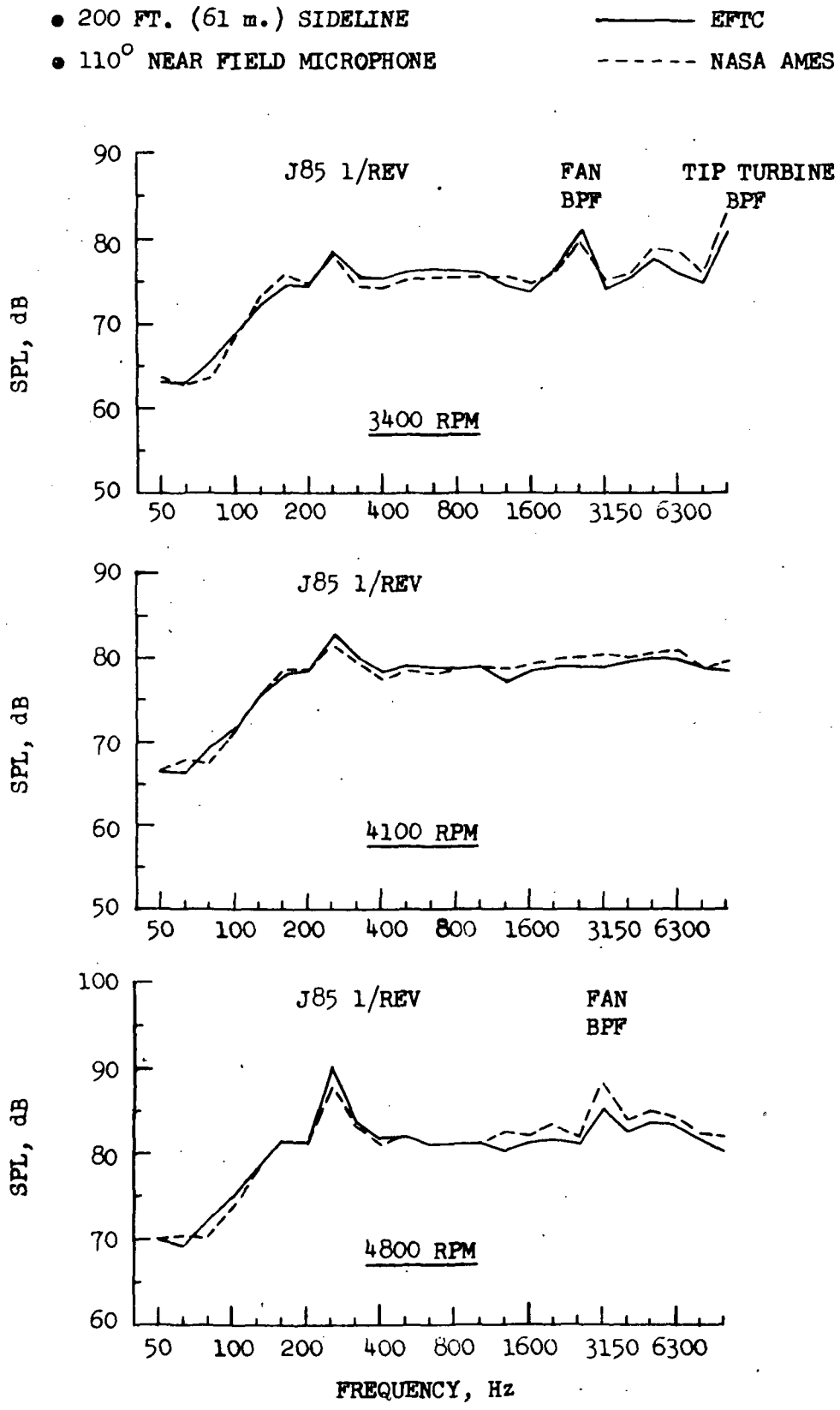

FIGURE 57 EFTC AND NASA AMES 110° NEAR FIELD 1/3 OCTAVE BAND SPECTRAL COMPARISON AT 3400, 4100, AND 4800 RPM

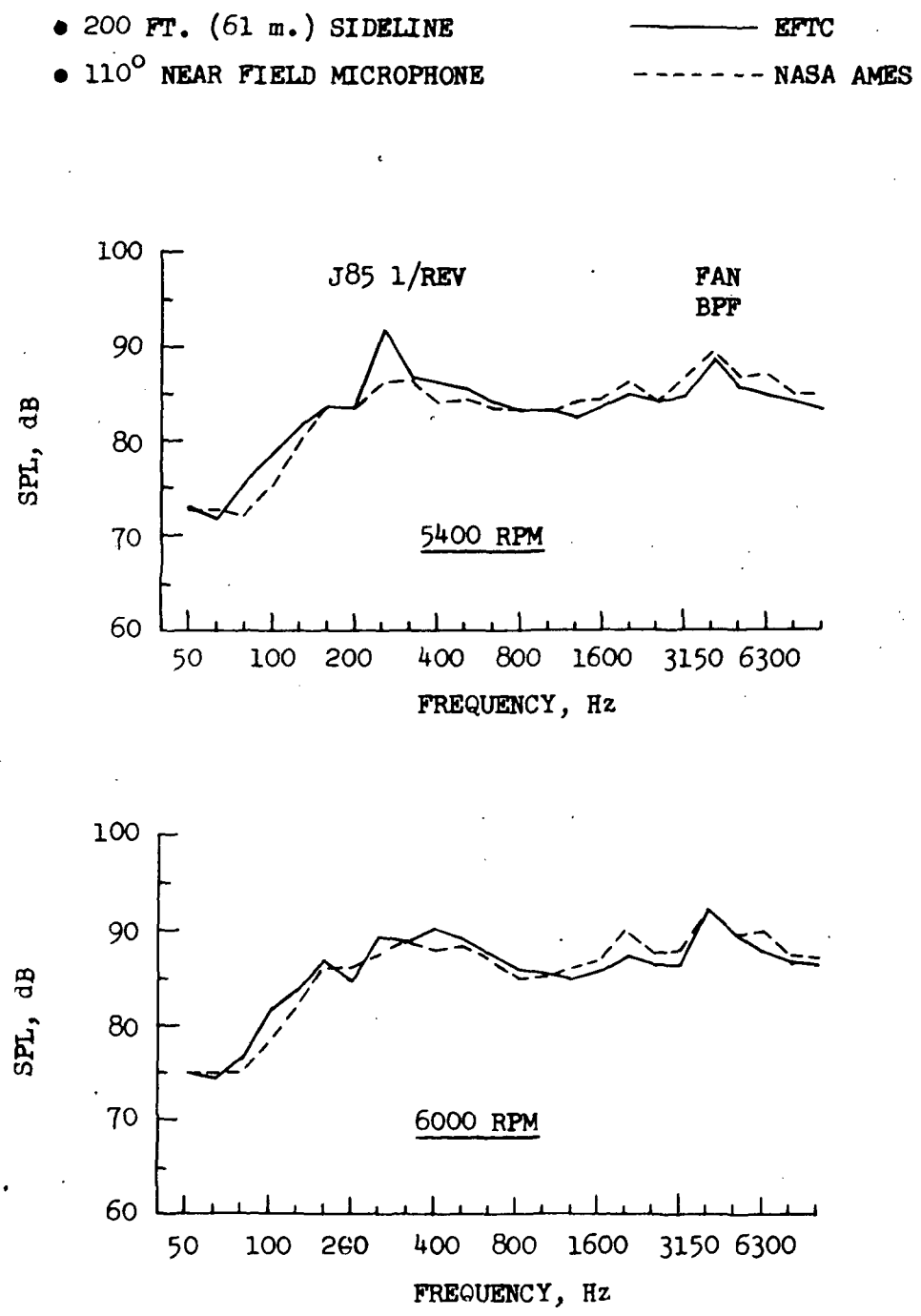

FIGURE 58 EFTC AND NASA AMES 110° NEAR FIELD 1/3 OCTAVE BAND SPECTRAL COMPARISON AT 5400 AND 6000 RPM

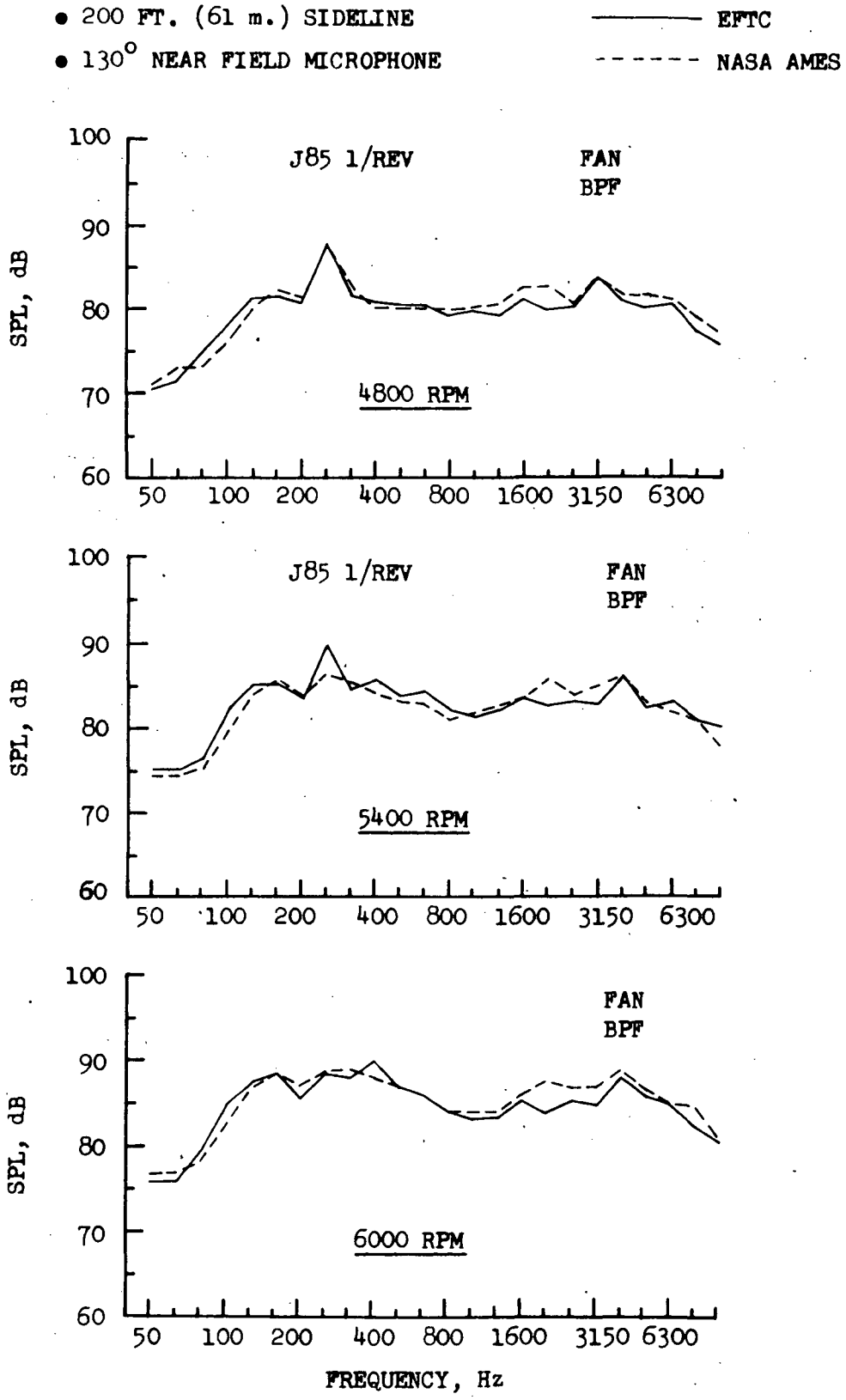

FIGURE 59 EFTC AND NASA AMES 130° NEAR FIELD 1/3 OCTAVE BAND SPECTRAL COMPARISON AT 4800, 5400, AND 6000 RPM

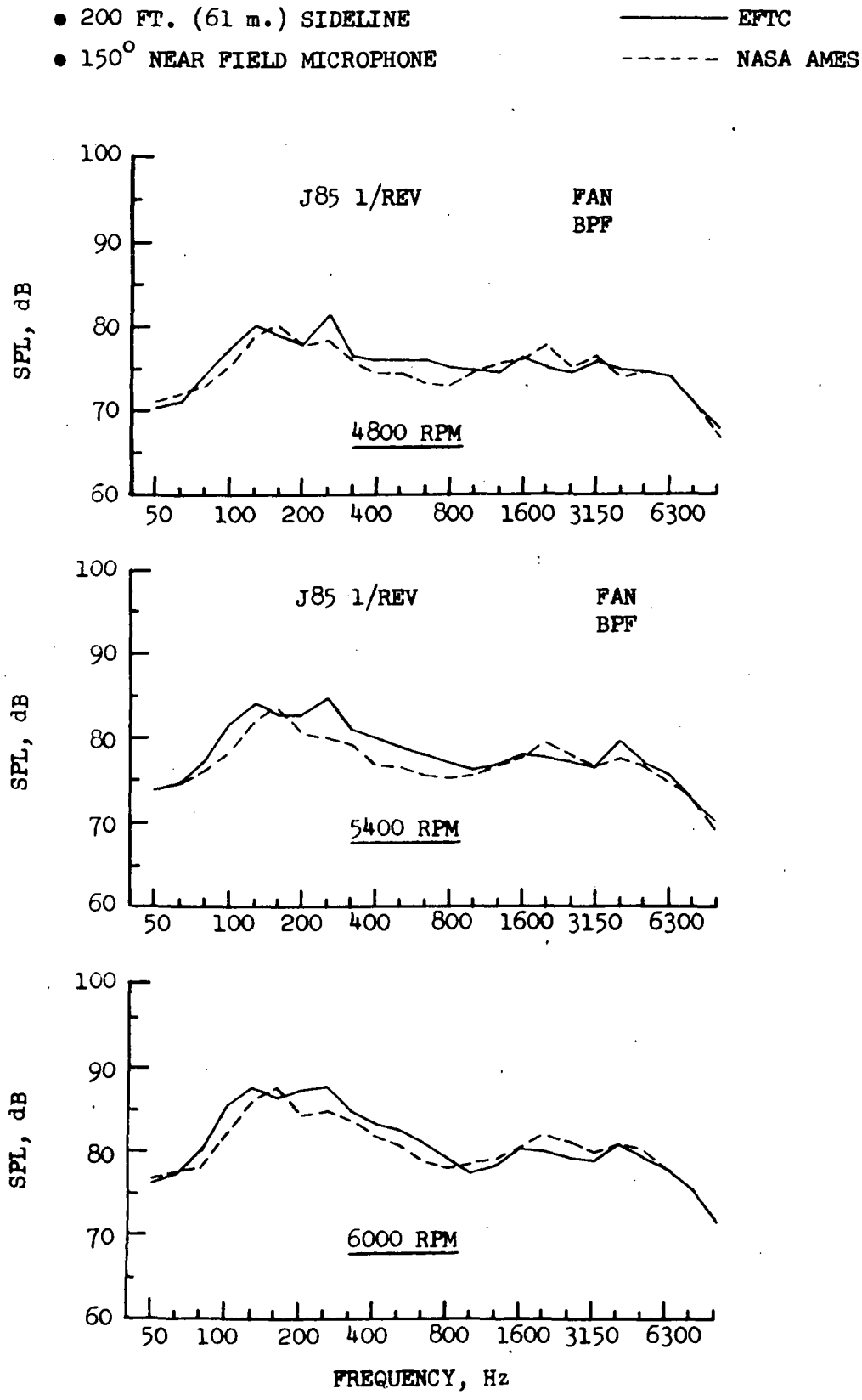

FIGURE 60 EFTC AND NASA AMES 150° NEAR FIELD 1/3 OCTAVE BAND SPECTRAL COMPARISON AT 4800, 5400, AND 6000 RPM

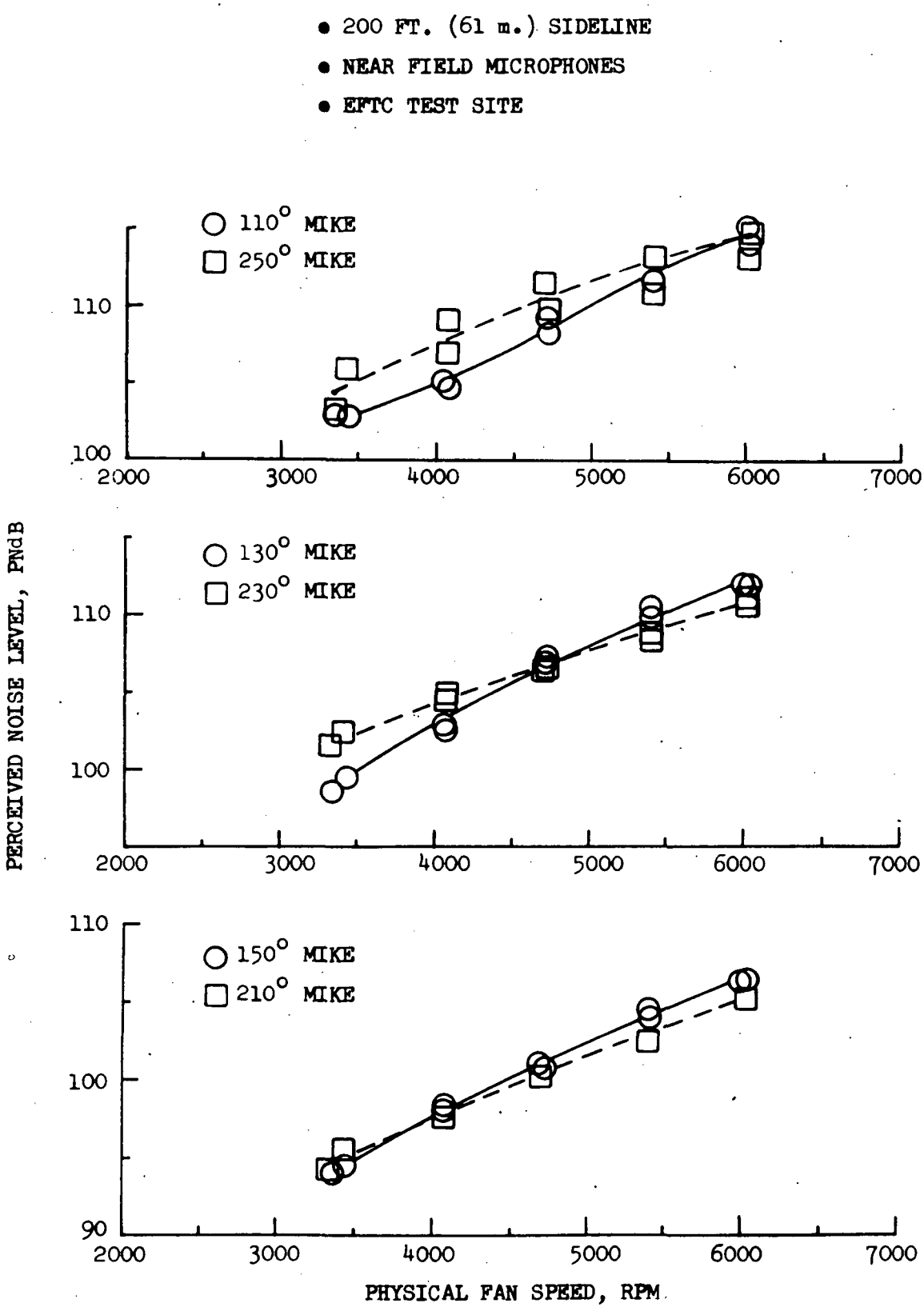

FIGURE 61 SYMMETRICALLY LOCATED NEAR FIELD MICROPHONE PNL COMPARISON AS A FUNCTION OF FAN SPEED

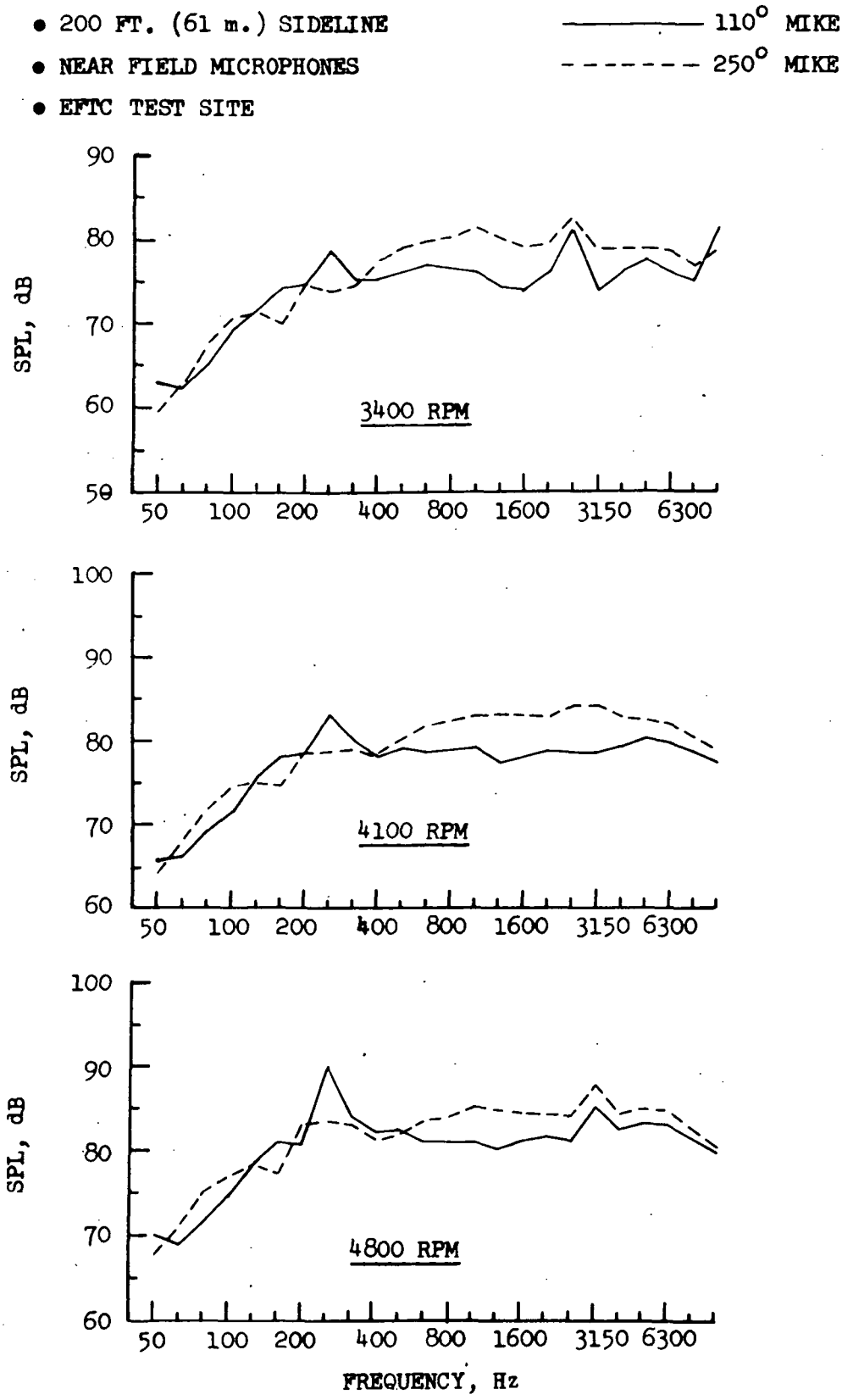

FIGURE 62 COMPARISON OF 110° AND 250° NEAR FIELD MICROPHONE 1/3 OCTAVE BAND SPECTRA AT 3400, 4100, AND 4800 RPM

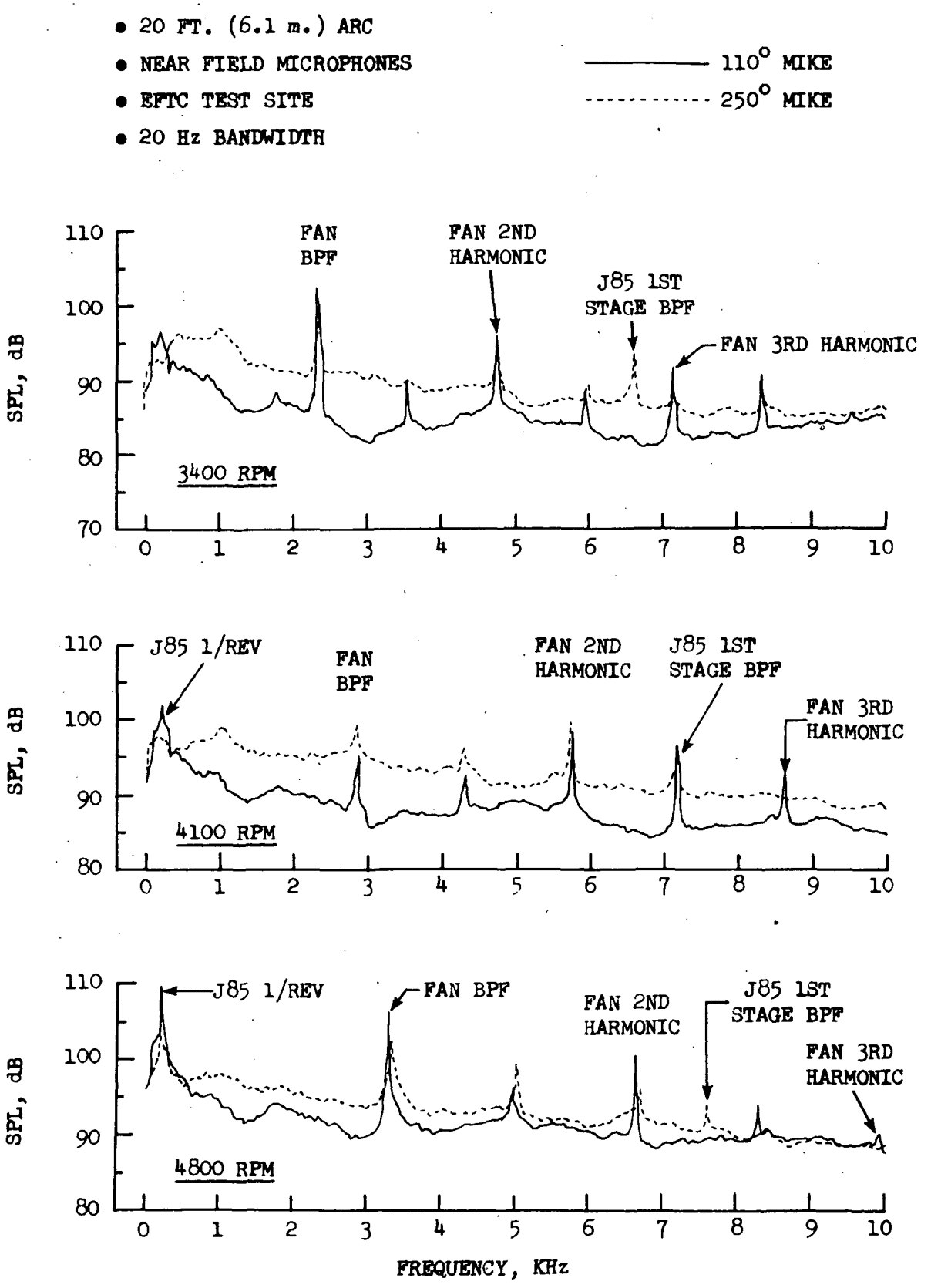

FIGURE 63 COMPARISON OF 110° AND 250° NEAR FIELD MICROPHONE 20 Hz NARROWBAND SPECTRA AT 3400, 4100, AND 4800 RPM

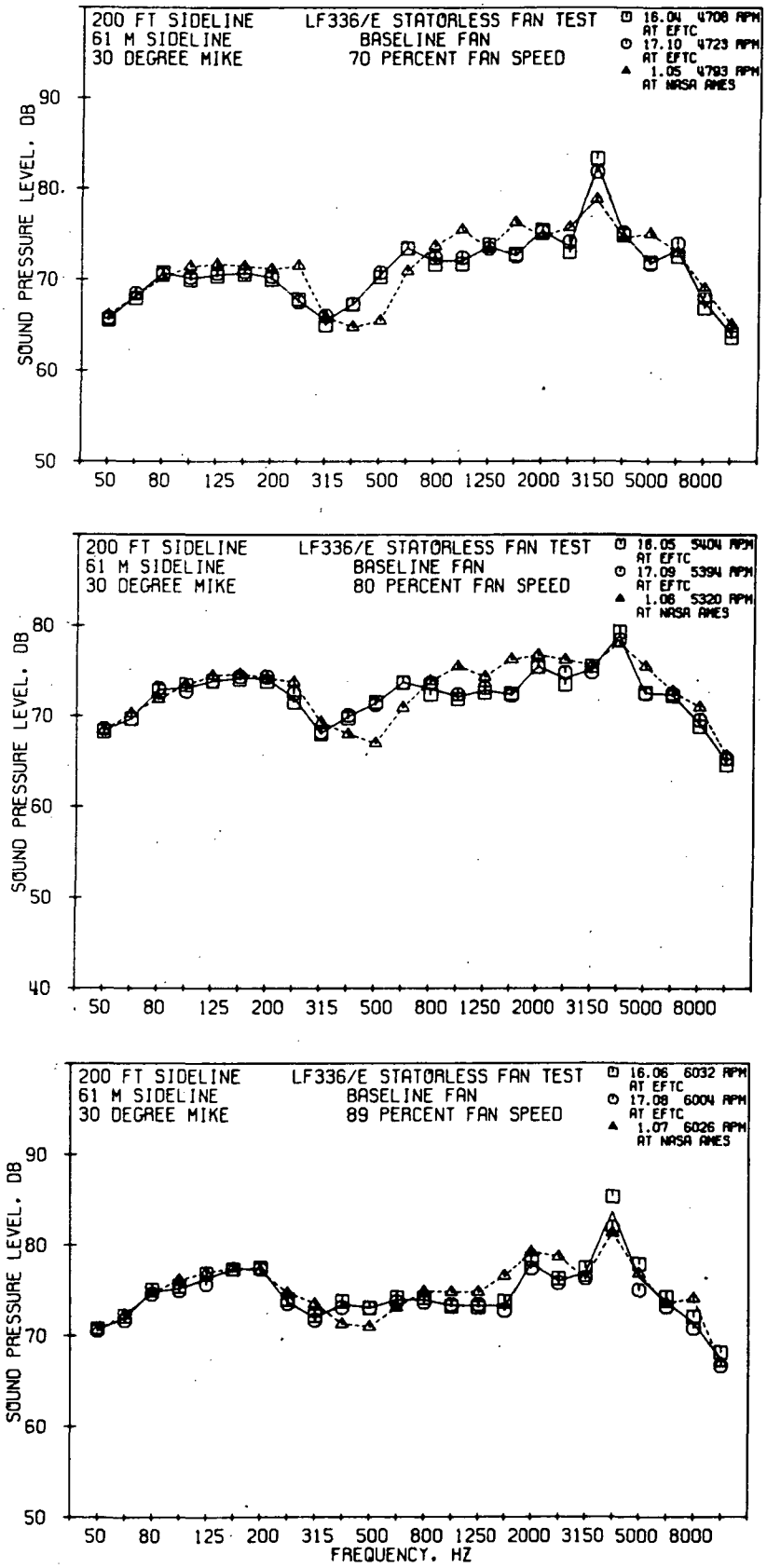

FIGURE 64 EFTC AND NASA AMES 30° FAR FIELD 1/3 OCTAVE BAND SPECTRAL COMPARISONS AT 4800, 5400, AND 6000 RPM

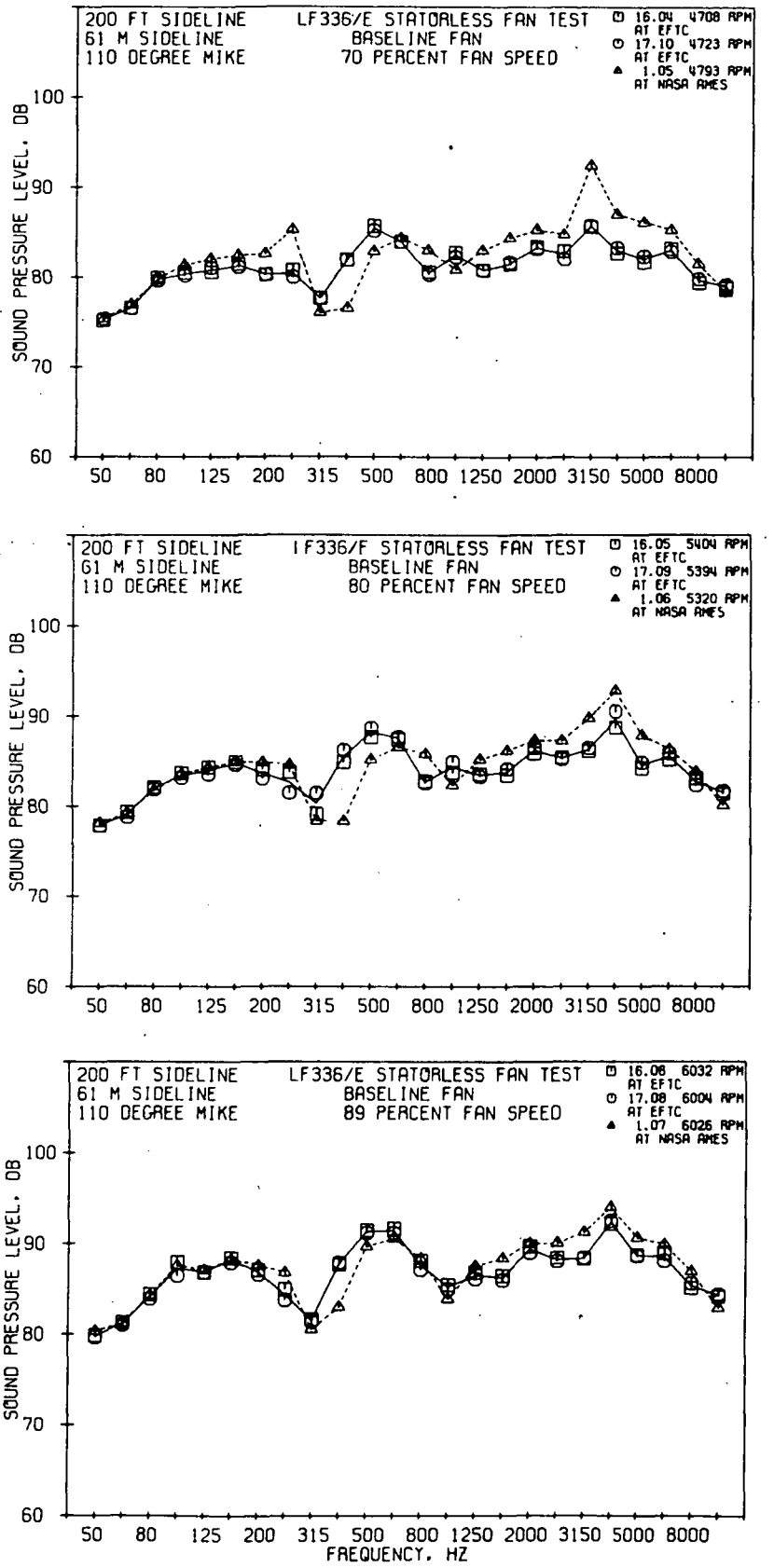

FIGURE 65 EFTC AND NASA AMES 110° FAR FIELD 1/3 OCTAVE BAND SPECTRAL COMPARISONS AT 4800, 5400, AND 6000 RPM

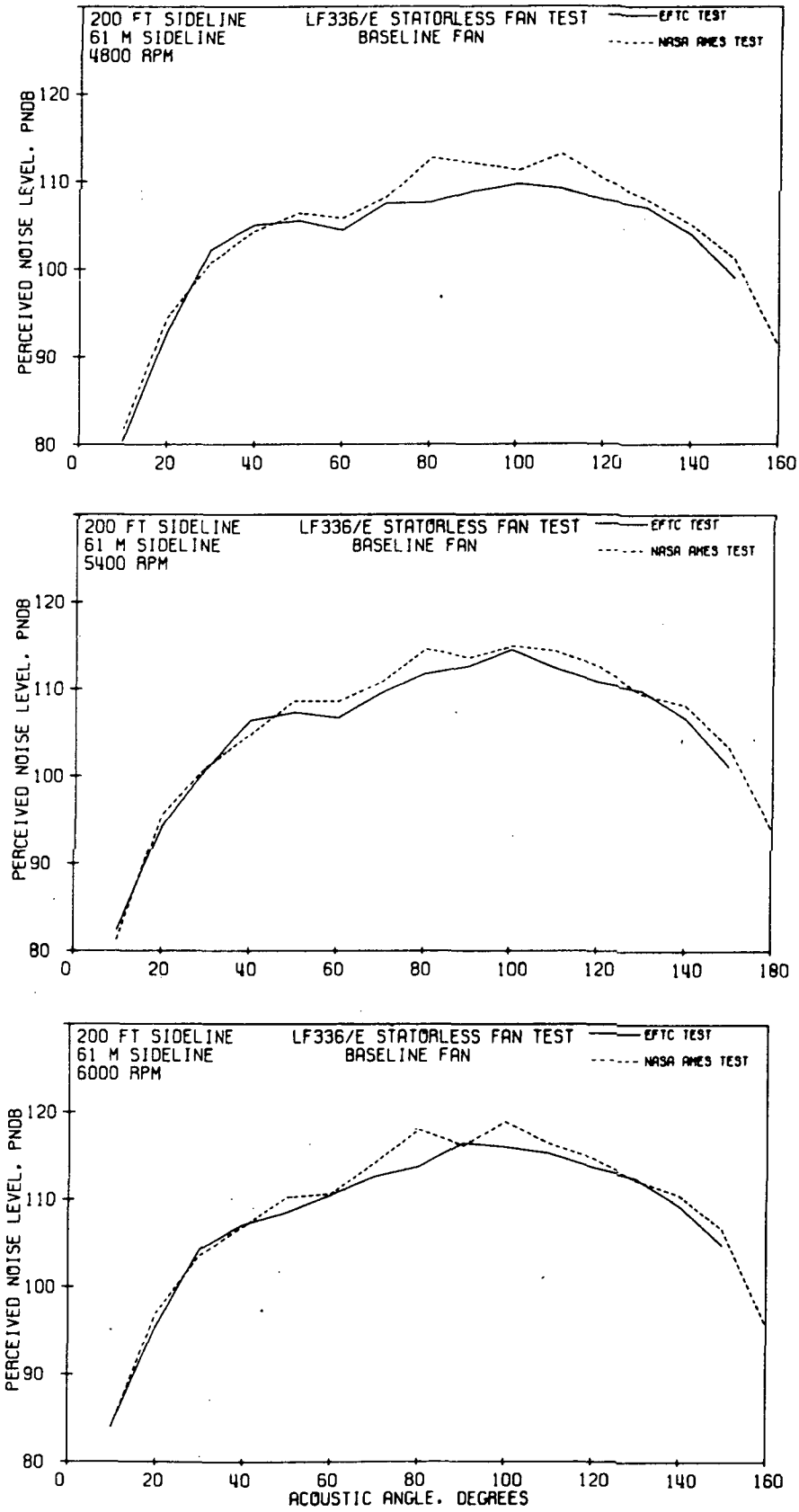

FIGURE 66 EFTC AND NASA AMES PNL DIRECTIVITY PATTERN COMPARISONS AT 5400 AND 6000 RPM

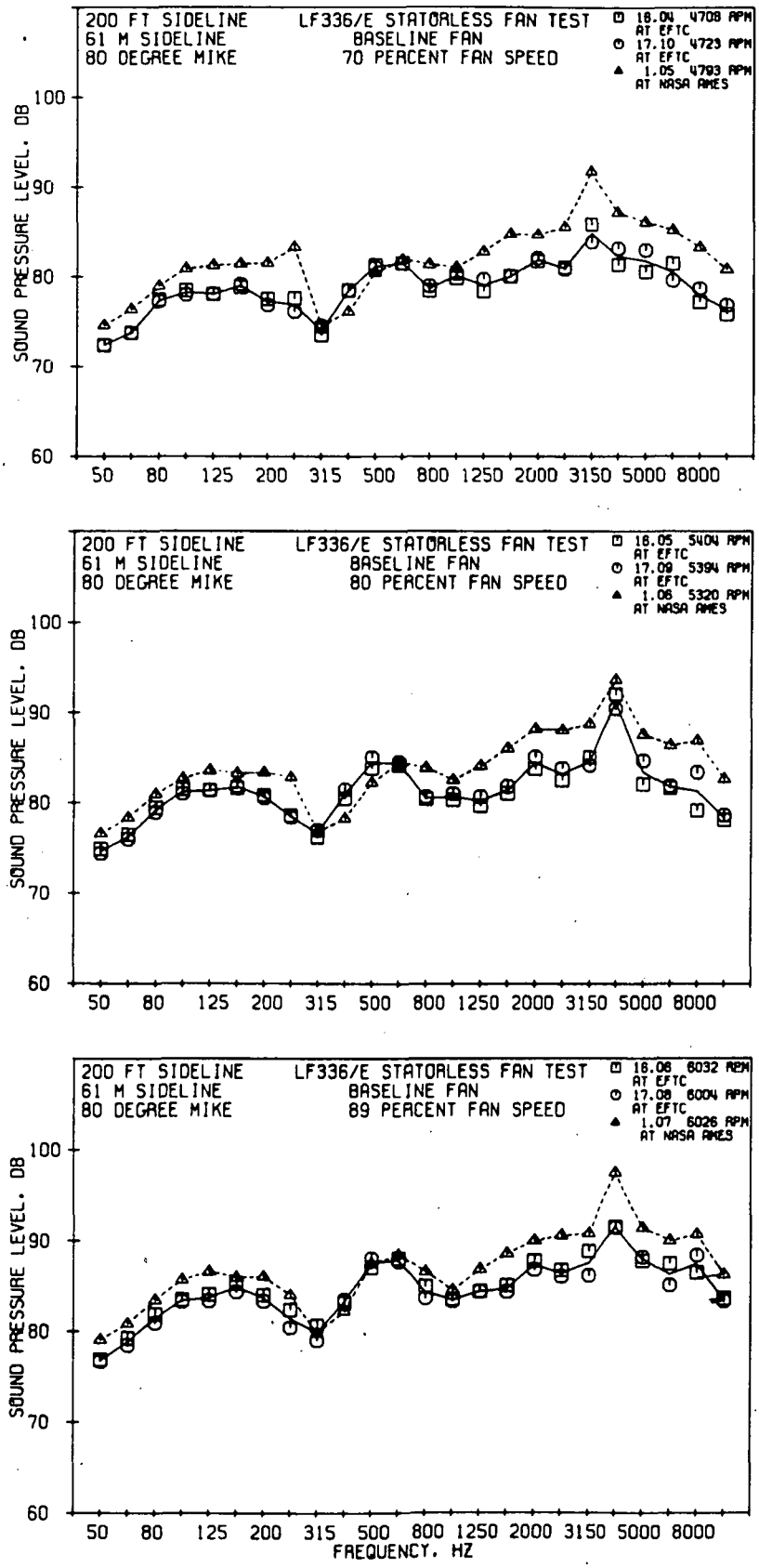

FIGURE 67 EFTC AND NASA AMES 80° FAR FIELD 1/3 OCTAVE BAND SPECTRAL COMPARISONS AT 5400 AND 6000 RPM

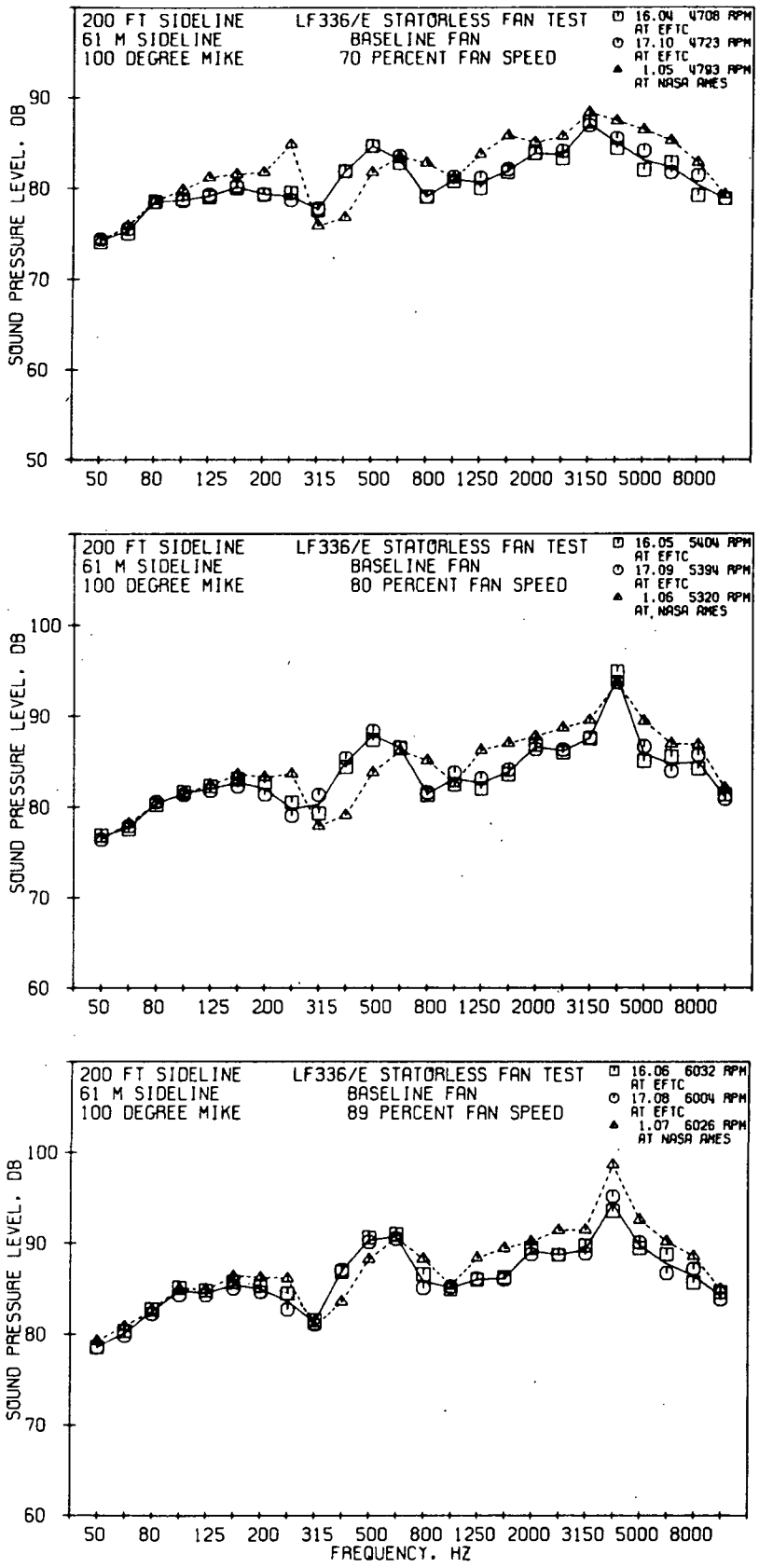

FIGURE 68 EFTC AND NASA AMES 100° FAR FIELD 1/3 OCTAVE BAND SPECTRAL COMPARISONS AT 5400 AND 6000 RPM

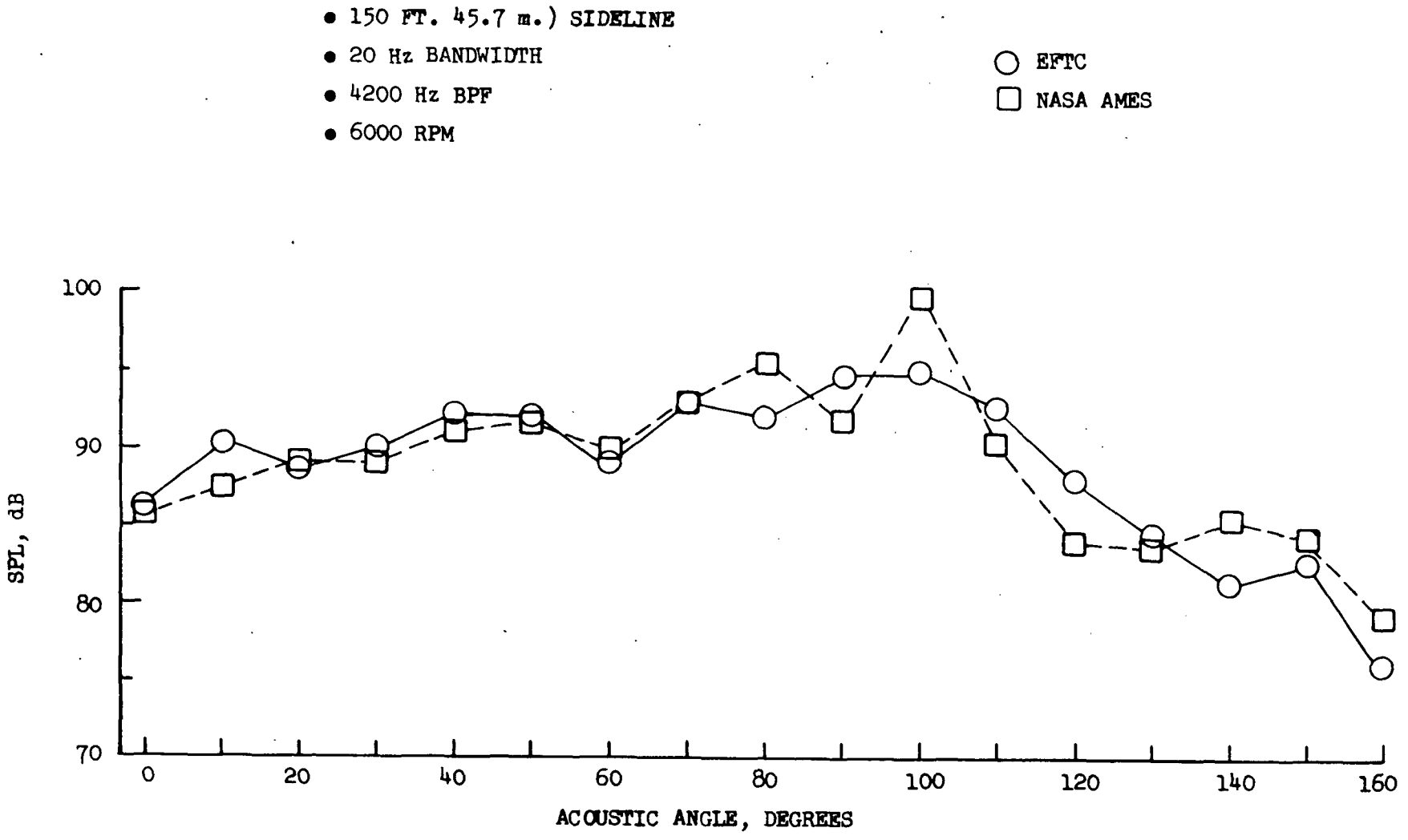

FIGURE 69 EFTC AND NASA AMES BPF DIRECTIVITY PATTERN COMPARISON AT 6000 RPM

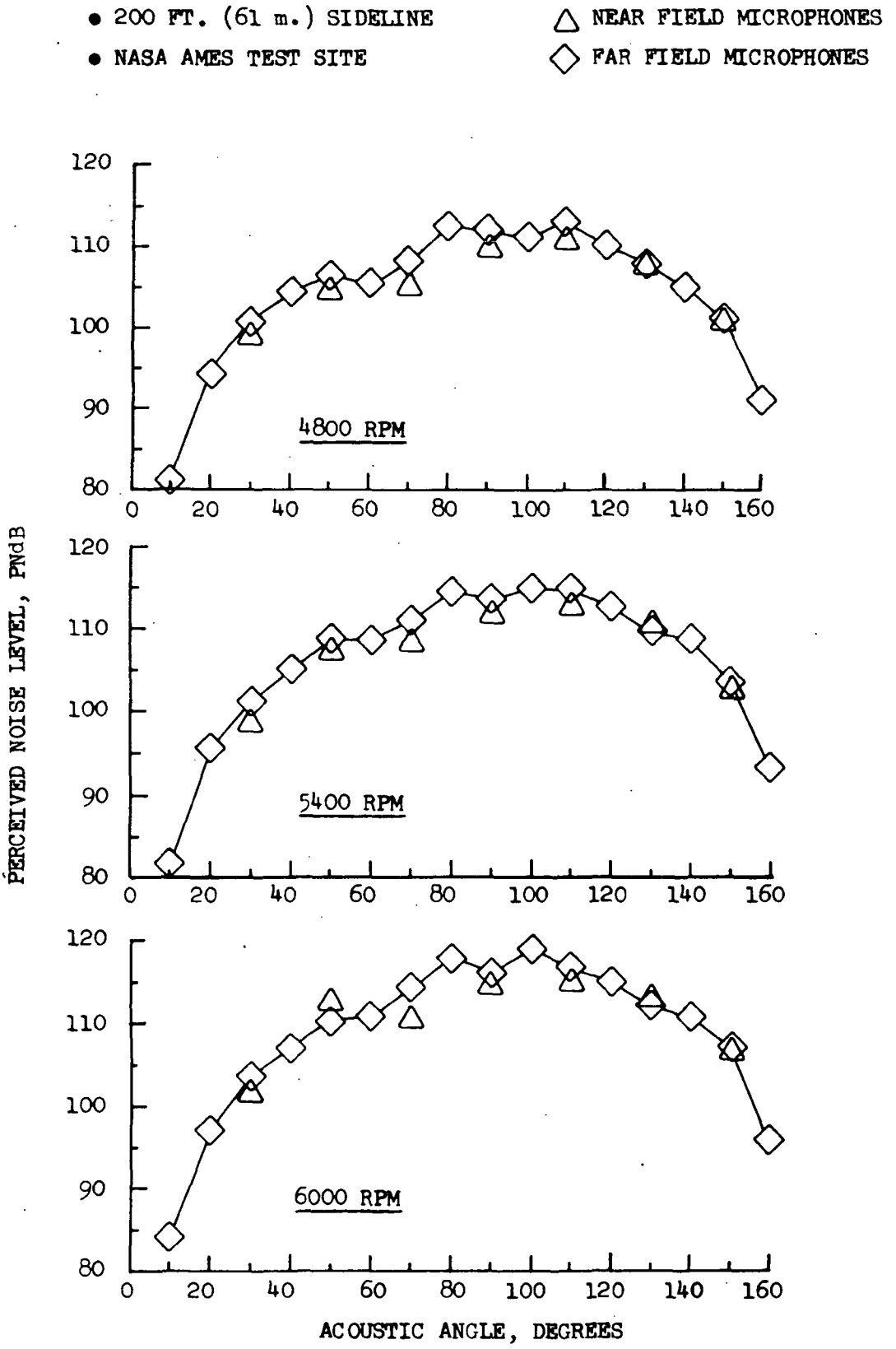

FIGURE 70 COMPARISON OF EXTRAPOLATED NEAR AND FAR FIELD PNL DIRECTIVITY PATTERNS AT 4800, 5400, AND 6000 RPM

- 200 FT. (61 m.) SIDELINE
- 50° MICROPHONE
- NASA AMES TEST SITE

——— NEAR FIELD MICROPHONE
- - - - - FAR FIELD MICROPHONE

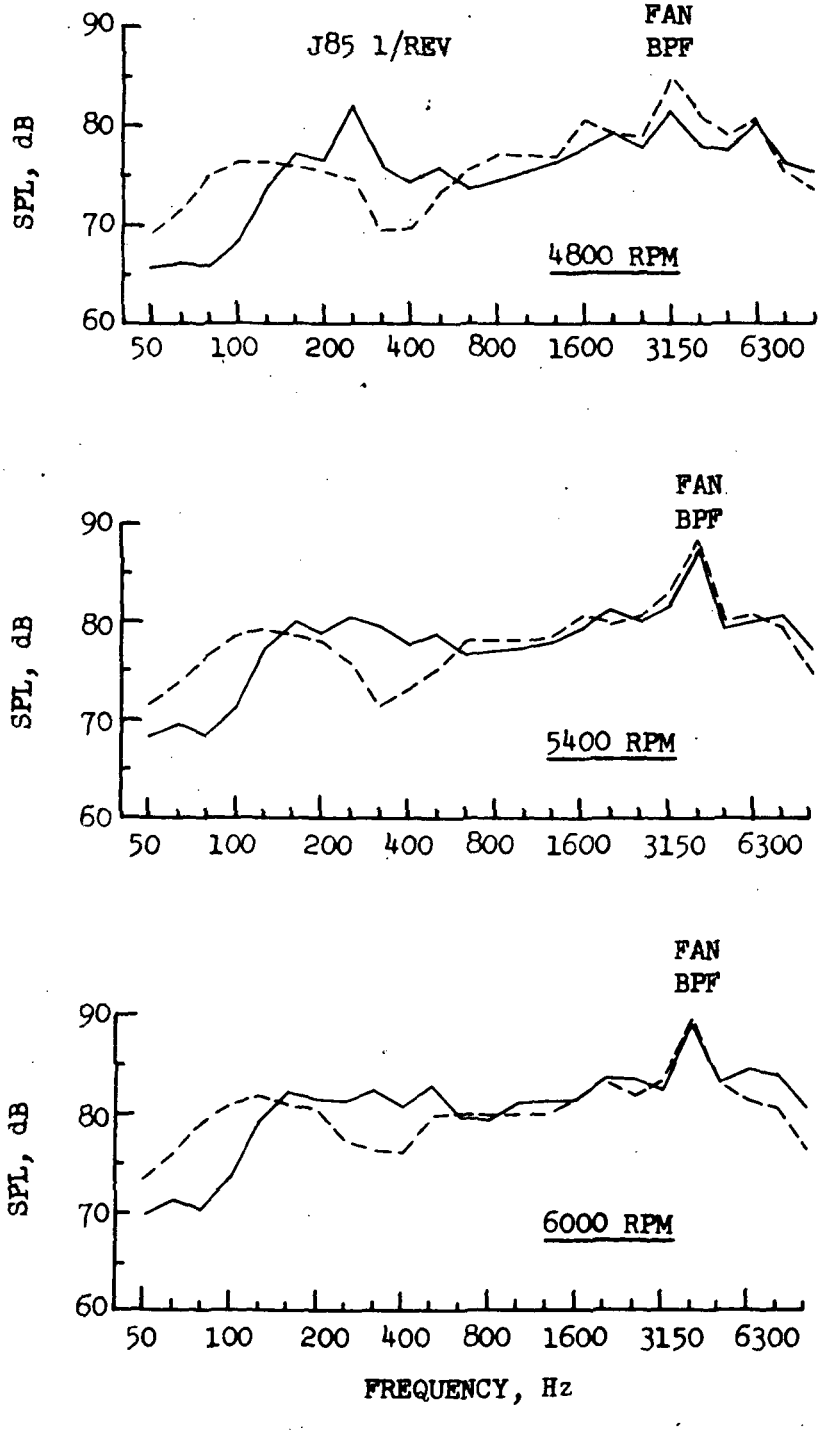

FIGURE 71 NEAR AND FAR FIELD 50° 1/3 OCTAVE BAND SPECTRAL COMPARISONS AT 4800, 5400, AND 6000 RPM

- 200 FT. (61 m.) SIDELINE
- 110° MICROPHONE
- NASA AMES TEST SITE

——— NEAR FIELD MICROPHONE
- - - - - FAR FIELD MICROPHONE

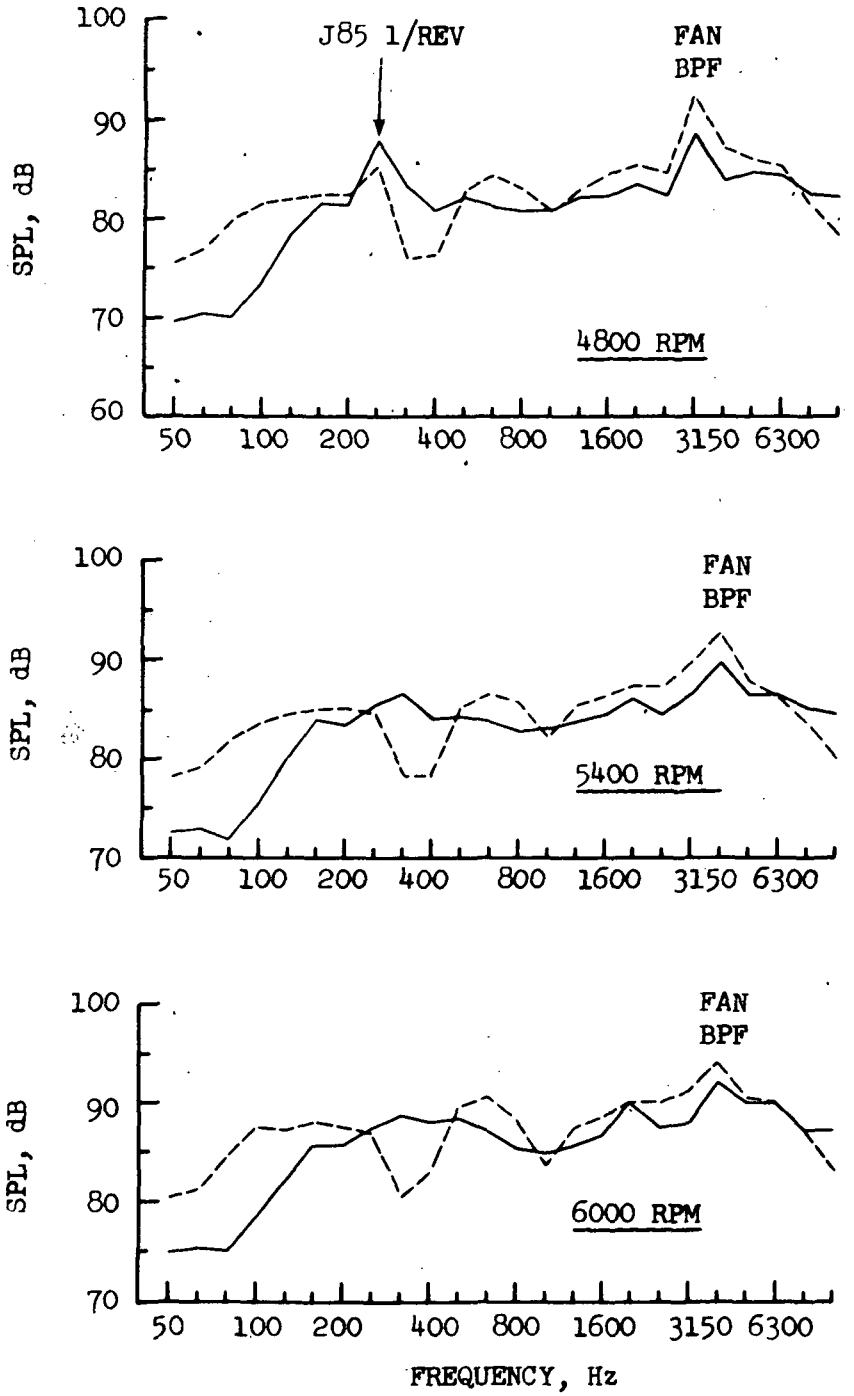

FIGURE 72 NEAR AND FAR FIELD 110° 1/3 OCTAVE BAND SPECTRAL COMPARISONS AT 4800, 5400, AND 6000 RPM